



Natural Resources
Canada

Ressources naturelles
Canada

**GEOLOGICAL SURVEY OF CANADA
OPEN FILE 8599**

**Passive seismic survey results of sediment thickness
at three 5200 cal yr BP landslide sites in eastern
Ontario and western Quebec**

B. Wang

2019

Canada



GEOLOGICAL SURVEY OF CANADA OPEN FILE 8599

Passive seismic survey results of sediment thickness at three 5200 cal yr BP landslide sites in eastern Ontario and western Quebec

B. Wang

Geological Survey of Canada, 601 Booth Street, Ottawa, Ontario K1A 0E8

2019

© Her Majesty the Queen in Right of Canada, as represented by the Minister of Natural Resources, 2019

Information contained in this publication or product may be reproduced, in part or in whole, and by any means, for personal or public non-commercial purposes, without charge or further permission, unless otherwise specified.

You are asked to:

- exercise due diligence in ensuring the accuracy of the materials reproduced;
- indicate the complete title of the materials reproduced, and the name of the author organization; and
- indicate that the reproduction is a copy of an official work that is published by Natural Resources Canada (NRCan) and that the reproduction has not been produced in affiliation with, or with the endorsement of, NRCan.

Commercial reproduction and distribution is prohibited except with written permission from NRCan. For more information, contact NRCan at nrcan.copyrightdroitdauteur.rncan@canada.ca.

Permanent link: <https://doi.org/10.4095/314939>

This publication is available for free download through GEOSCAN (<https://geoscan.nrcan.gc.ca/>).

Recommended citation

Wang, B., 2019. Passive seismic survey results of sediment thickness at three 5200 cal yr BP landslide sites in eastern Ontario and western Quebec; Geological Survey of Canada, Open File 8599, 78 p.
<https://doi.org/10.4095/314939>

Publications in this series have not been edited; they are released as submitted by the author.

Passive seismic survey results of sediment thickness at three 5200 cal yr BP landslide sites in eastern Ontario and western Quebec

Baolin Wang

ABSTRACT

Passive seismic surveys or Horizontal-to-Vertical Spectral Ratio (HVSR) measurements can be used to estimate sediment thickness or depth to bedrock.

Three landslide sites were selected strategically for potential geotechnical studies. The bedrock depth estimates obtained from passive seismic surveys may aid in the planning of the geotechnical drilling programs. Geotechnical investigations of paleo-landslides are important for earthquake research as they can provide more precise estimates of the location and magnitude of pre-historic earthquakes.

This document reports results of passive seismic surveys at three prehistoric landslide sites near Cheney and Wendover in eastern Ontario, and Masson in western Quebec. The sites are among 13 landslides previously dated to have occurred about 5200 cal yr BP. The landslides are Champlain Sea clay failures and are hypothesized in previous studies as triggered by an earthquake around that time.

Passive seismic surveys are conducted along the approximate centerlines of the landslides to estimate the thickness of the Champlain Sea sediments. The range of the sediment thickness is found to be around 30, 40 and 50 m at Cheney, Masson and Wendover site respectively. Sediment profiles are interpreted along the longitudinal sections. The results show variable bedrock depths at Cheney and Masson sites. The interpreted bedrock at the Wendover site is deeper and appears more even. These bedrock depth estimates form the planning basis of potential future geotechnical drilling programs. Upon borehole confirmation, the survey results may help construct models for slope stability analysis.

1. INTRODUCTION

Geological Survey of Canada (GSC) has been conducting paleoseismicity research in the Western Quebec Seismic Zone (WQSZ). Aylsworth et al. (2000) reported 11 landslides of about 5200 cal yr BP in the WQSZ (Fig. 1). Brooks (2015) identified another two landslides of similar ages in the region. All of the 13 landslides are Champlain Sea clay failures. They were hypothesized to have been triggered by an earthquake about 5200 cal yr BP. The earthquake magnitude (M_w 6.4) was estimated based on the area of landslides using a magnitude-to-area-of-landsliding correlation by Keefer (1984) and Rodriguez et al. (1999). However, the correlation is rather crude as it is based on worldwide data that does not specifically address soft clay landslides nor the region's ground-motion characteristics. For example, smaller earthquakes may trigger landslides in a larger area of Champlain Sea sediments due to the high sensitivity of the clay. It is also well known that ground-motion characteristics in eastern North America is different from that of other regions, e.g., western North America (Hassani and Atkinson 2015, Shahjouei and Pezeshk 2016, Yenier and Atkinson 2015). An earthquake in one region may induce different ground accelerations at a given distance than that in another region for the same magnitude and at the same distance.

Understanding paleoearthquakes helps improve the building code by extending seismic database to prehistoric times (Adams 2011). Due to the importance of prehistoric events to the building code, the magnitude of the earthquake deserves further investigation. Geotechnical studies of the landslides may help improve the understanding of the earthquake. Particularly, slope stability analyses of the landslides may help establish the threshold ground accelerations that can be used to locate the earthquake and estimate its magnitude more accurately. This report provides estimates of sediment thicknesses at select landslide sites as the first step towards this objective.

Three of the 13 landslides are selected for the study. Passive seismic surveys are conducted at the selected sites, and the thicknesses of the Champlain Sea sediments are estimated based on the survey results. Upon borehole confirmation, the survey results may help establish the sediment depth profiles for construction of slope stability models.



Fig. 1 Locations of ~5200 cal yr BP landslides (Round red dots mark the locations of the landslides reported in Aylsworth et al. 2000. Square blue dots are locations of the landslides identified by Brooks 2015. Map © Google Inc.)

2. SITE SELECTION

Selecting suitable landslides is required for geotechnical studies to further investigate the earthquake. Properly selected landslides allow slope stability studies to be carried out with more certainty and earthquake magnitude calculated with higher confidence. Several factors may be considered on the site selection, e.g. landslide size, distance between sites and location relation among the sites. Larger landslides may be better candidates for various reasons. For example, slope stability analyses of larger landslides may incur less errors associated with local geometric variations. The slope failure process and mechanism can be easier to establish with larger landslides (Wang 2016, 2019). Ground accelerations derived from slope stability analyses are of better quality if fewer uncertainties about the landslides are involved.

The distance between the study landslides needs to be considered. Calculations of earthquake magnitude from ground accelerations may bear less geometrical error with data from distant sites than from those of tighter spacing. This requires choosing the landslide sites as farther apart as possible.

A minimum of three landslides are needed for triangulation of the earthquake. A more regularly shaped triangle formed by the sites incurs less geometrical distortion when pinpointing the earthquake.

Other considerations on site selection may include accessibility of the site, potential quality of data that can be acquired and cost associated with field works etc.

A field reconnaissance was conducted at the 11 landslide sites identified by Aylsworth et al. (2000). Three sites, i.e., at Cheney, Masson and Wendover (Fig. 1) were identified as good candidates for geotechnical studies based on the above screening criteria. Details about the sites are discussed in the subsequent sections. Other sites are limited in terms of site accessibility, extent of the slope failure, or certainty about the failure mechanism. Note that the two landslides reported by Brooks (2015) may also be good candidates due to their far distance from others and potential large size. However, the two landslides appear very complex and details are yet to be confirmed and finalized.

3. METHOD OF INVESTIGATION

Passive seismic surveys were carried out at the three selected landslide sites with an ultra-portable instrument Tromino®. The device is a 3-component seismograph designed to measure ambient noise in the ground (Micromed 2012). It records the horizontal (H) and vertical (V) components of the noise over a certain period of time. The horizontal to vertical spectral ratio (HVSR) is calculated. This is useful for estimating the thickness of sediments overlying stiffer materials (e.g., bedrock) of sharp shear-wave velocity contrast (Nakamura, 1989, SESAME 2004). The method is also referred to as H/V (or HVSR) method and has been applied successfully in various industries, e.g., Lane et al. (2008); Scheib (2014); Smith et al. (2013); Chandler and Lively (2016).

Typically, the Champlain Sea sediments in the study region have a predominant seismic impedance boundary at the base underlain by glacial sediments or bedrock (Hunter et al. 2010). This stratigraphy usually exhibits a strong impedance contrast forming a strong resonator and yields a well-defined sharp peak period (resonant period). The study sites are therefore suitable for

application of the HVSR method.

The Tromino surveys were done along road shoulders in most cases at the study sites. Some other locations surveyed were in wooded areas away from roads. At each acquisition site, the ground surface was cleared with a hand shovel to remove loose materials. A level base was prepared on the firm ground. The unit was orientated to the north. The three spikes at the bottom of the unit were pushed into the ground until the lower plate touched the ground. The unit was leveled with the built-in leveling bubble. The acquisition was set for 30 minutes at each location. A traffic pylon was used to cover the device to minimize wind effect when necessary.

A proprietary software, Grilla® developed for Tromino was used to analyze the data and to calculate a resonant frequency (F_0) or period ($T_0 = 1/F_0$) of the site. The Tromino recordings were downloaded on to a laptop computer and inspected for data quality immediately after each acquisition. If poor quality data is observed from the Grilla graphic display, the measurement is repeated at a nearby location.

Crow et al. (2017) presents an empirical correlation between depth to impedance contrast (H) and resonant frequency (F_0) specifically for Champlain Sea sediments in the general Ottawa-Gatineau region:

$$H = 60.38 F_0^{-1.158} \pm 17.66 \text{ m} \quad (1)$$

This correlation is used to calculate the sediment thickness with the resonant frequency obtained from the Tromino measurement.

4. CHENEY LANDSLIDE

Cheney is part of the City of Clarence-Rockland in the United Counties of Prescott and Russell, Ontario. The ~5200 cal yr BP landslide scar is right beside (northwest of) Cheney and is about 33 km east of Ottawa (Figs. 1 and 2). The scar is about 1.9 km long and about 1.5 km wide. The Champlain Sea plain in the area is about 80 m above sea level (asl.). The landslide occurred at the north bank of an abandoned Mer Bleue Channel (Aylsworth et al. 2010). The eroded channel side slope is about 15 m high. The debris surface in the landslide source zone dropped by about 8 m from the pre-failure Champlain Sea plain. An isolated area of about 250 m by 200 m at the toe of the slope appears to have not been affected by the landslide as seen on the LiDAR image in Fig. 2. The scar zone is mostly wooded. Canaan Road runs across the landslide scar along the approximate center line of the landslide (Fig. 2). The road surface in this area is gravel (Fig. 3) and some areas are muddy and uneven. There is little traffic along this part of the road. It provides an ideal access for geotechnical site investigations along the approximate centerline of the landslide.

A total of 15 locations along Canaan Road were surveyed with Tromino®. The survey locations (CT01 to CT15) are marked in Fig. 2. The Tromino® measurements were on the shoulders of Canaan Road or in the field slightly away from the road shoulder. The graphic display of the Grilla software indicates high quality recordings with sharp impedance contrast at most locations. Figures 4 to 6 are example (CT04) charts of HVSR, spectral windows, and the average spectra interpreted by the Grilla software. The charts for all 15 survey locations are provided in Appendix A.

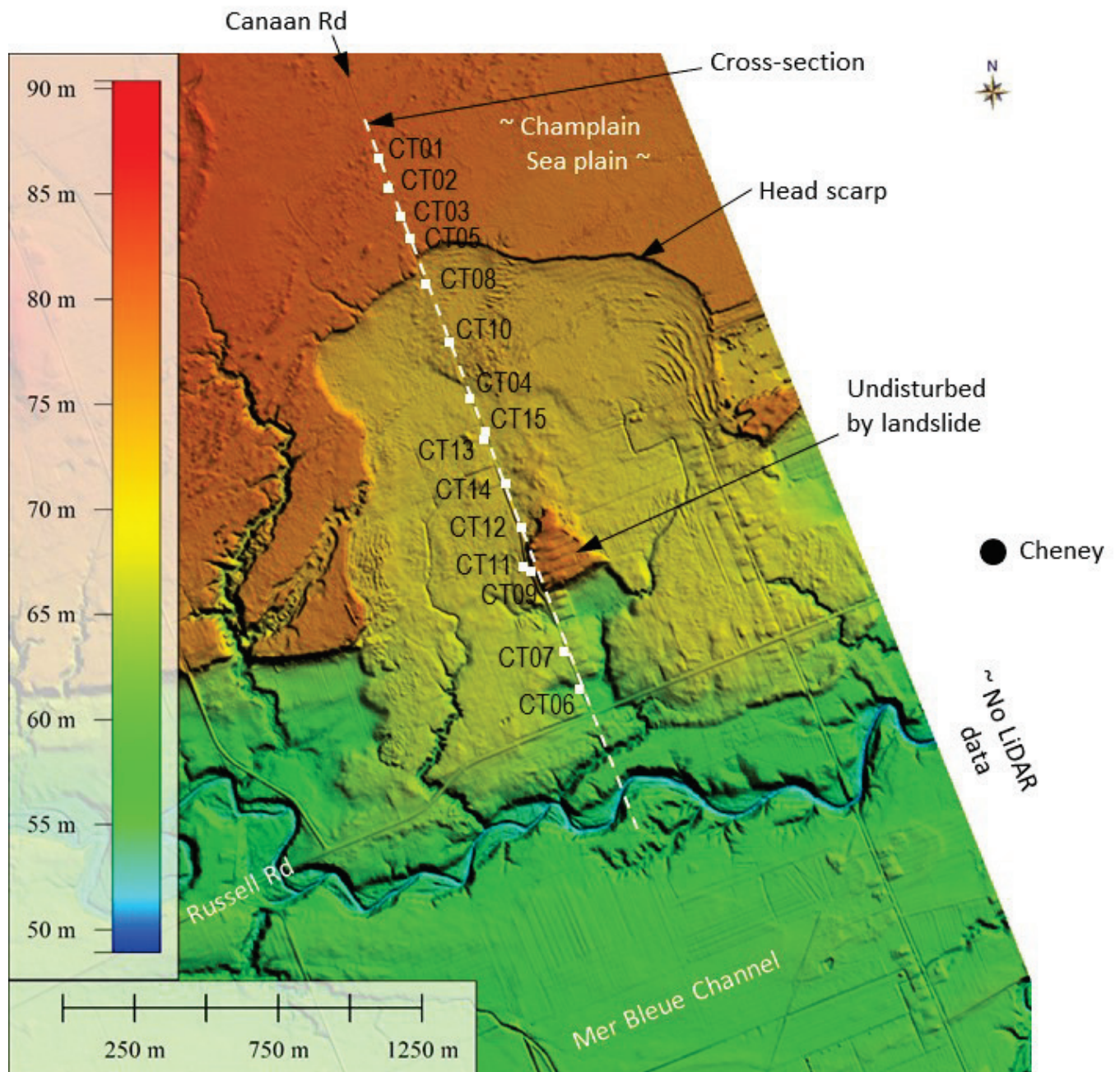


Fig. 2 LiDAR image of Cheney landslide site (Square dots mark Tromino survey locations and labelled as CT. LiDAR© City of Ottawa)



Fig. 3 Photo of Canaan Road at Cheney landslide site (Taken July 4, 2018 at CT15, facing north. See Fig. 2 for location.)

Table 1 Tromino survey results from Cheney landslide site

Location	Coordinates (UTM WGS 84)		Distance from North of Section (m)	F_0 (Hz)	T_0 (Sec.)	Soil Thickness (m)	Surface Elevation from LiDAR (m, asl.)	Resonator Elevation (m, asl.)
	Easting (m)	Northing (m)						
CT01	478255	5029832	151	1.66	0.60	34	80	46
CT02	478293	5029725	264	1.66	0.60	34	80	46
CT03	478332	5029627	370	1.69	0.59	33	79	46
CT05	478359	5029549	452	1.66	0.60	34	79	45
CT08	478416	5029391	620	1.75	0.57	32	74	42
CT10	478490	5029184	840	1.53	0.65	37	73	36
CT04	478562	5028986	1,051	1.59	0.63	35	71	36
CT15	478615	5028869	1,179	1.88	0.53	29	71	42
CT13	478608	5028846	1,198	1.94	0.52	28	71	43
CT14	478680	5028690	1,369	3.34	0.30	15	71	56
CT12	478735	5028541	1,528	4.66	0.21	10	71	61
CT11	478737	5028397	1,664	3.69	0.27	13	70	57
CT09	478762	5028380	1,689	3.78	0.26	13	72	59
CT07	478874	5028101	1,989	3.22	0.31	16	67	51
CT06	478927	5027967	2,133	2.25	0.44	24	62	38

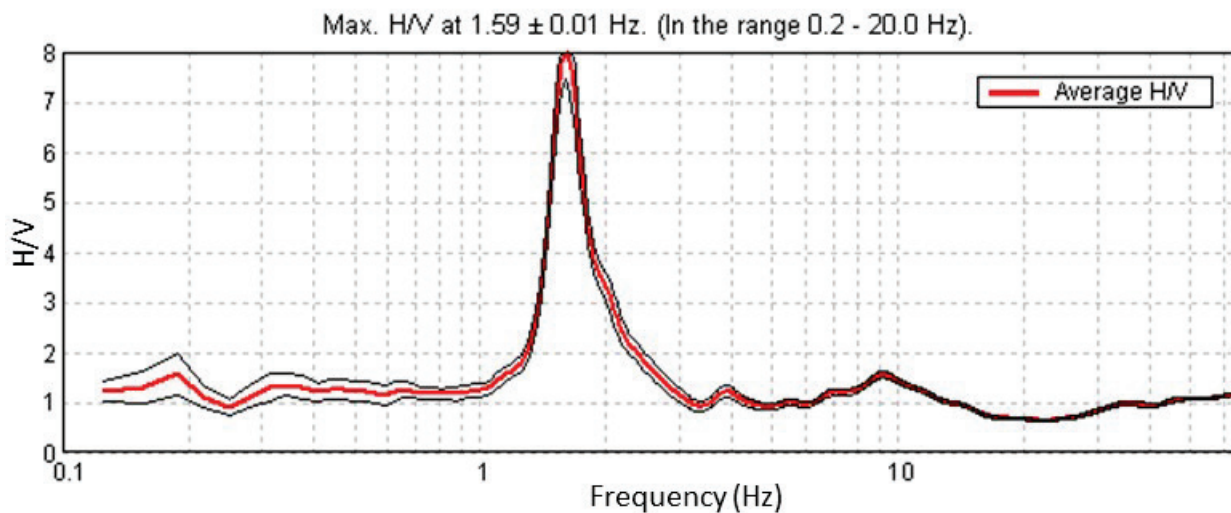


Fig. 4 Example chart of Horizontal to Vertical Spectral Ratio (Cheney landslide site, CT04)

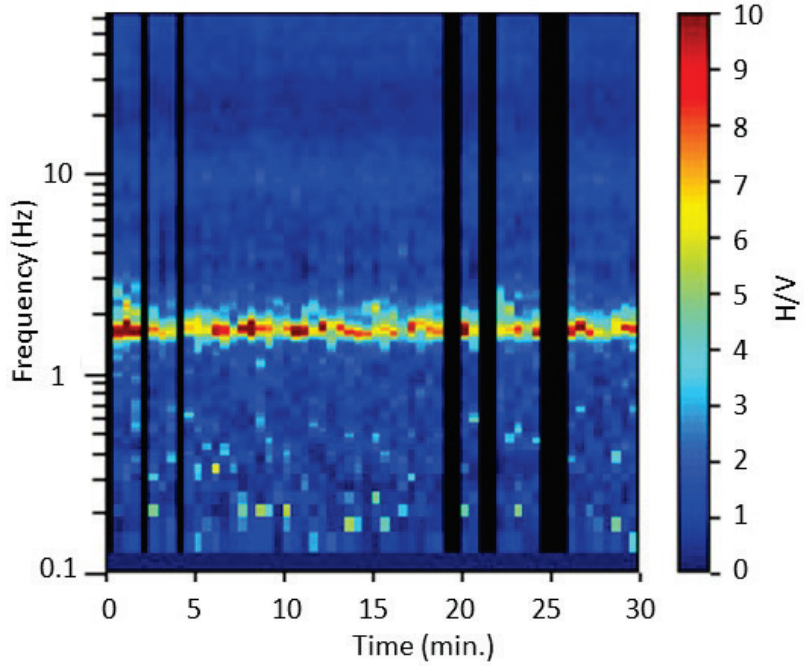


Fig. 5 Example chart of spectral windows (Cheney landslide site, CT04). Black bars are windows of noisy signals recorded (usually due to traffic) and removed from calculations.

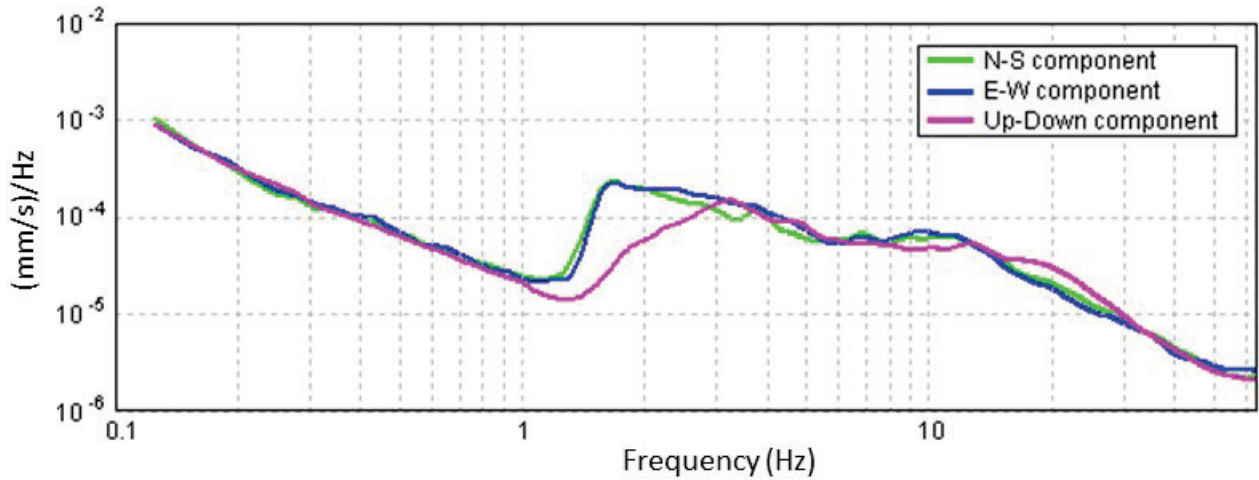


Fig. 6 Example chart of the north-south, east-west and vertical average spectra for all selected windows used in the interpretation (Cheney landslide site, CT04)

The recordings at CT09 exhibit a broader band of frequency (Fig. 7.a) than most other cases. This measurement was on the road shoulder. Another measurement was made at CT11 to replicate CT09. CT11 is in a nearby grass field where the surface is relatively even and the elevation is about 2 m lower than the road. The signals recorded from CT11 (Fig. 7.b) are similar to that from CT09.

The recordings at CT13 were noisy (Fig. A-13). A repeat measurement was made at CT15 and better signals were recorded (Fig. A-15).

Table 1 provides the resonant frequencies calculated from the Grilla software. Also provided in

the table are the sediment thicknesses estimated with eq. (1). An interpreted sediment profile of a cross-section parallel to Canaan Road is shown in Fig. 8 (the location of the section is shown in Fig. 2). The current ground surface is based on the LiDAR data. The pre-failure surface is interpreted from the Champlain Sea terraces along the shoulders of the landslide as well as the undisturbed ground in the middle of the scar zone.

The interpreted elevation of the impedance surface at CT11 is slightly lower than that at CT09 (due to surface elevation difference) although the estimated sediment thickness is identical at the two locations (Table 1). The elevations of the resonant surface at CT09 and CT11 are consistent with those measured from other nearby locations (Fig. 8). From the cross-sectional profile in Fig. 8, a bedrock knoll likely exists near CT09, CT11 and CT12. This correlates with the observations on the surface where the isolated area unaffected by the landslide is visible (Fig. 2). It is interesting to note that CT11 is slightly further away from the undisturbed “island” than CT09. The impedance surface at CT11 is about 2 m below that at CT09. It is an indication of bedrock sloping down from CT09 to CT11, which, again, is consistent with the observations on the surface. The bedrock is likely shallower further into the central area of the “island”. The broader bands of high-amplitude H/V signal at CT09 and CT11 (Fig. 7) are likely attributed to the slope of the impedance surface. The consistency of these and other data indicates that the quality of the data acquired at Cheney landslide site is reasonably high and the estimated sediment thicknesses are likely accurate and well within the uncertainty margin.

In summary, the Champlain Sea sediments at the Cheney landslide along Canaan Road are about 10 m to 37 m thick. There is likely a bedrock knoll at the toe of the landslide source zone. The shallow bedrock knoll is probably the reason why the isolated 250x200 m area inside the scar was unaffected by the landslide. The Tromino survey results provide a basis for planning of further geotechnical investigations. The HVSR measurements are likely accurate, but borehole verification is required to confirm the actual thickness of the sediments.

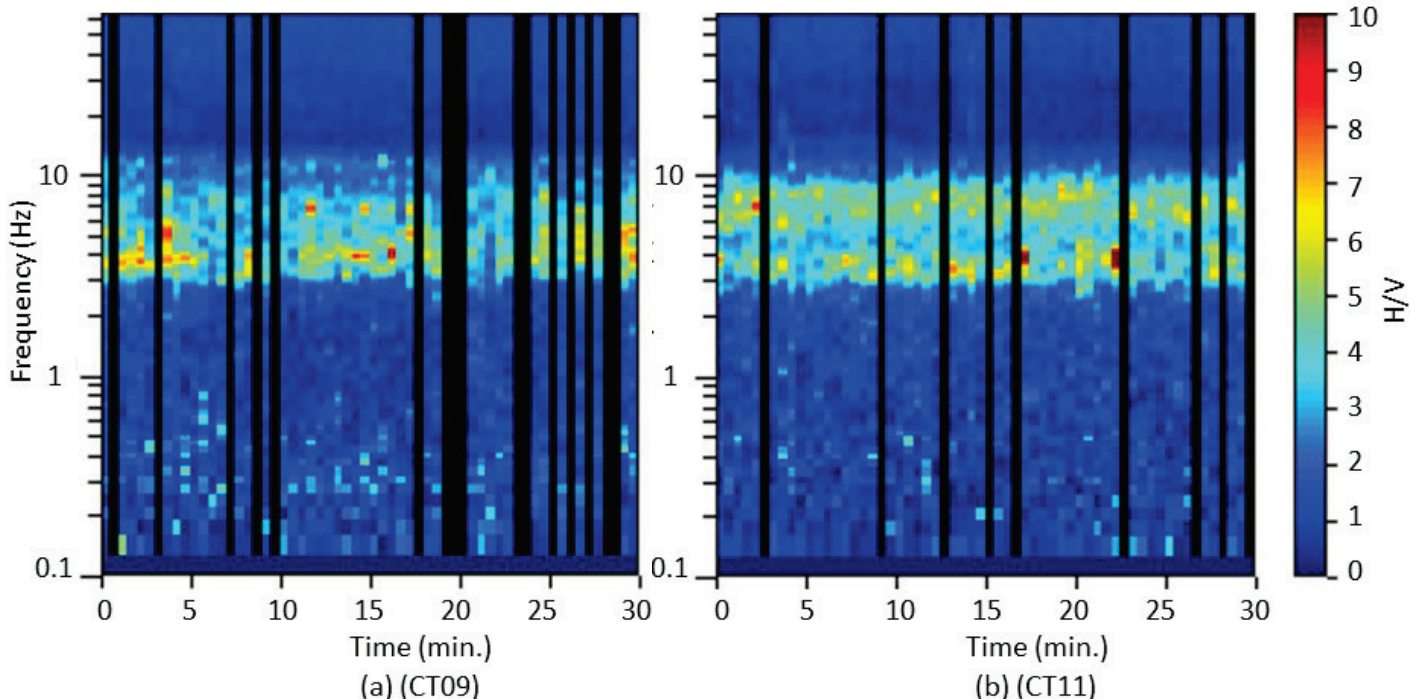


Fig. 7 Spectral windows at (a) CT09, and (b) CT11, Cheney landslide site (note broader frequency band of high-amplitude H/V signals compared to Fig. 5)

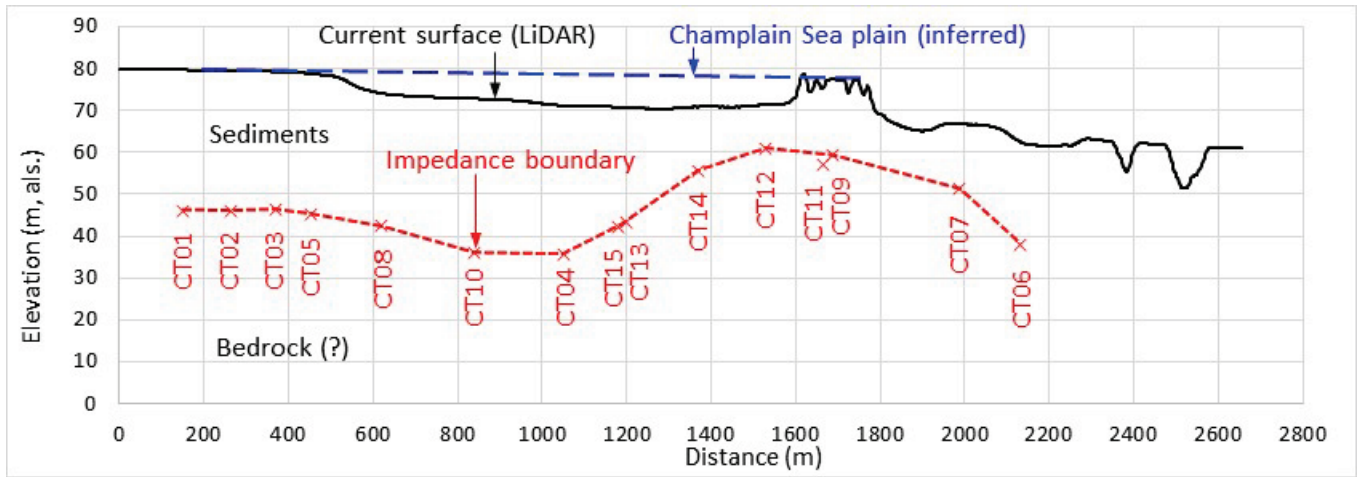


Fig. 8 Cross-sectional profile along Canaan Road, Cheney landslide site (see Fig. 2 for location. Vertical exag.: 10x)

5. MASSON LANDSLIDE

The landslide at Masson, Quebec is about 28 km northeast of Ottawa (Fig. 1). Figure 9 shows a LiDAR image of the landslide site. The source zone of the landslide is about 1.4 km long and about 1.8 km wide. Findlay Road runs across the approximate centerline of the landslide (Fig. 9). The road is separated by Hwy 50. The road segment between Hwy 50 and Hélène Impasse appears to have not been maintained for an extended period of time. This portion of the Road is blocked with large concrete barriers at Hélène Impasse to prevent vehicle access (Fig. 10). The northern portion of Findlay Road (Fig. 11) can be accessed from Lépine Ave. and the southern portion (Fig. 12) from Hwy 148. The road provides an ideal access for geotechnical site investigations along the approximate centerline of the landslide.

A total of 29 locations (MT01 to MT29) were surveyed with Tromino along Findlay Road, Hélène Impasse and in an open area north of Hwy 50. The survey locations are shown in Fig. 9 and the coordinates are provided in Table 2. Clear signals were recorded at most locations. Due to uncertainty of the recordings at MT23, the measurement was immediately repeated at the nearby location MT24 and similar data were recorded. The charts of HVSR, spectral windows, and the average spectra interpreted by the Grilla software for all the survey locations are provided in Appendix B. The peak frequency, amplitude, and estimated sediment thickness are summarized in Table 2. The current ground elevations at the survey locations are obtained from the LiDAR data. Also listed in Table 2 are calculated bedrock or resonator depth. An interpreted cross-sectional profile parallel to Findlay Road is shown in Fig. 13.

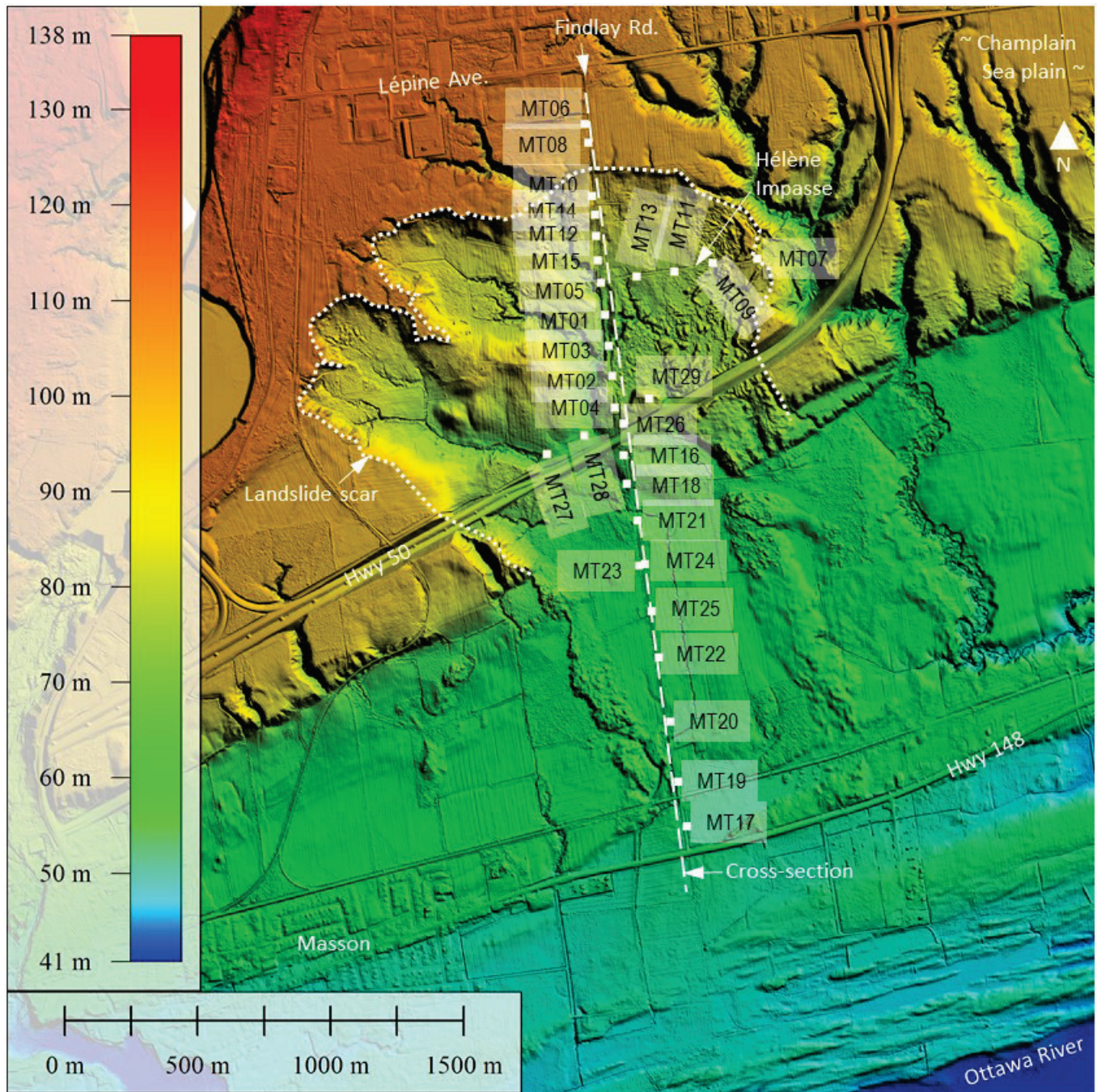


Fig. 9 LiDAR image of Masson landslide site and Tromino survey locations (Square dots mark Tromino survey locations. LiDAR © Government of Quebec)



Fig. 10 Photo of blocked portion of Findlay Road (taken from intersection at Hélène Impasse on July 05, 2018, facing south)



Fig. 11 Photo of Findlay Road north of Hélène Impasse (taken from intersection at Hélène Impasse on July 05, 2018, facing north)



Fig. 12 Photo of Findlay Road south of Hwy 50 (taken from northern end of road next to Hwy 50 on July 05, 2018, facing south)

As seen from Table 2 and Fig. 13, the depth to impedance varies from 6 m to 33 m from the current surface along Findlay Road. The general slope of the impedance (bedrock) surface is towards the Ottawa River, which correlates with the Ottawa River valley. Locally however, the resonance surface elevation changes by about 20 to 30 m along Findlay Road. The pre-failure Champlain Sea sediments could be 20 to 50 m thick in the source zone of the landslide. Weaker signals were recorded at MT23/24 and MT25 making the depth estimates at the two locations somewhat less reliable. This could be due to complications of ground conditions caused by landslide debris deposition. The results provide a basis for planning of geotechnical drillhole investigations. Verification from drillholes is required to confirm the actual thickness of the sediments.

Table 2 Tromino survey results from Masson landslide site

Location	Coordinates (UTM WGS 84)		Distance from North of Section (Sites on Findlay Rd) (m)	F_0 (Hz)	T_0 (Sec.)	Soil Thickness (m)	Surface Elevation from LiDAR (m, asl.)	Resonator Elevation (m, asl.)
	Easting (m)	Northing (m)						
MT06	468955	5046777	121	2.69	0.37	19	102	83
MT08	468968	5046707	191	2.53	0.40	21	101	80
MT10	468977	5046505	393	2.50	0.40	21	91	70
MT14	468988	5046436	463	2.53	0.40	21	89	68
MT12	468990	5046355	544	2.75	0.36	19	84	65
MT15	468995	5046264	635	2.78	0.36	18	81	63
MT05	469003	5046179	720	2.63	0.38	20	79	59
MT01	469019	5046059	841	2.34	0.43	23	75	52
MT03	469029	5045941	960	2.00	0.50	27	73	46
MT02	469041	5045829	1072	2.28	0.44	23	76	53
MT04	469047	5045709	1192	3.38	0.30	15	76	61
MT26	469080	5045648	1256	3.63	0.28	14	76	62
MT16	469078	5045531	1372	3.22	0.31	16	71	55
MT18	469089	5045423	1481	3.69	0.27	13	66	53
MT21	469126	5045284	1623	2.72	0.37	19	63	44
MT24	469150	5045120	1788	1.69	0.59	33	61	28
MT23	469129	5045115	1791	1.69	0.59	33	61	28
MT25	469173	5044943	1967	7.03	0.14	6	60	54
MT22	469196	5044768	2143	3.13	0.32	16	58	42
MT20	469234	5044526	2388	3.88	0.26	13	56	43
MT19	469261	5044300	2615	3.41	0.29	15	54	39
MT17	469290	5044132	2786	2.31	0.43	23	53	30
MT07	469594	5046258	-	2.16	0.46	25	89	64
MT09	469427	5046246	-	2.63	0.38	20	82	62
MT11	469283	5046216	-	2.47	0.40	21	80	59
MT13	469141	5046201	-	2.44	0.41	21	80	59
MT27	468790	5045540	-	3.66	0.27	13	72	59
MT28	468932	5045607	-	3.22	0.31	16	70	54
MT29	469177	5045740	-	2.69	0.37	19	83	64

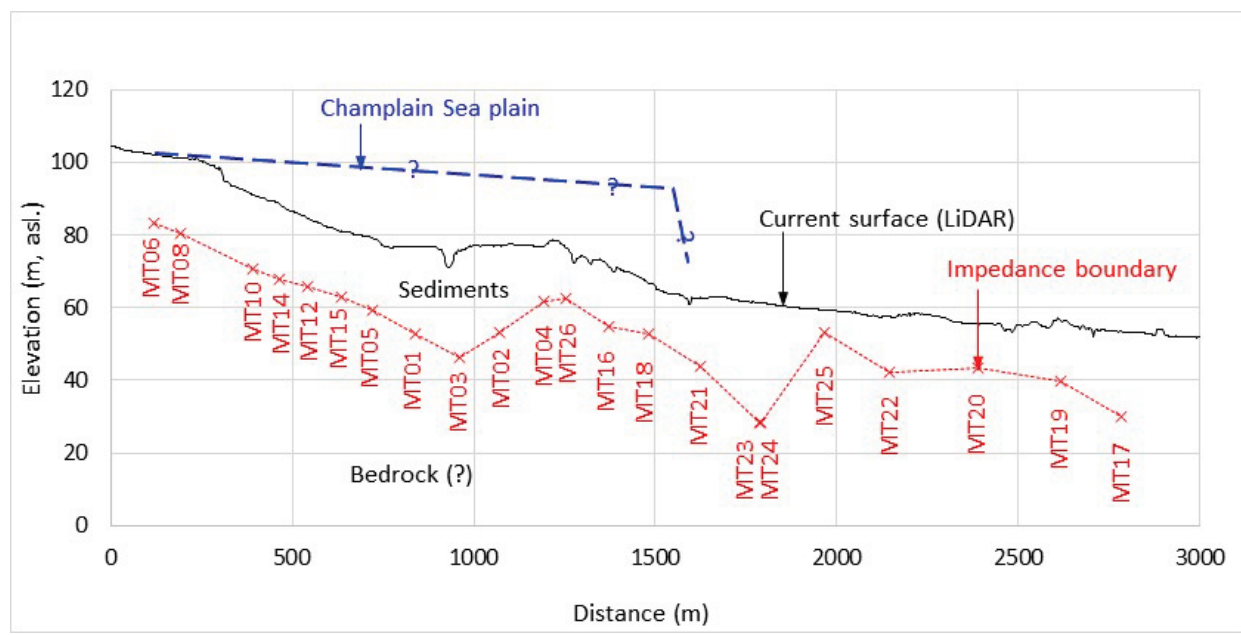


Fig. 13 Longitudinal section of Masson landslide (parallel to Findlay Road. See Fig. 9 for location. Vertical exag.: 10x)

6. WENDOVER LANDSLIDE

This landslide is located 3 km southwest of Wendover, Ontario or about 45 km east of Ottawa (Fig. 1). Figure 14 is a satellite image of the landslide site. Unfortunately LiDAR data is not available for this site. The landslide scar in Fig. 14 was delineated with reference to airphotos. Its size is about 2 km long (including an estimated 0.8 km source zone and 1.2 km deposition zone) and about 2.5 km wide in the east-west direction. The estimates need to be reassessed when LiDAR data becomes available.

Division Road is located along the approximate centerline of the landslide. The road north of the intersection with Concession 2 Road has a gravel surface (Fig. 15). There is little to moderate traffic on this road. To the south of Concession 2, Division Road is a gravel/dirt road for local access (Fig. 16). Apparently, trees have been cut recently in the landslide source zone to the east of Division Road and south of Concession 2 Road (Fig. 16). Division Road provides ideal access for geotechnical site investigations along the approximate centerline of the landslide.

A total of 11 locations (WT01 to WT11, Fig. 14) were surveyed with Tromino along Division Road. The coordinates of the survey locations are provided in Table 3. The charts of HVSR, spectral windows, and the average spectra interpreted by the Grilla software for all the survey locations are provided in Appendix C. Clear signals were recorded at almost all locations at this site. The interpretations of the sediment thickness are provided in Table 3.

The toe of the debris deposition zone is likely located at WT01 as estimated from the airphotos and visual observations in the field (Fig. 17). The impedance depth at WT01 is estimated to be 25 m. Located inside the debris deposition zone, at WT03, WT05, and WT07, the impedance depths are all estimated to be 40 m from the current surface. The landslide source zone was measured to have a slightly variable sediment thickness of 43 to 48 m increasing gradually upslope from WT09 to WT06 (Fig. 14 and Table 3). The locations above the landslide head scarp were estimated to have a sediment thickness of 55 and 58 m at WT04 and WT02 respectively. Although difficult to interpret a cross-sectional profile without LiDAR data, the above results indicate that the bedrock underlying this landslide site is probably more even and deeper compared to the other two landslide sites. In order to appreciate the above results visually, the ground surface elevations are estimated from Google Earth®. Note that the resolution of the elevation data is much lower than that of LiDAR and cannot be used for geotechnical model construction. Figure 18 shows a section of the ground surface and sediment depth profile along Division Road (location shown in Fig. 14). As seen in Fig. 18, the interpreted bedrock is remarkably smooth and consistent despite the uneven ground surface and the coarse elevation data. This is another indication that the data quality of this study is quite high. However, this is only a first estimate for future drilling investigation plans. Drillhole verification is required to confirm the estimates.

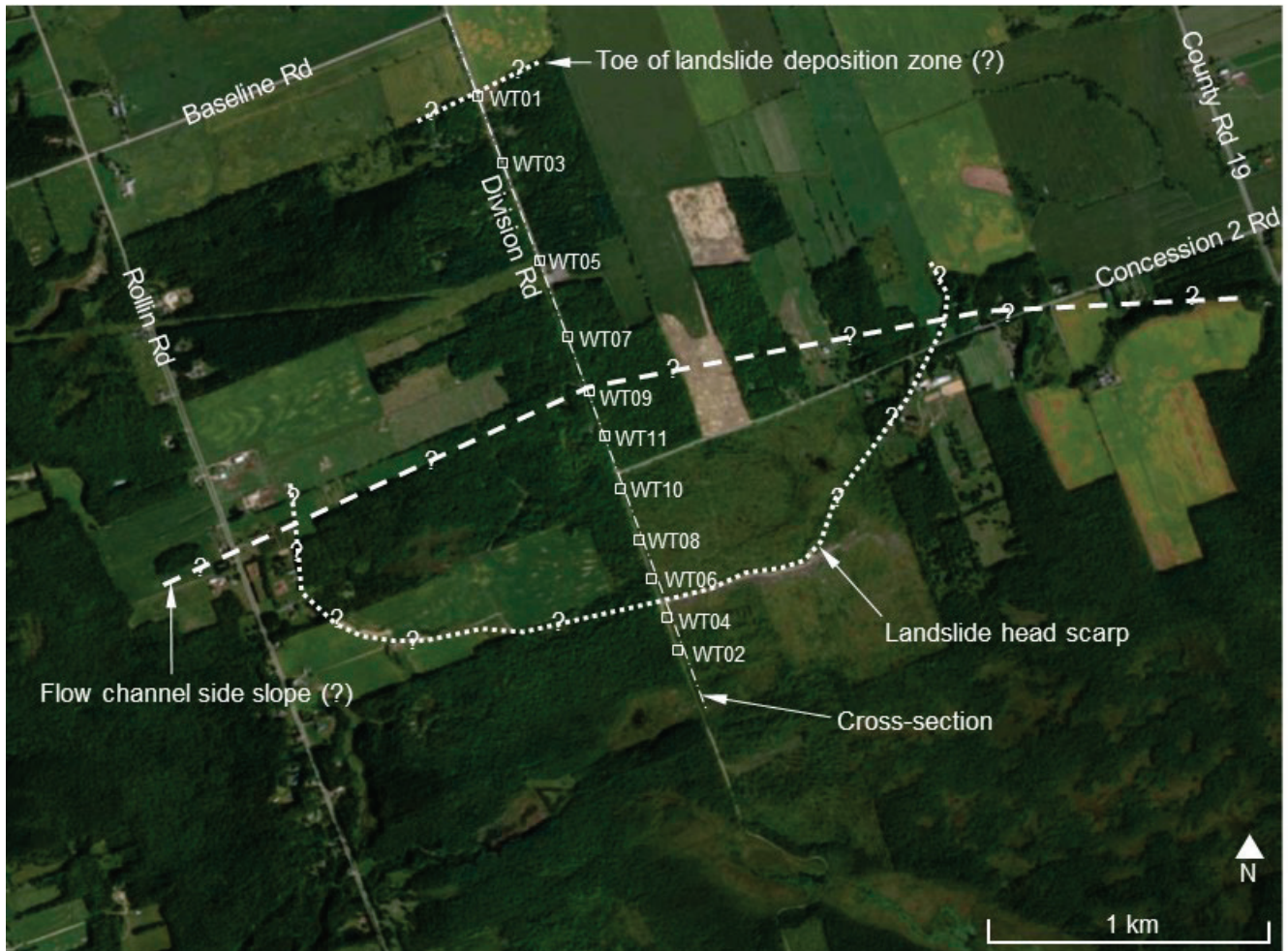


Fig. 14 Satellite image of Wendover landslide site and Tromino survey locations (Satellite image © Google Inc.)



Fig. 15 Photo of Division Road north of intersection with Concession 2 Road (taken from WT11 on July 10, 2018, facing north. See Fig. 14 for location)



Fig. 16 Photo of Division Road south of Concession 2 Road (taken from WT08 on July 10, 2018, facing south. See Fig. 14 for location. Note trees cut recently to the left of the road. Dark piles are cut wood branches. The red arrow points to a truck on the crest of the landslide head scarp for scale.)



Fig. 17 Photo of possible toe of landslide debris deposition zone (taken from WT01 on July 10, 2018, facing south. See Fig. 14 for location. Note road sloping up from where the photo is taken)

Table 3 Tromino survey results from Wendover landslide site

Location	Coordinates (UTM WGS 84)		Distance from Baseline Rd (m)	F_0 (Hz)	T_0 (Sec.)	Soil Thickness (m)
	Easting (m)	Northing (m)				
WT01	488297	5044308	312	2.13	0.47	25
WT03	488385	5044082	555	1.44	0.69	40
WT05	488515	5043729	931	1.44	0.69	40
WT07	488621	5043460	1220	1.44	0.69	40
WT09	488693	5043271	1422	1.34	0.75	43
WT11	488743	5043112	1589	1.34	0.75	43
WT10	488802	5042925	1784	1.31	0.76	44
WT08	488865	5042749	1971	1.25	0.80	47
WT06	488914	5042604	2124	1.22	0.82	48
WT04	488961	5042472	2265	1.09	0.92	55
WT02	489007	5042356	2389	1.03	0.97	58

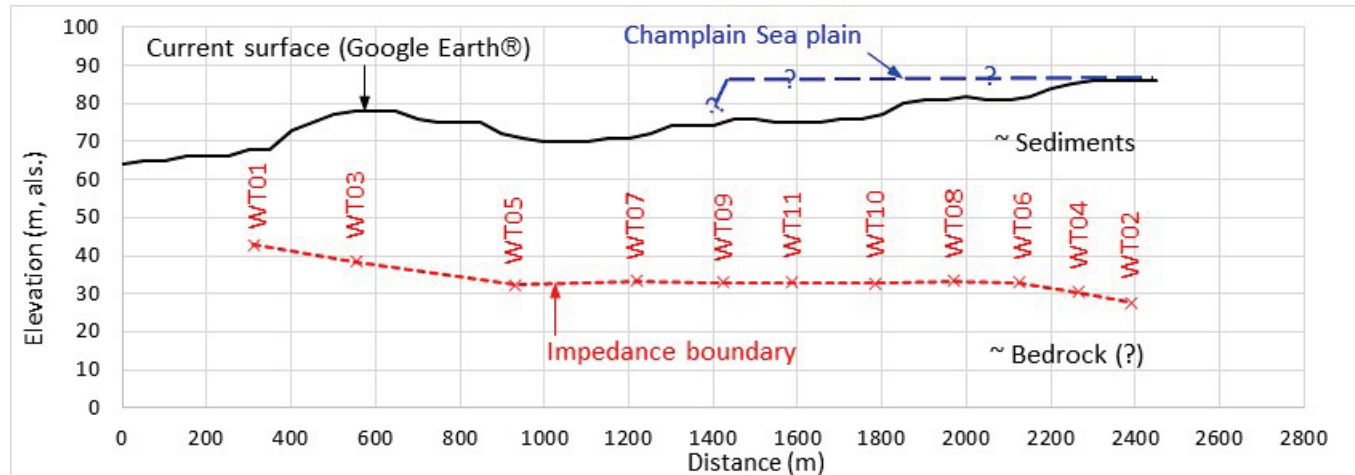


Fig. 18 Cross-sectional profile along Division Road, Wendover landslide site (see Fig. 14 for location. Surface elevation estimated from Google Earth®. Vertical exag.: 10x)

7. CONCLUSIONS

Three landslides at Cheney, Masson and Wendover were selected as candidate sites for potential geotechnical studies to investigate the earthquake that was previously hypothesized to have triggered the slope failures about 5200 cal yr BP. The landslides are relatively large, fairly distant from each other forming a regularly shaped triangle, and easy to access. Initial site investigations were conducted with passive seismic surveys at each site. These measurements allow depth estimates of stiffer materials (e.g. bedrock) overlain by soft materials like Champlain Sea sediments. The interpreted bedrock surfaces at Cheney and Masson sites are found to be irregular, with nominal thicknesses of the Champlain Sea sediments of about 30 m and 40 m, respectively. At the Wendover site, the interpreted bedrock surface is likely fairly even and in the range of around 50 m depth. Good impedance signals have been recorded at most locations surveyed. The data comprise a preliminary basis for planning of potential geotechnical drilling programs. Upon confirmation from borehole testing, the survey data may also help establish the sediment cross-sectional profiles for slope stability analysis. The results can then be used to estimate the threshold ground accelerations

required to trigger the landslides, which, in turn, can be used to calculate the epicenter and magnitude of the earthquake.

ACKNOWLEDGEMENTS

The author would like to thank James Hunter for access to two Tromino units that have been essential to the work, Greg Brooks for access to LiDAR data, and Alain Grenier for assistance in field works. He would also like to thank Barbara Dietiker for her kind review and comments on the manuscript.

REFERENCES

- Adams J (2011) Seismic hazard maps for the National Building Code of Canada. In: Proc. Symp. of the CSCE 2011 General Conference, Ottawa, 14-17 June 2011, pp JHS-1-1 to 9
- Alysworth JM, Lawrence DE, Guertin J (2000) Did two massive earthquakes in the Holocene induce widespread landsliding and near-surface deformation in part of the Ottawa Valley, Canada? *Geology* 28(10): 903-906
- Brooks GR (2015) Evidence of paleoseismicity within the West Quebec Seismic Zone, eastern Canada, from the age and morphology of sensitive clay landslides. Proc. 6th international INQUA Meeting on Paleoseismology, Active Tectonics and Archaeoseismology, 19-24 Apr. 2015, Pescina, Fucino Basin, Italy. pp 59-62
- Chandler VW and Lively RS (2016) Utility of the horizontal-to-vertical spectral ratio passive seismic method for estimating thickness of Quaternary sediments in Minnesota and adjacent parts of Wisconsin. *Interpretation*, 4(3) SH71-SH90.
- Crow H, Alpay S, Hinton M, Knight R, Oldenborger G, Percival JP, Pugin AJM, Pelchat P (2017) Geophysical, geotechnical, geochemical, and mineralogical datasets collected in Champlain Sea sediments in the Municipality of Pontiac, Quebec. Geological Survey of Canada, Open File 7881. 45 p. doi: 10.4095/301664
- Hassani B, Atkinson GM (2015) Referenced empirical ground-motion model for Eastern North America. *Seismological Research Letters* 86(2A):477-491
- Hunter JA, Crow H, Brooks GR, Pyne M, Lamontagne M, Pugin A, Pullan SE, Cartwright T, Douma M, Burns RA, Good RL, Motazedian D, Kaheshi-Banab K, Caron R, Kolaj M, Folahan I, Dixon L, Dion K, Duxbury A, Landriault A, Ter-Emmanuil V, Jones A, Plastow G, and Muir D (2010) Seismic site classification and site period mapping in the Ottawa area using geophysical methods, *Geol. Surv. Can., Open-File Rept.* 6273
- Keefer DK (1984) Landslides caused by earthquakes. *Geological Society of America Bulletin* 95:406-421
- Lane, JW, White, EA, Steele, GV and Cannia, JC (2008) Estimation of bedrock depth using the horizontal-to-vertical (H/V) ambient-noise seismic method, in Proceedings of the Symposium on the Application of Geophysics to Engineering and Environmental Problems: Environmental and Engineering Geophysical Society; Symposium on the Application of Geophysics to Engineering and Environmental Problems, Philadelphia, Pennsylvania, US, 6 April 2008, 13p.
- Micromed (2012) Tromino – Portable ultra-light acquisition system for seismic noise and vibrations, User's Manual. 139p.
- Nakamura Y (1989) A method for dynamic characteristics estimation of subsurface using microtremor on the ground surface. *Quarterly Report of Railway Technical Research Institute (RTRI)*, Japan, 30(1) 25-33.

- Rodríguez CE, Bommer JJ, Chandler RJ (1999) Earthquake-induced landslides: 1980–1997. *Soil Dynamics and Earthquake Engineering* 18:325-346
- Scheib AJ (2014) The application of passive seismic to estimate cover thickness in Greenfields areas of Western Australia – Method, data interpretation and recommendations. Geological Survey of Western Australia, Rocord 2014/9, 67p.
- SESAME (2004) Guidelines for the implementation of the H/V spectral ratio technique using ambient noise measurements, processing and interpretation, SESAME European Research Project WP12, Deliverable D23.12. 62p.
- Shahjouei A, Pezeshk S (2016) Alternative hybrid empirical ground-motion model for Central and Eastern North America using hybrid simulations and NGA-West2 models. *Bulletin of the Seismological Society of America* 106(2):734-754
- Smith, NRA, Reading, AM, Asten, MW and Funk, CW (2013), Constraining depth to basement for mineral exploration using microtremor: A demonstration study from remote inland Australia: *Geophysics* 78(5) B227–B242
- Wang B (2016) Local shaking intensity of an earthquake that triggered Quyon Valley landslide 1020 cal yr BP. Proc. 69th Canadian Geotechnical Conference, Vancouver, 2-5 Oct. 2016
- Wang, B (2019) Failure mechanism of an ancient sensitive clay landslide in eastern Canada. *Landslides* 16(8):1483-1495
- Yenier E, Atkinson GM (2015) Regionally adjustable generic ground-motion prediction equation based on equivalent point-source simulations: Application to Central and Eastern North America. *Bulletin of the Seismological Society of America* 105(4):1989-2009

Appendix A

Charts of Tromino Measurements from Cheney Landslide Site

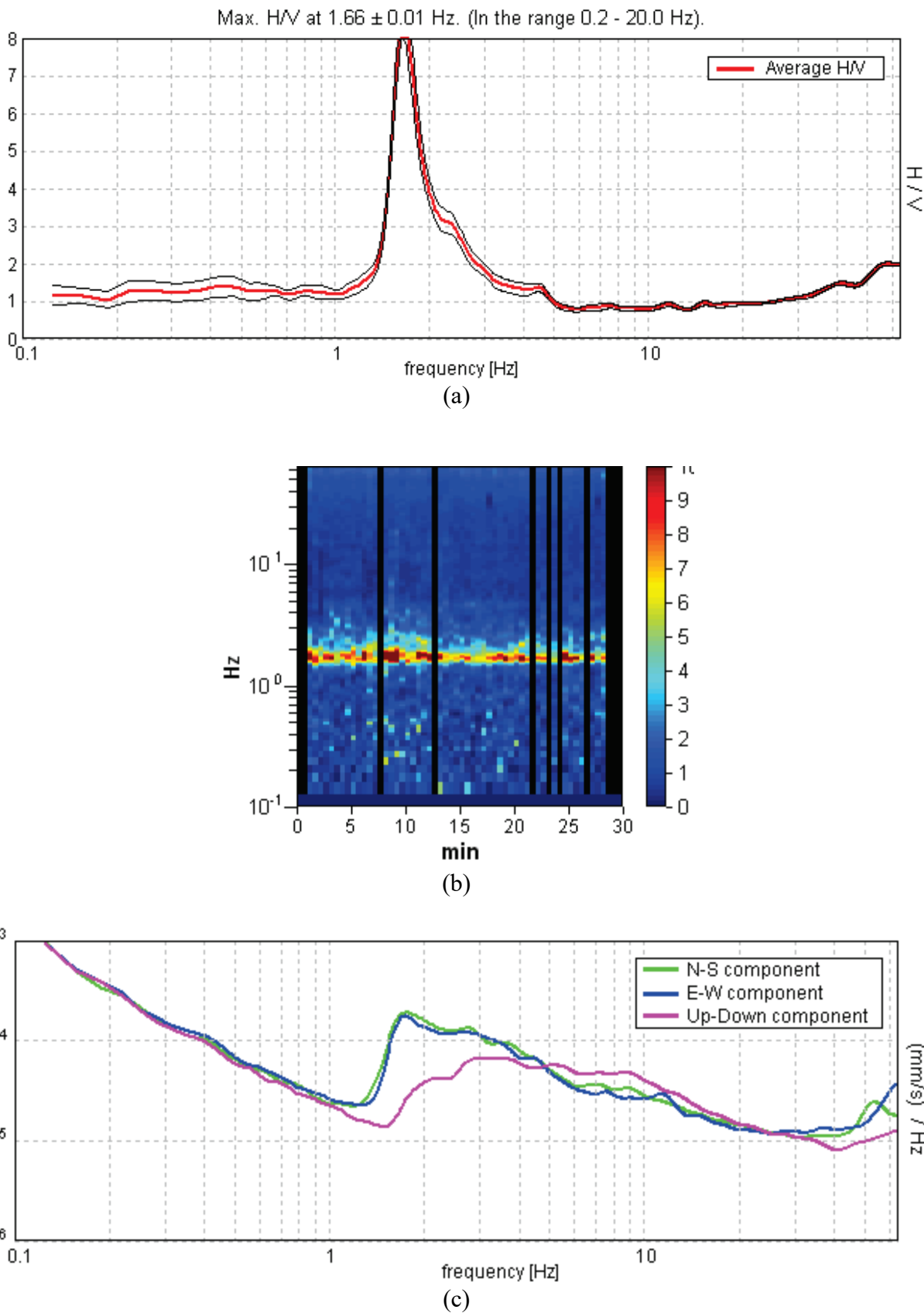


Fig. A-01 Tromino results at Cheney landslide site CT01. (a) HVSR; (b) Spectral windows; (c) Horizontal and vertical average spectra for all windows used.

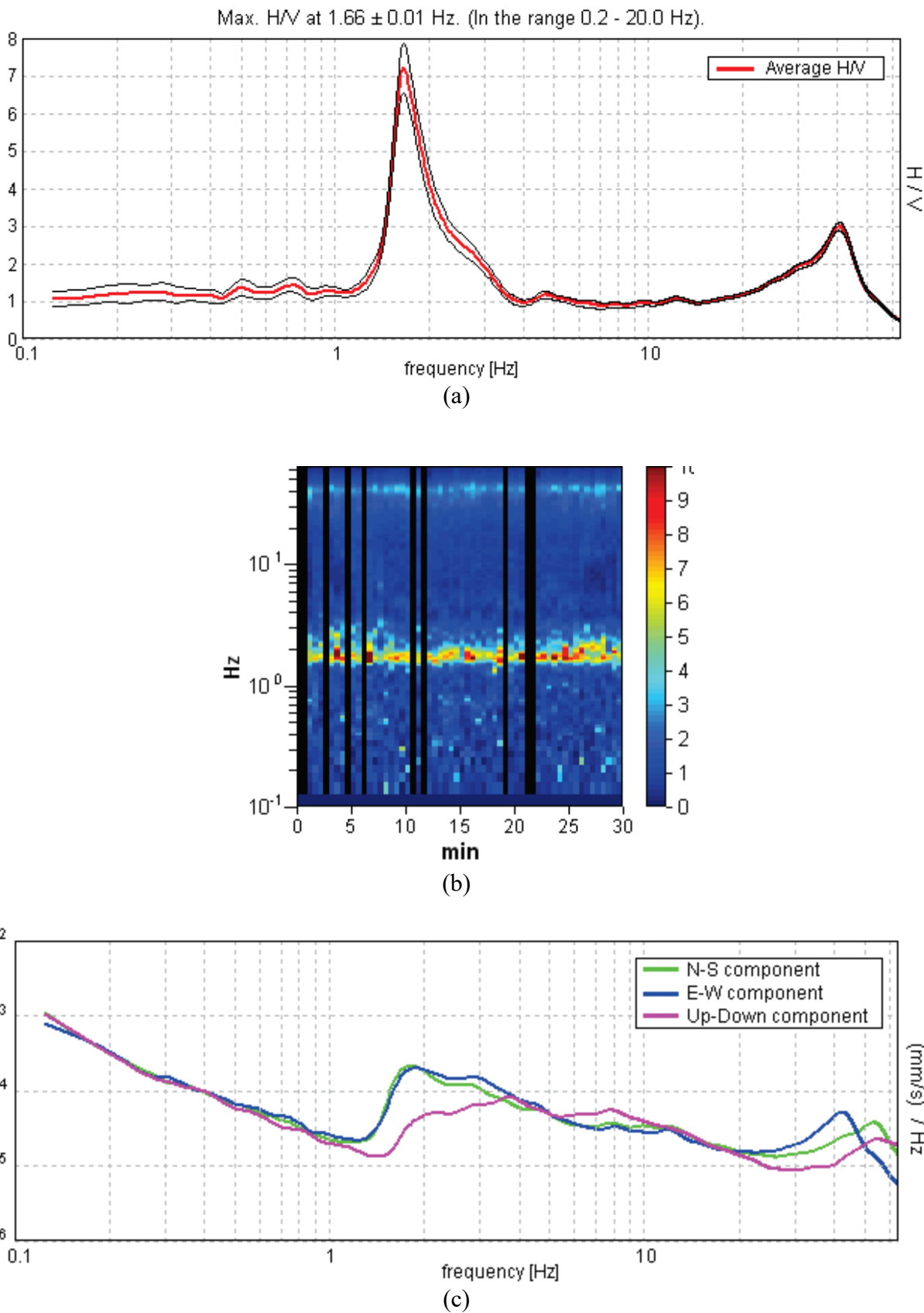


Fig. A-02 Tromino results at Cheney landslide site CT02. (a) HVSR; (b) Spectral windows; (c) Horizontal and vertical average spectra for all windows used.

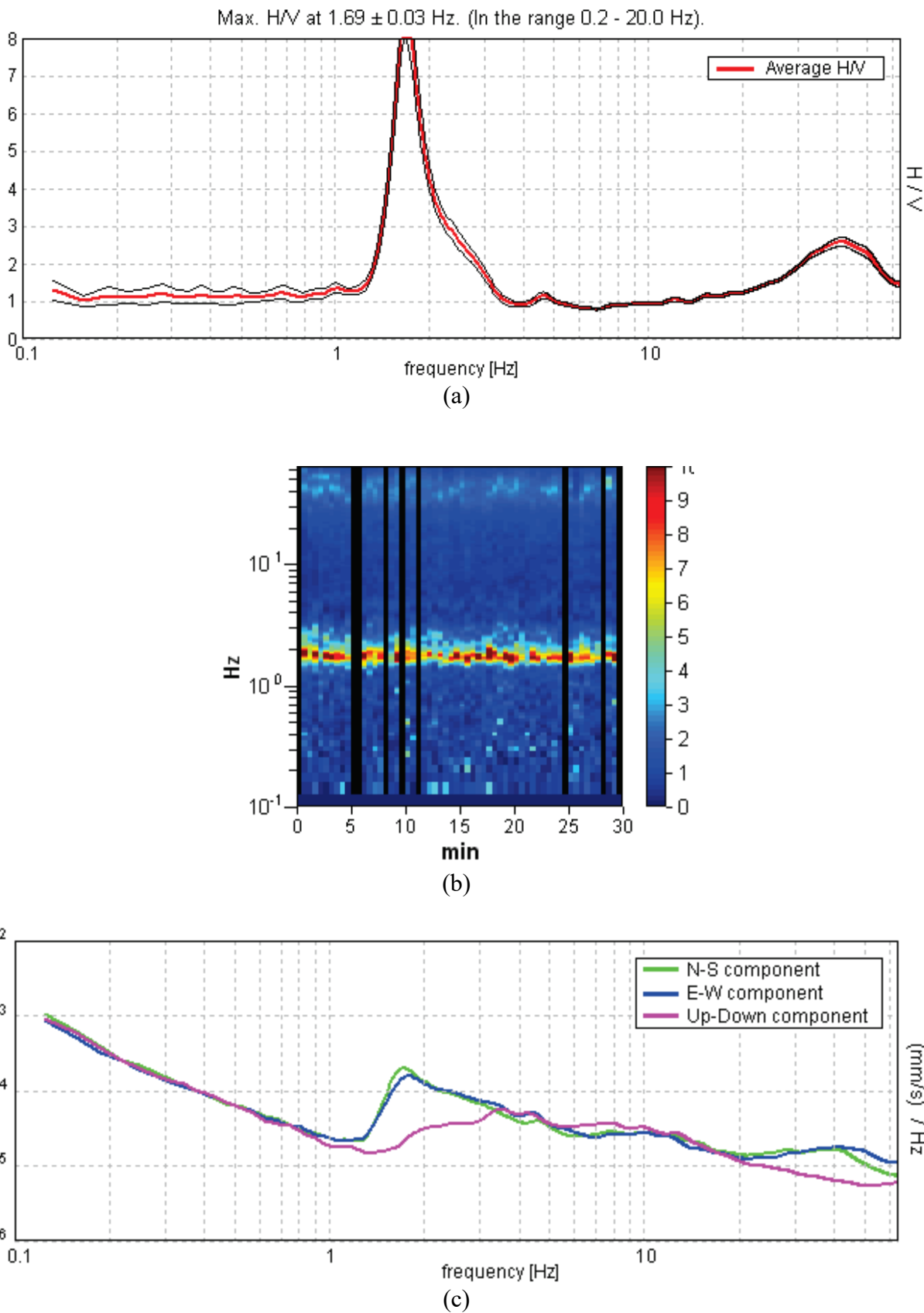


Fig. A-03 Tromino results at Cheney landslide site CT03. (a) HVSR; (b) Spectral windows; (c) Horizontal and vertical average spectra for all windows used.

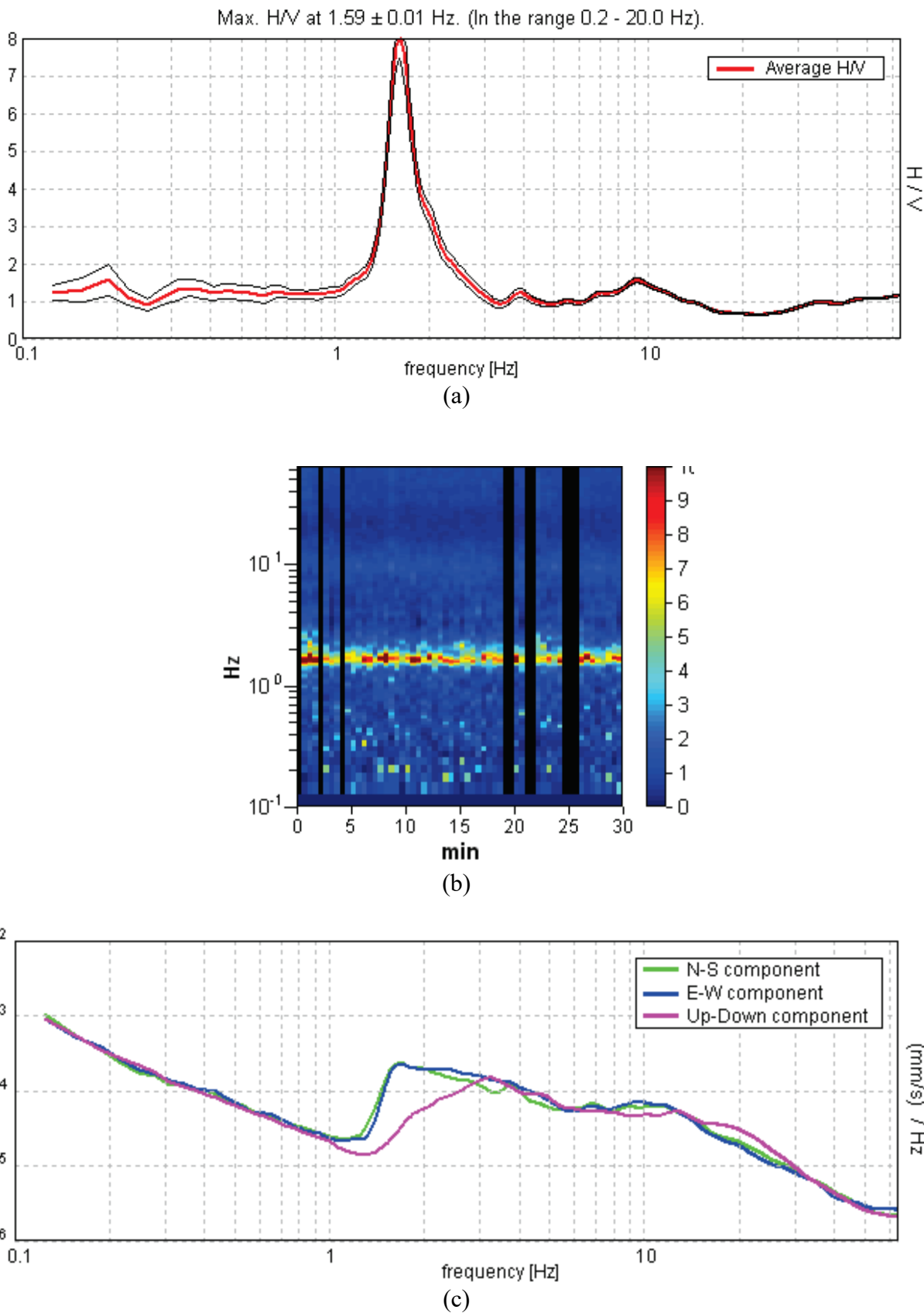


Fig. A-04 Tromino results at Cheney landslide site CT04. (a) HVSR; (b) Spectral windows; (c) Horizontal and vertical average spectra for all windows used.

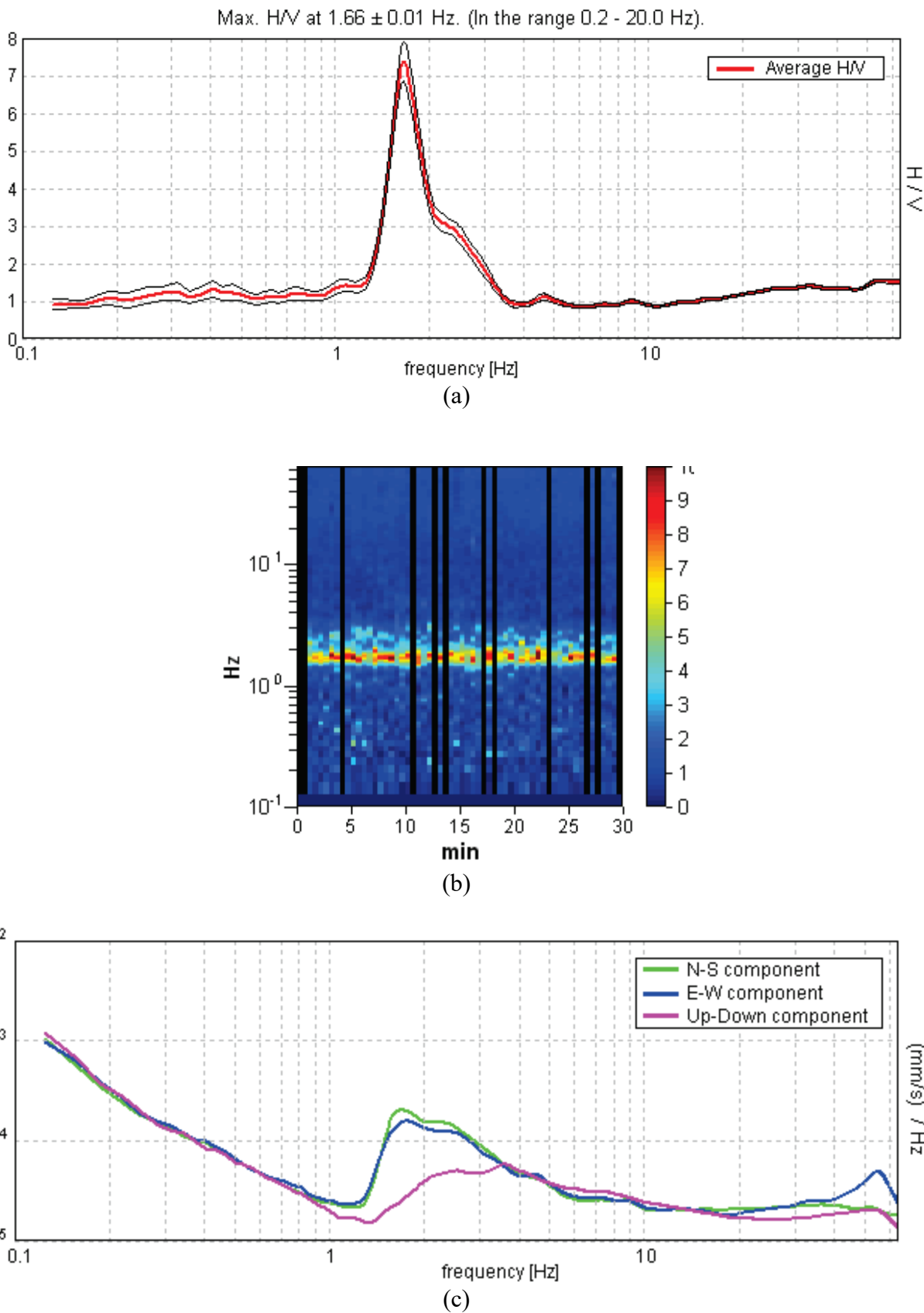


Fig. A-05 Tromino results at Cheney landslide site CT05. (a) HVSR; (b) Spectral windows; (c) Horizontal and vertical average spectra for all windows used.

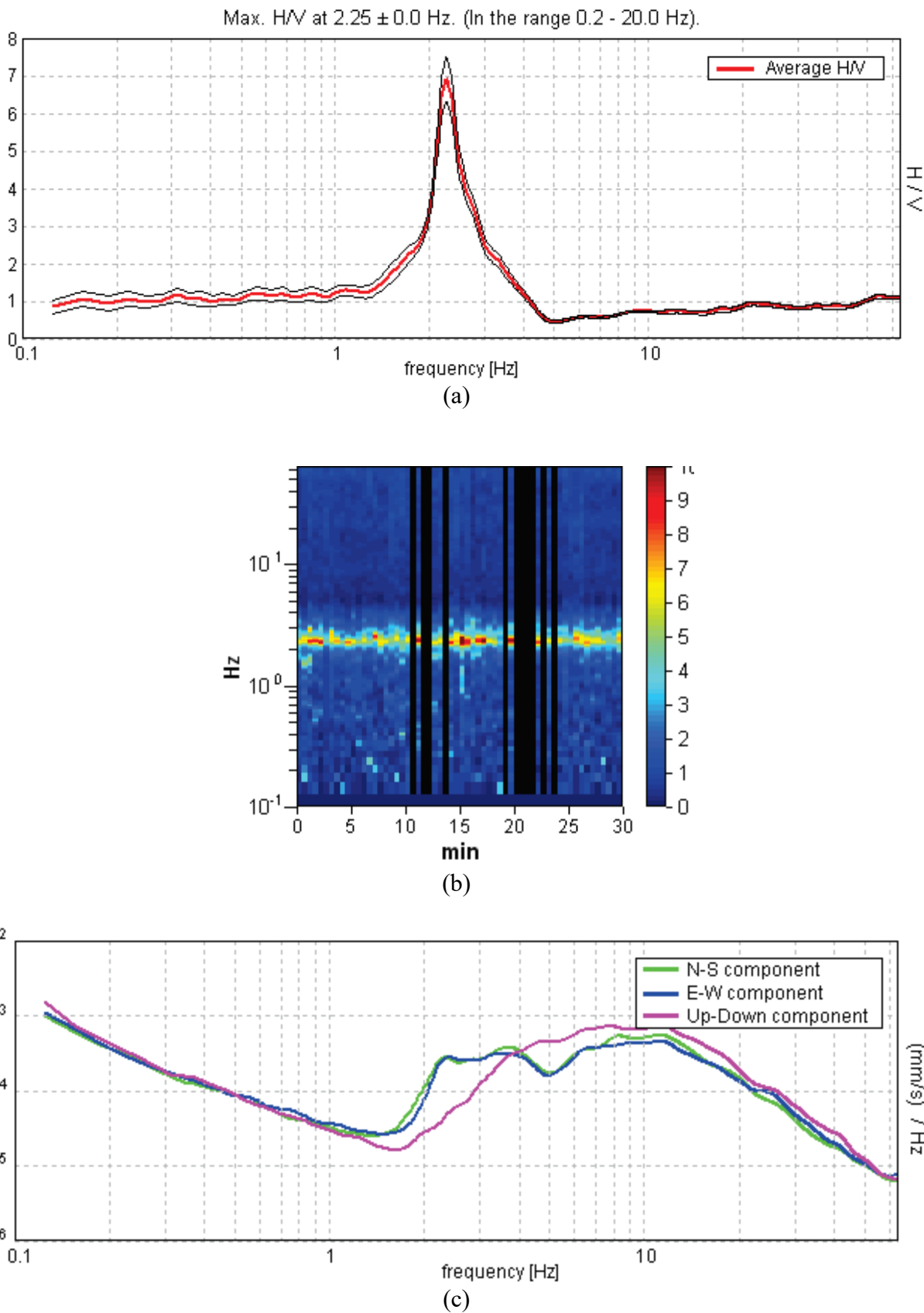


Fig. A-06 Tromino results at Cheney landslide site CT06. (a) HVSR; (b) Spectral windows; (c) Horizontal and vertical average spectra for all windows used.

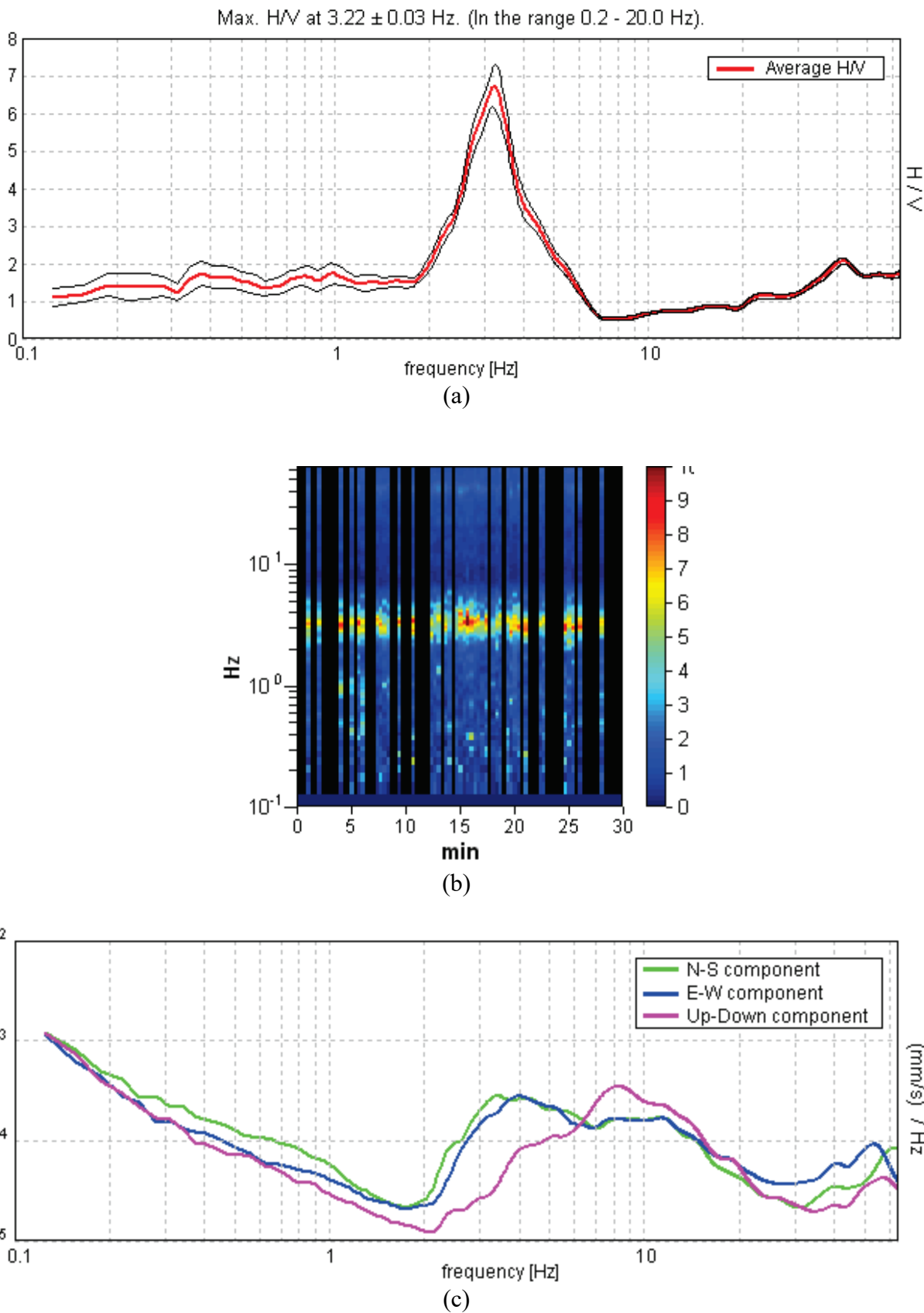


Fig. A-07 Tromino results at Cheney landslide site CT07. (a) HVSR; (b) Spectral windows; (c) Horizontal and vertical average spectra for all windows used.

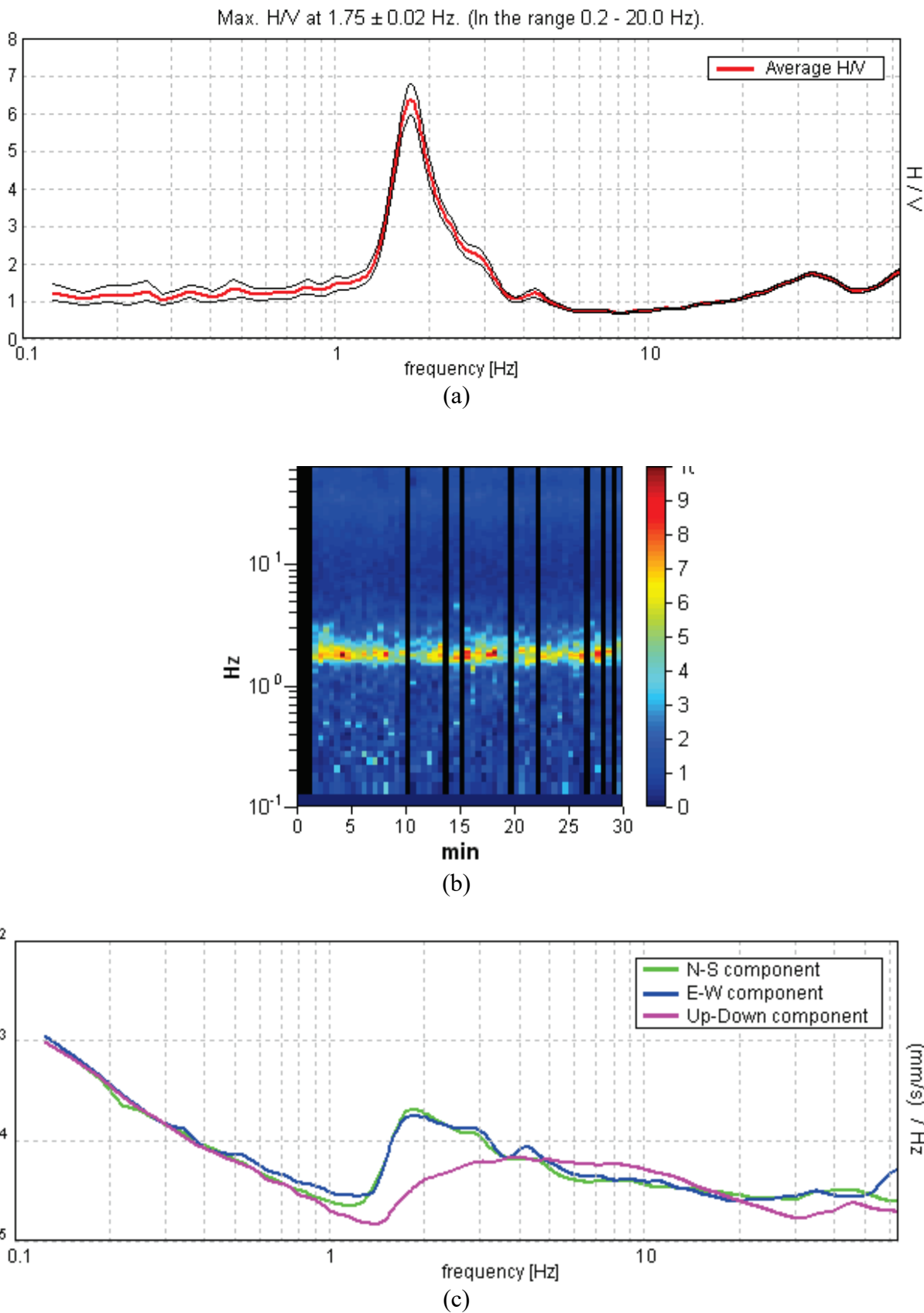


Fig. A-08 Tromino results at Cheney landslide site CT08. (a) HVSR; (b) Spectral windows; (c) Horizontal and vertical average spectra for all windows used.

Max. H/V at 3.78 ± 0.1 Hz. (In the range 0.2 - 20.0 Hz).

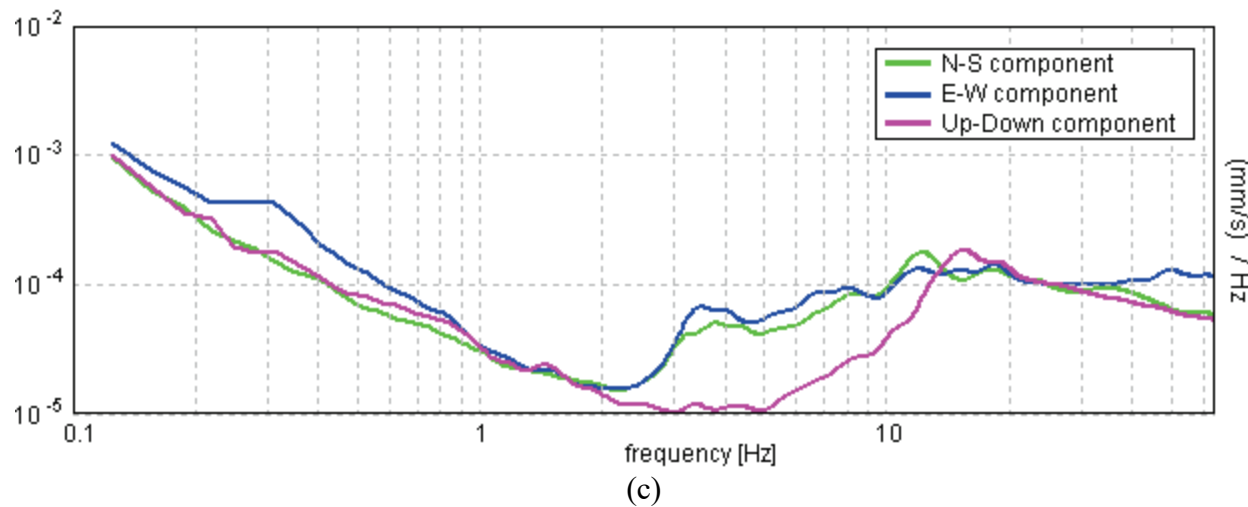
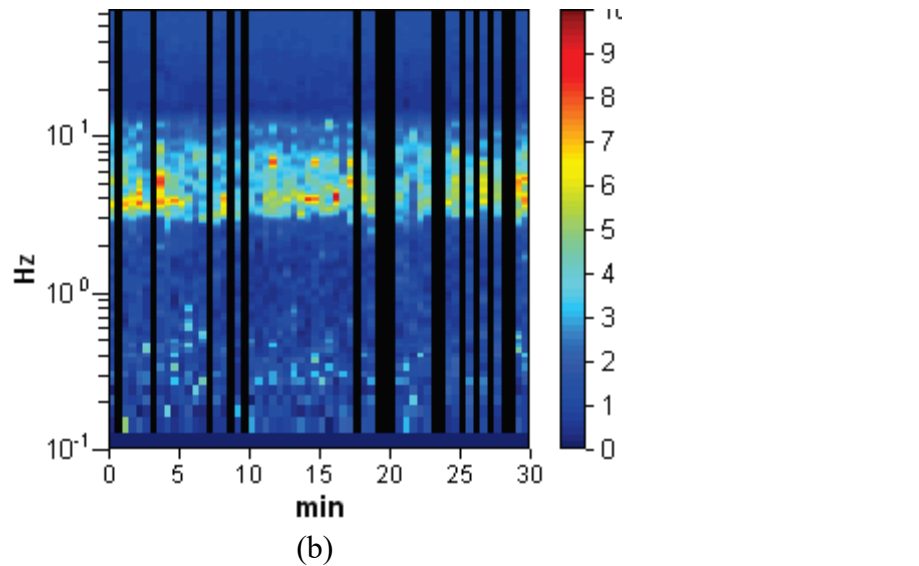
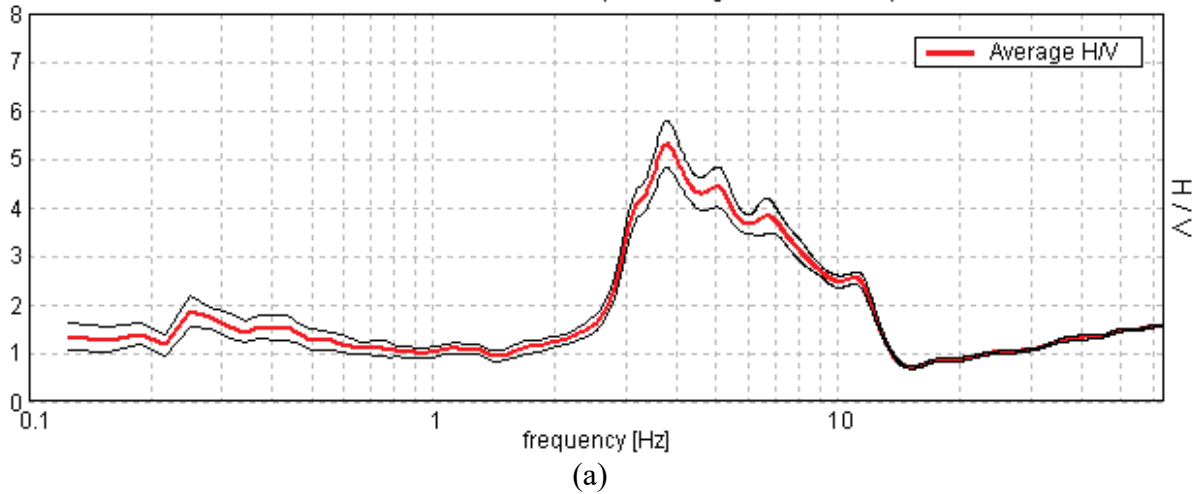


Fig. A-09 Tromino results at Cheney landslide site CT09. (a) HVSR; (b) Spectral windows; (c) Horizontal and vertical average spectra for all windows used.

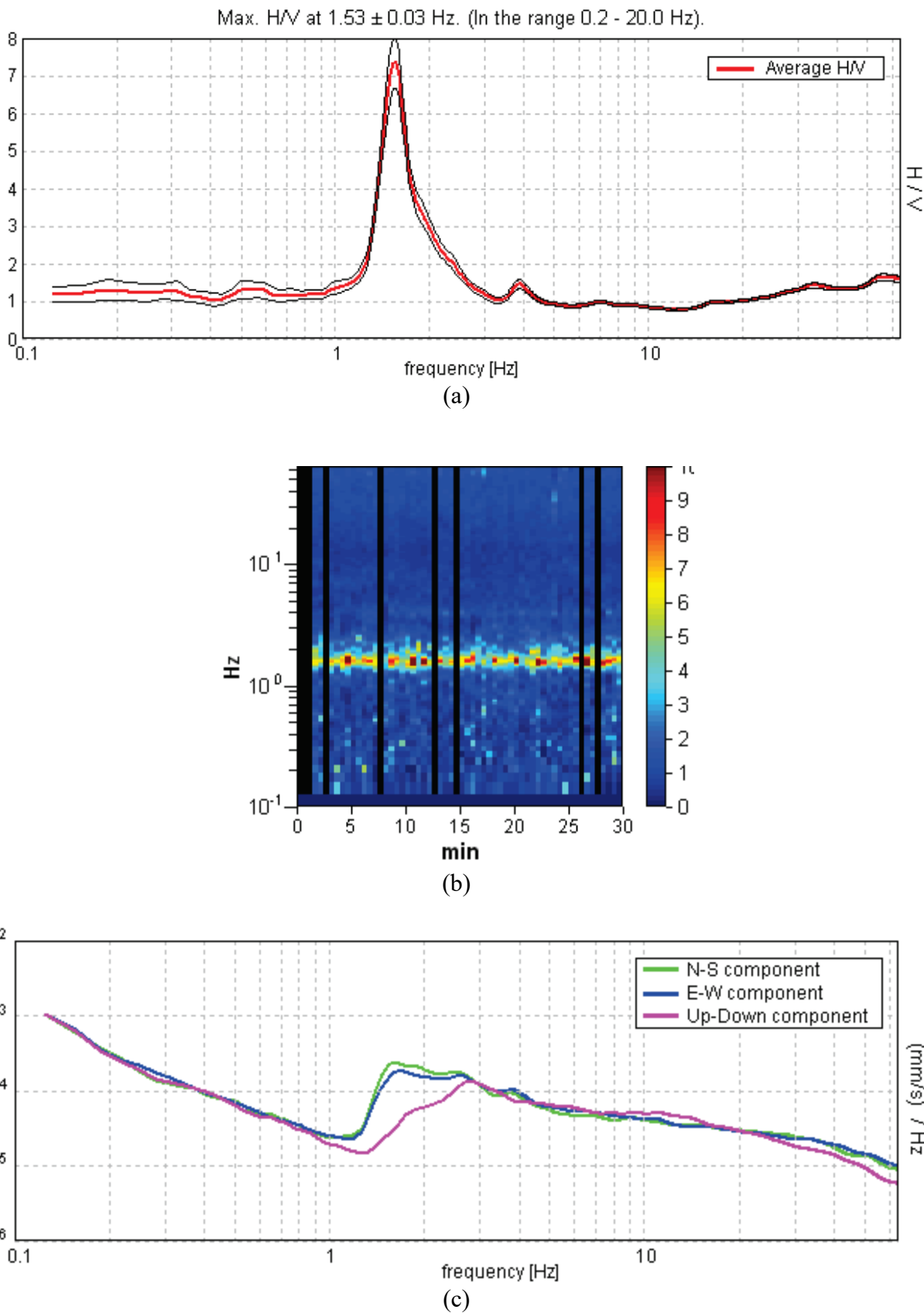


Fig. A-10 Tromino results at Cheney landslide site CT10. (a) HVSR; (b) Spectral windows; (c) Horizontal and vertical average spectra for all windows used.

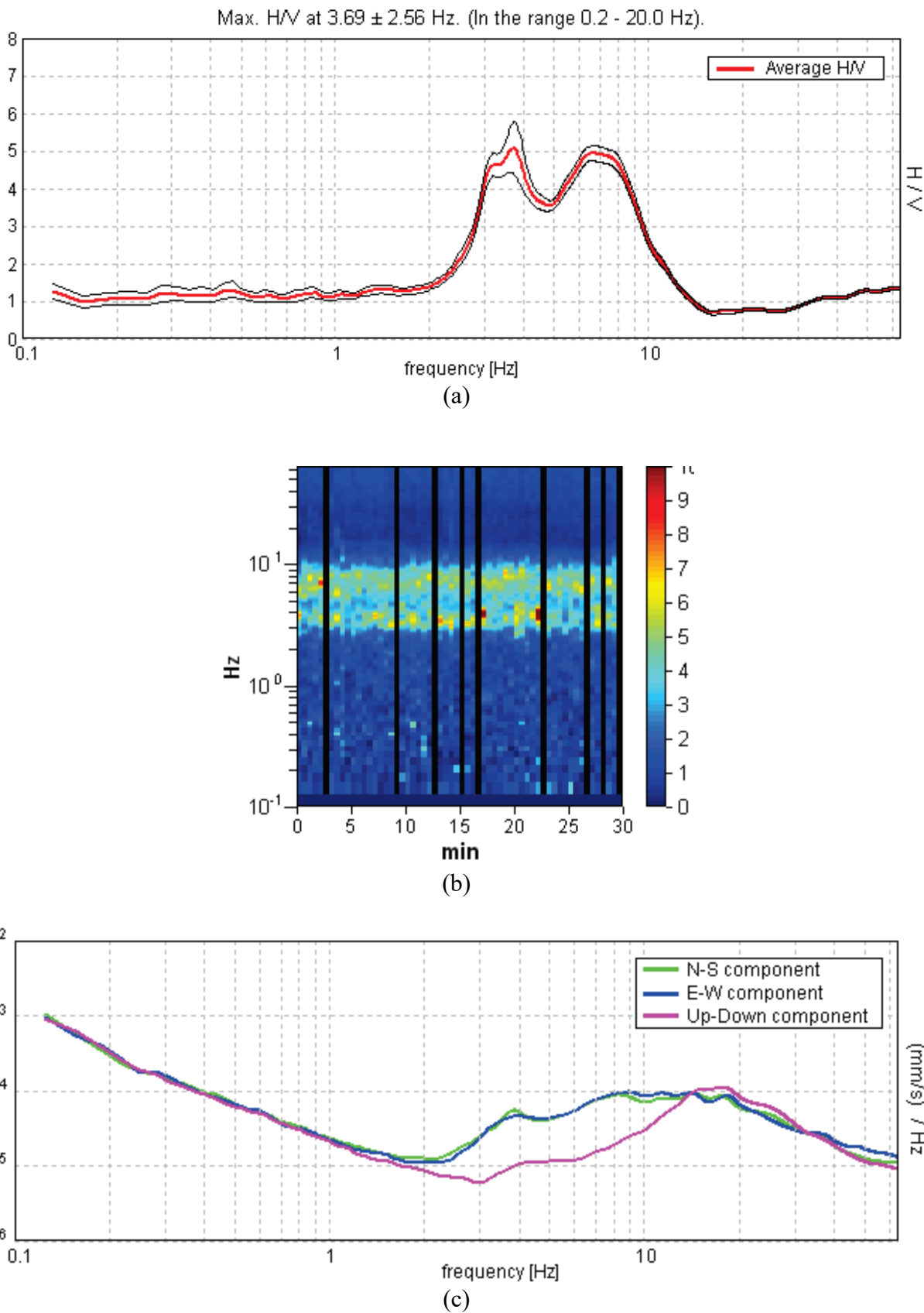


Fig. A-11 Tromino results at Cheney landslide site CT11. (a) HVSR; (b) Spectral windows; (c) Horizontal and vertical average spectra for all windows used.

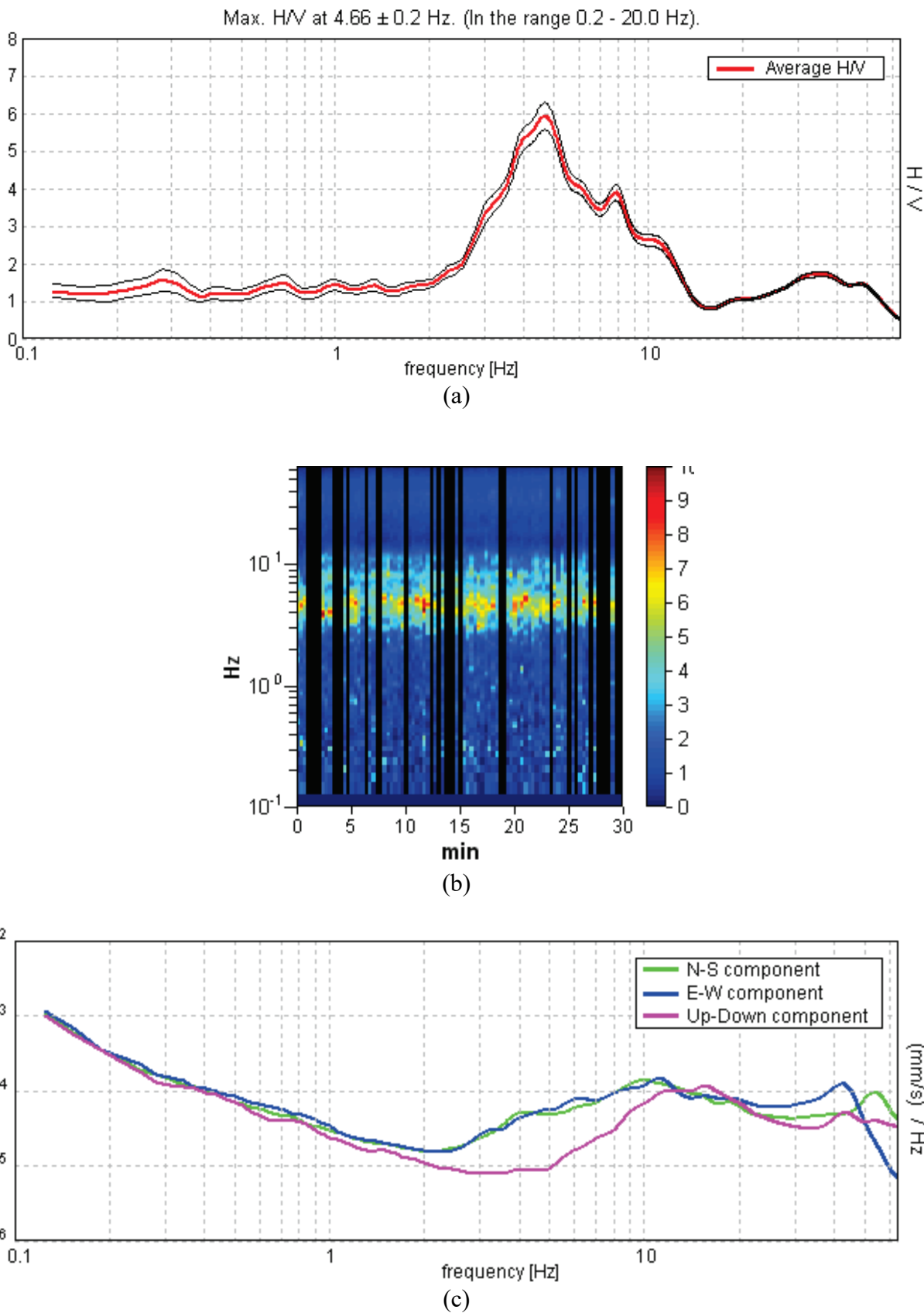


Fig. A-12 Tromino results at Cheney landslide site CT12. (a) HVSR; (b) Spectral windows; (c) Horizontal and vertical average spectra for all windows used.

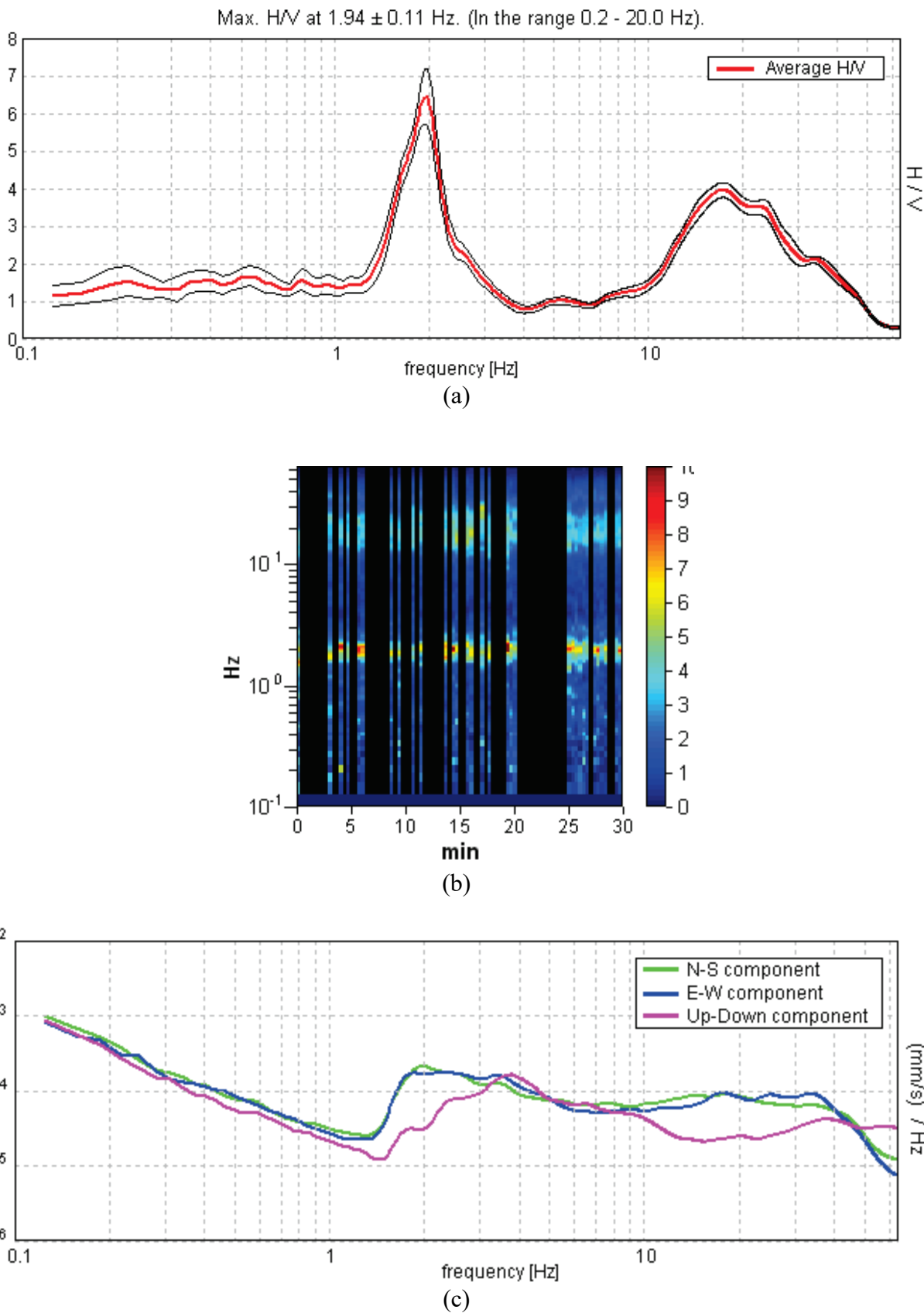


Fig. A-13 Tromino results at Cheney landslide site CT13. (a) HVSR; (b) Spectral windows; (c) Horizontal and vertical average spectra for all windows used.

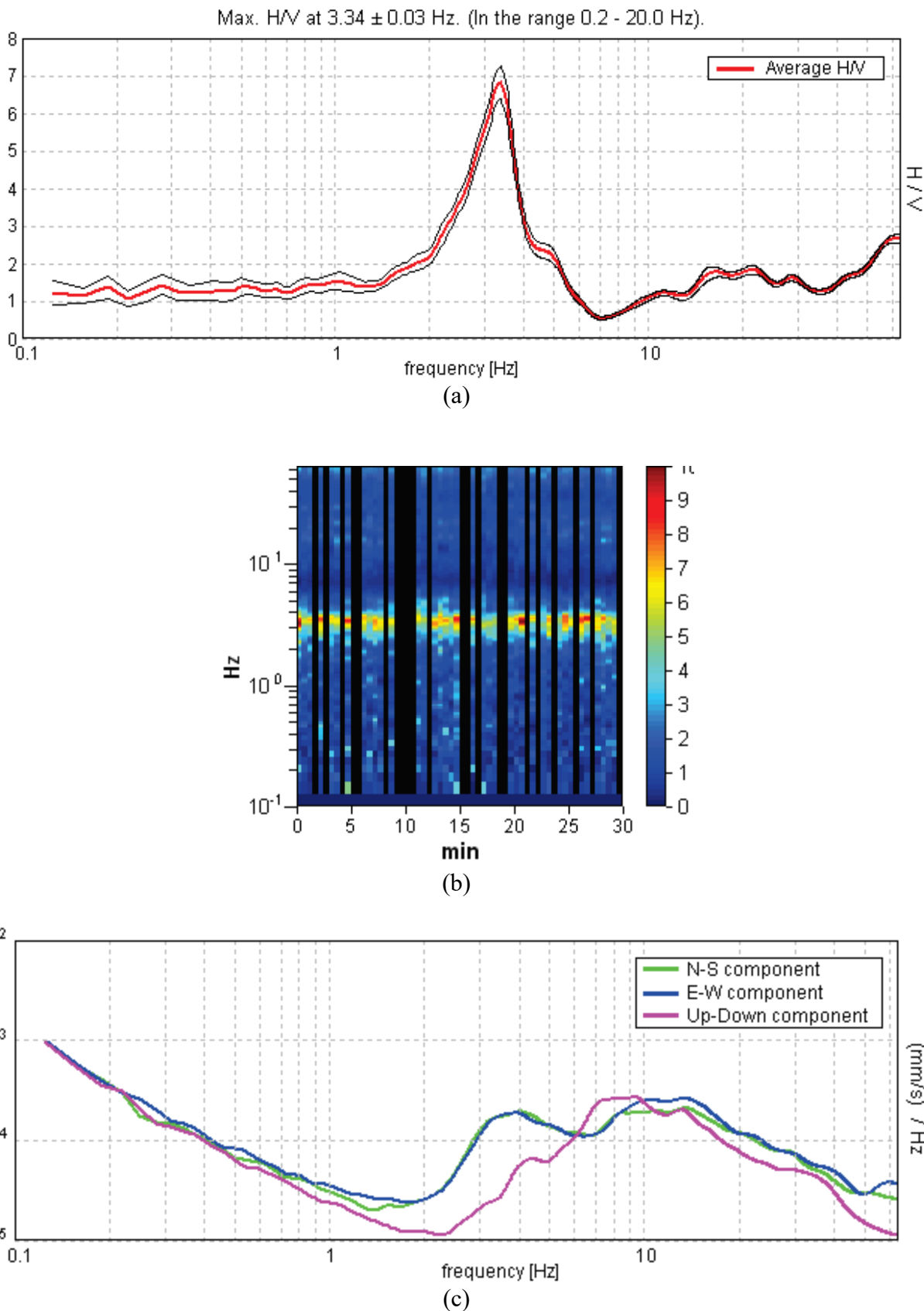


Fig. A-14 Tromino results at Cheney landslide site CT14. (a) HVSR; (b) Spectral windows; (c) Horizontal and vertical average spectra for all windows used.

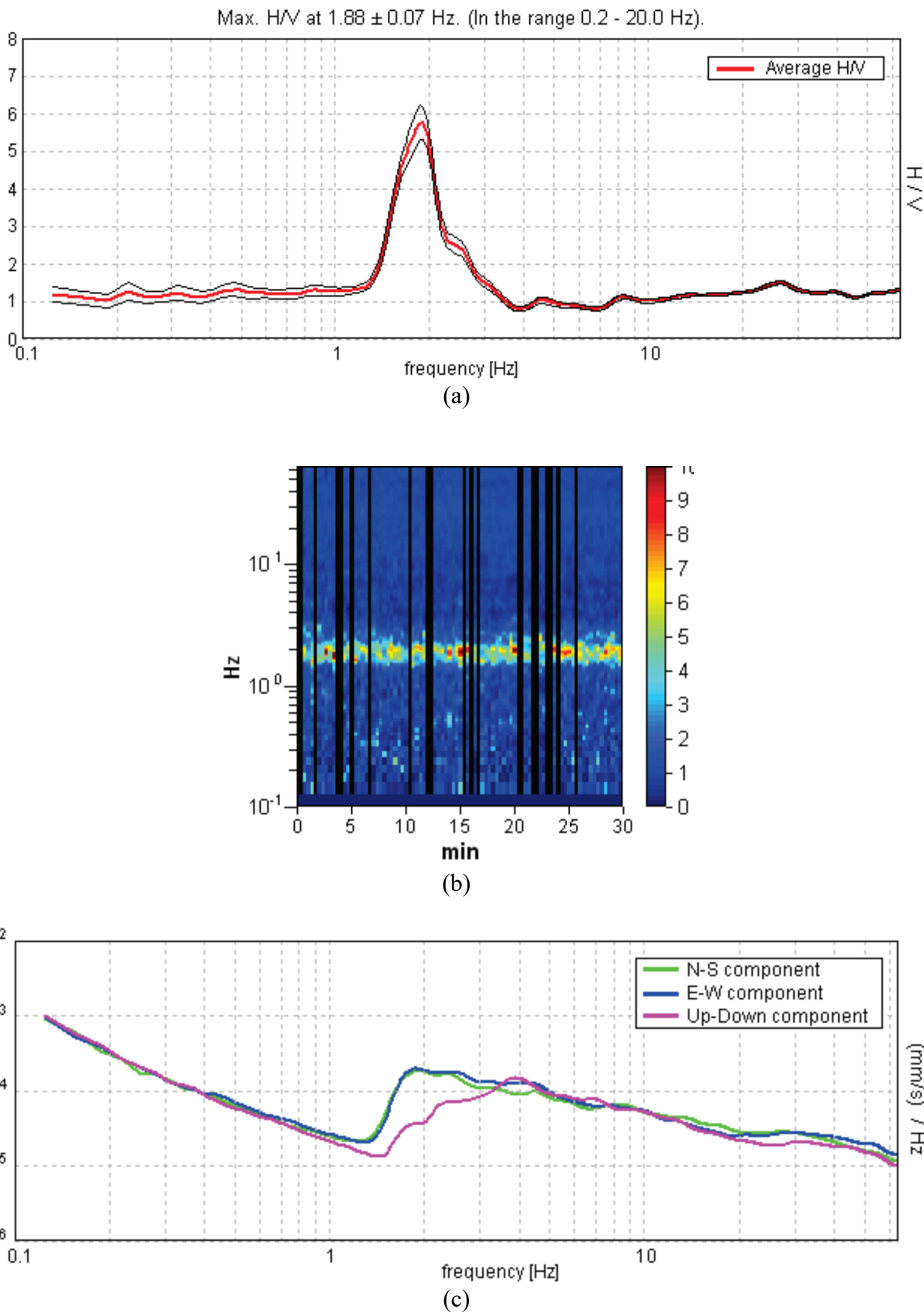


Fig. A-15 Tromino results at Cheney landslide site CT15. (a) HVSR; (b) Spectral windows; (c) Horizontal and vertical average spectra for all windows used.

Appendix B

Charts of Tromino Measurements from Masson Landslide Site

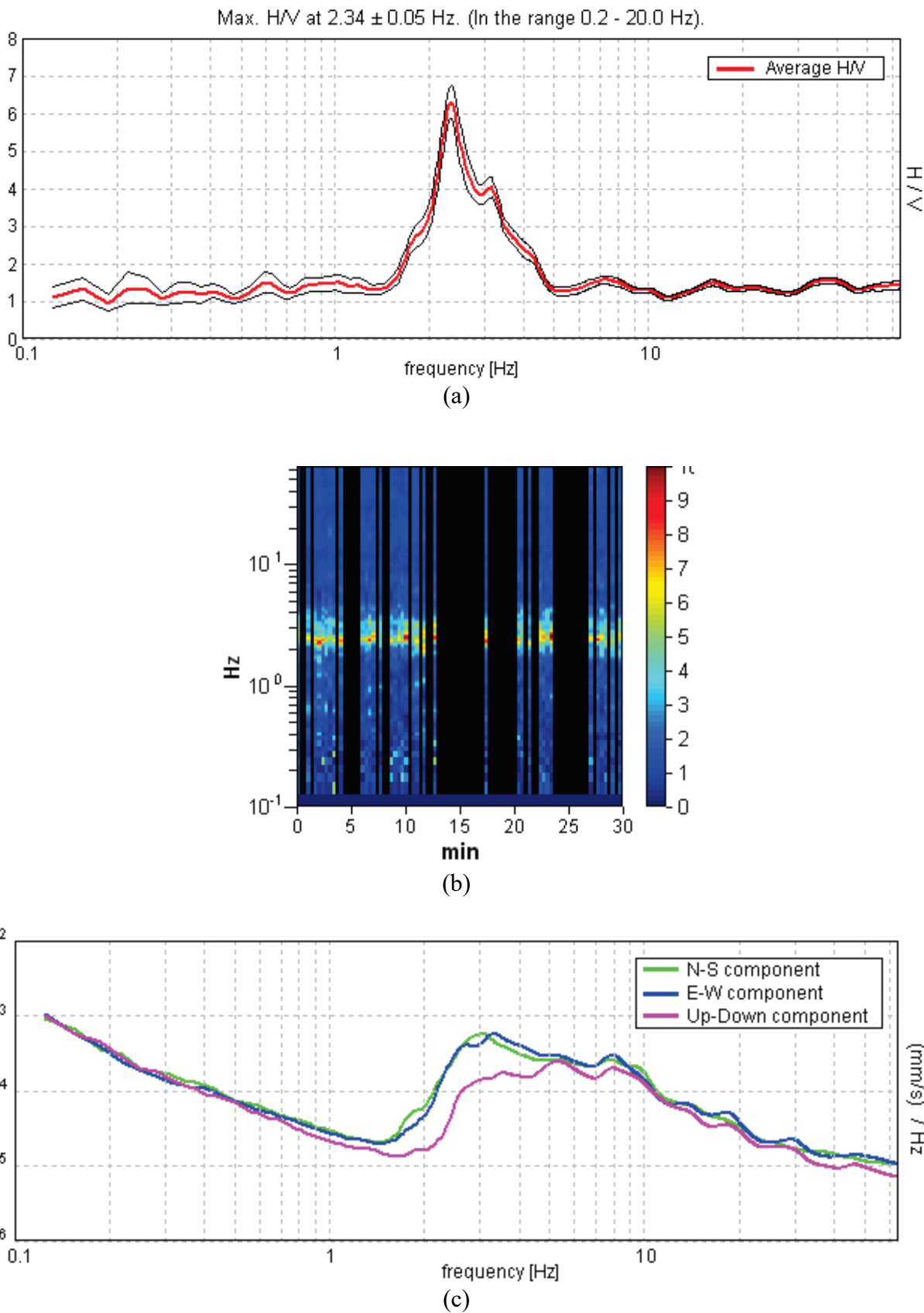


Fig. B-01 Tromino results at Masson landslide site MT01. (a) HVSR; (b) Spectral windows; (c) Horizontal and vertical average spectra for all windows used.

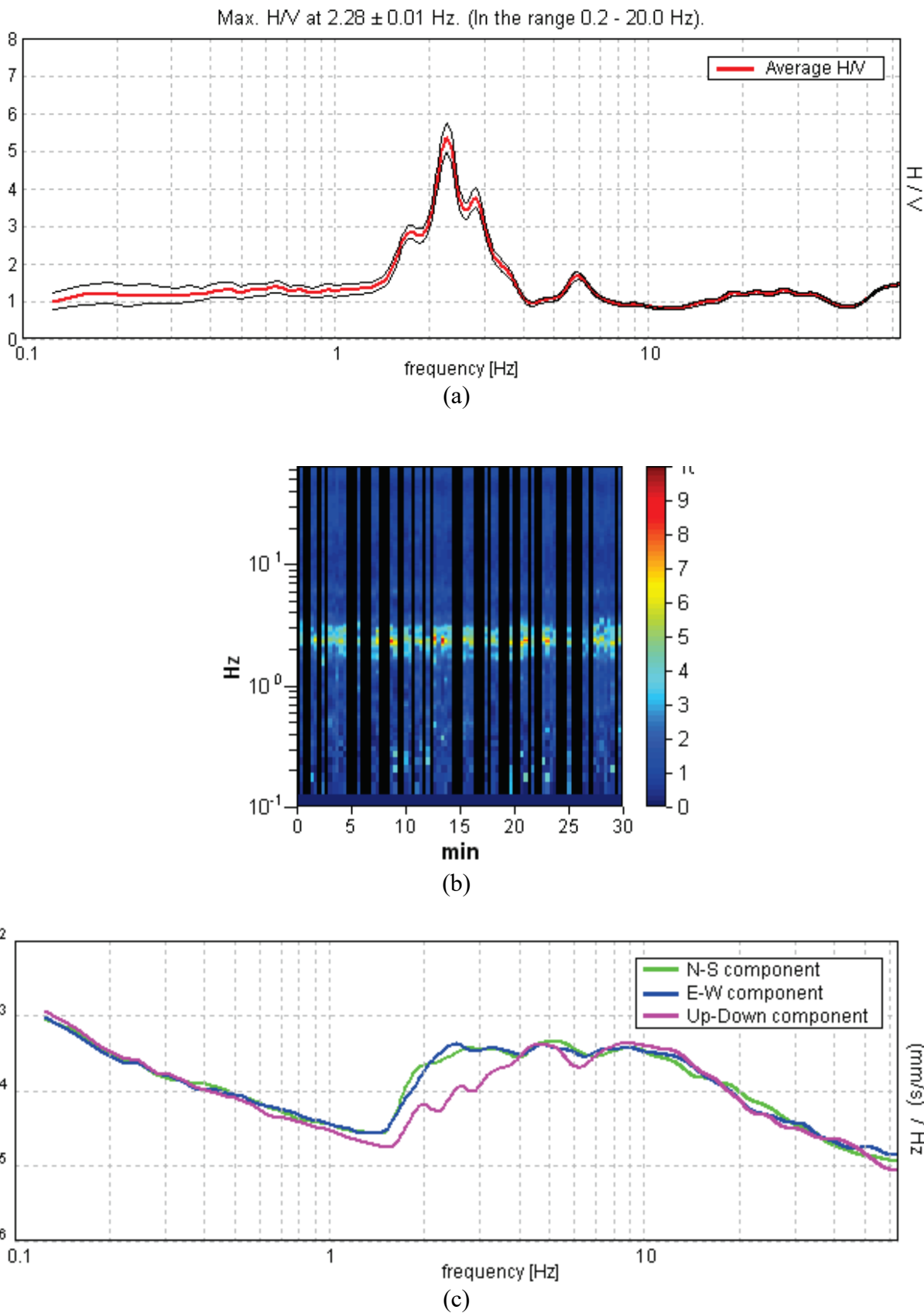


Fig. B-02 Tromino results at Masson landslide site MT02. (a) HVSR; (b) Spectral windows; (c) Horizontal and vertical average spectra for all windows used.

Max. H/V at 2.0 ± 0.03 Hz. (In the range 0.2 - 20.0 Hz).

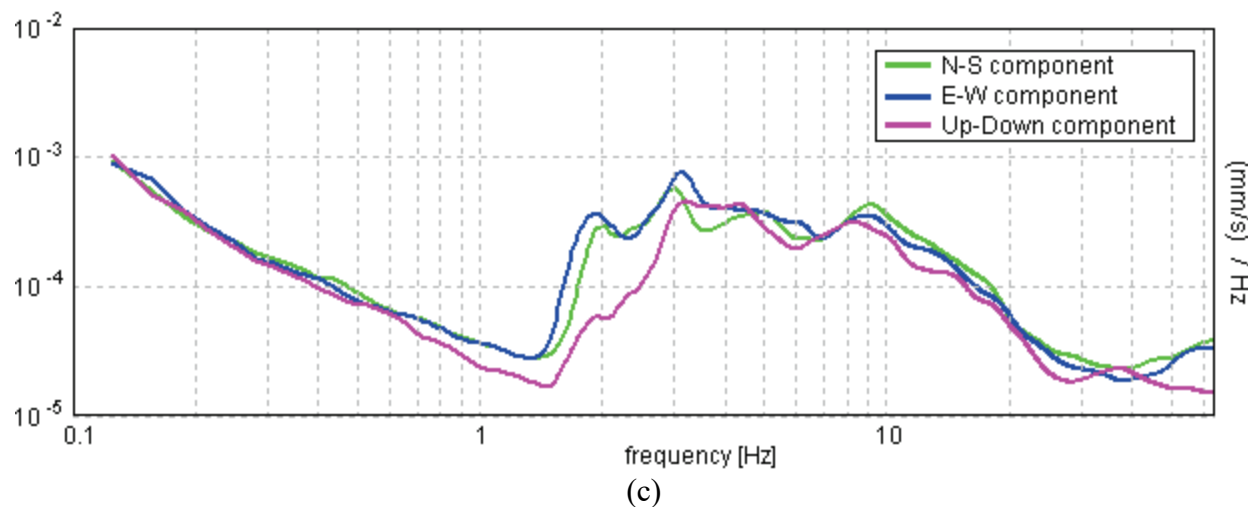
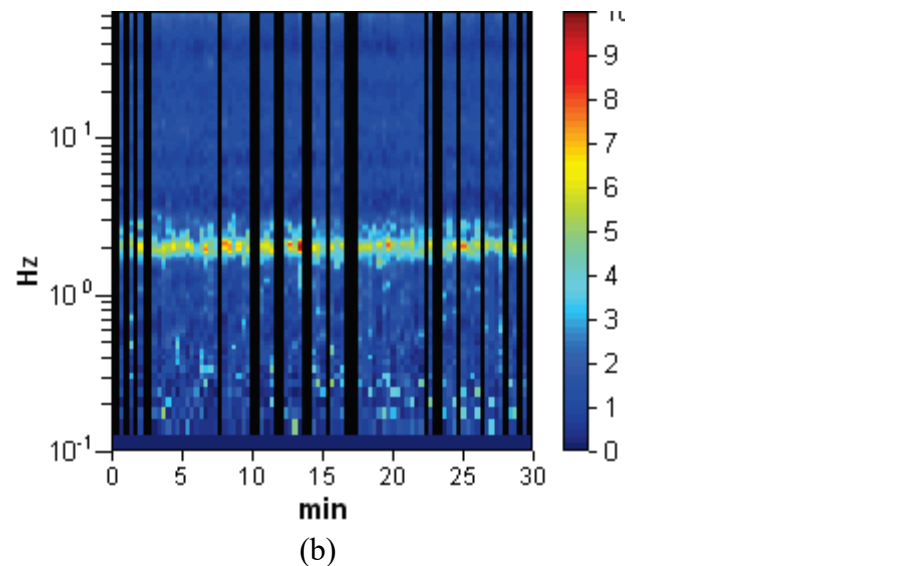
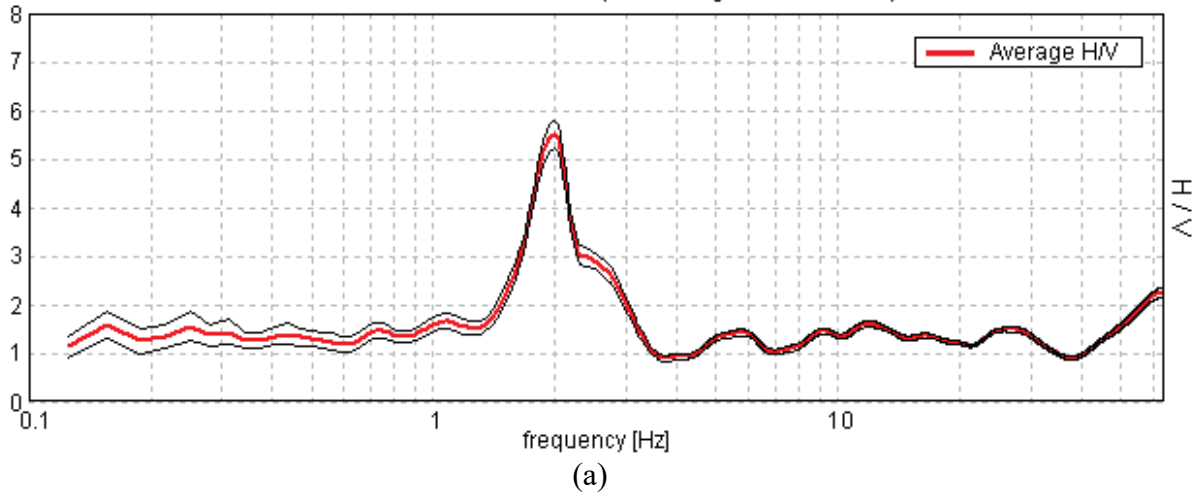


Fig. B-03 Tromino results at Masson landslide site MT03. (a) HVSR; (b) Spectral windows; (c) Horizontal and vertical average spectra for all windows used.

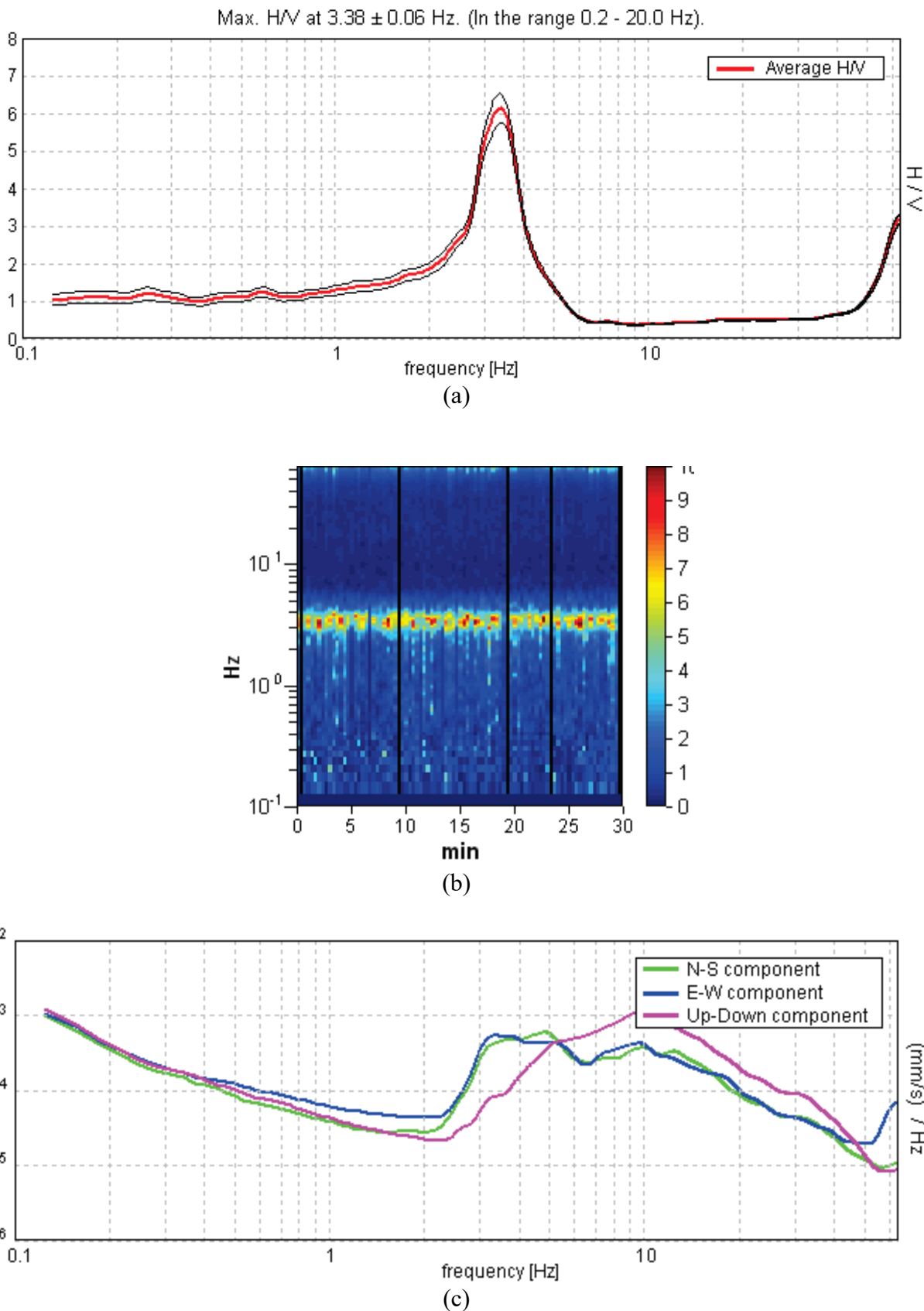


Fig. B-04 Tromino results at Masson landslide site MT04. (a) HVSR; (b) Spectral windows; (c) Horizontal and vertical average spectra for all windows used.

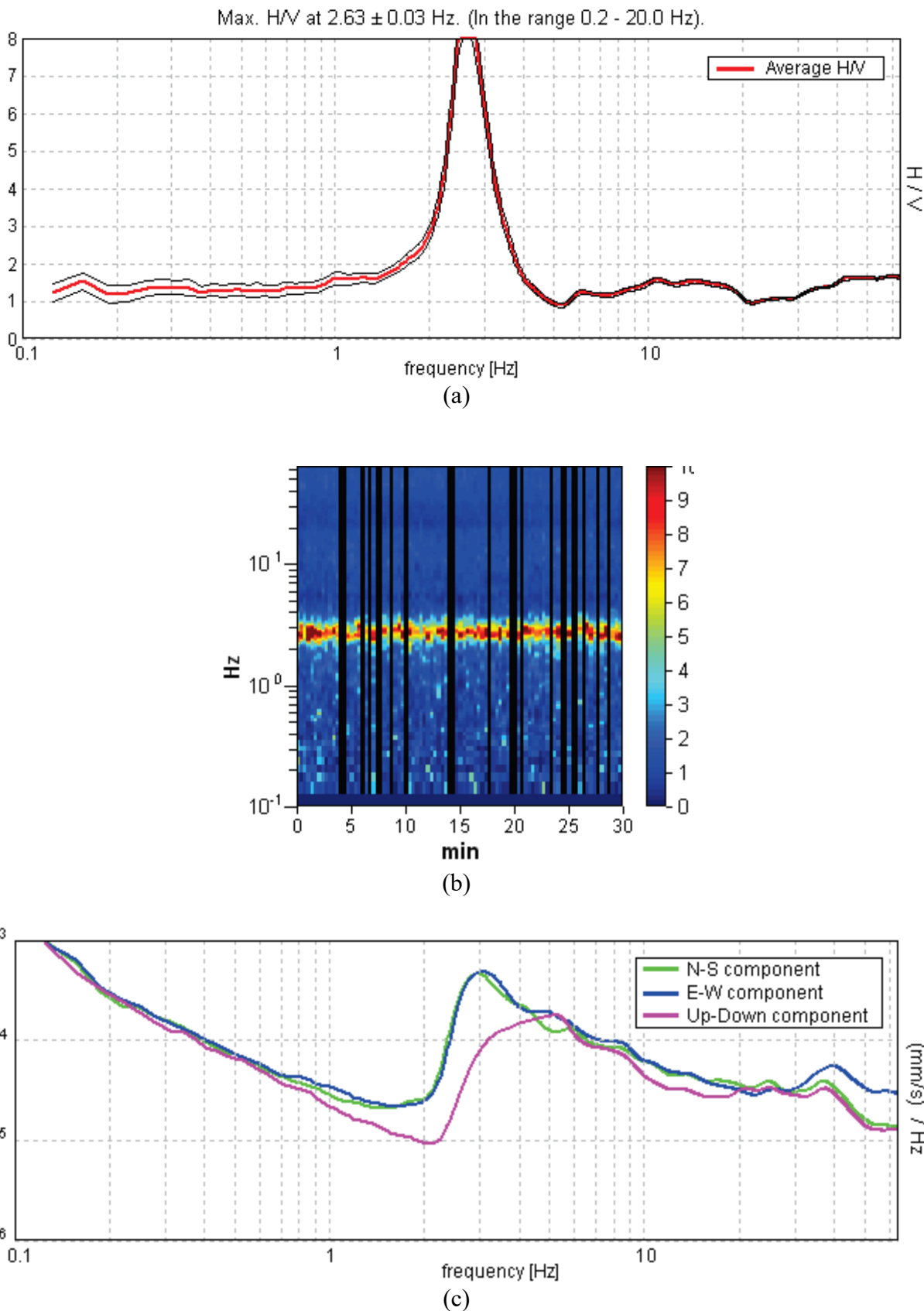


Fig. B-05 Tromino results at Masson landslide site MT05. (a) HVSR; (b) Spectral windows; (c) Horizontal and vertical average spectra for all windows used.

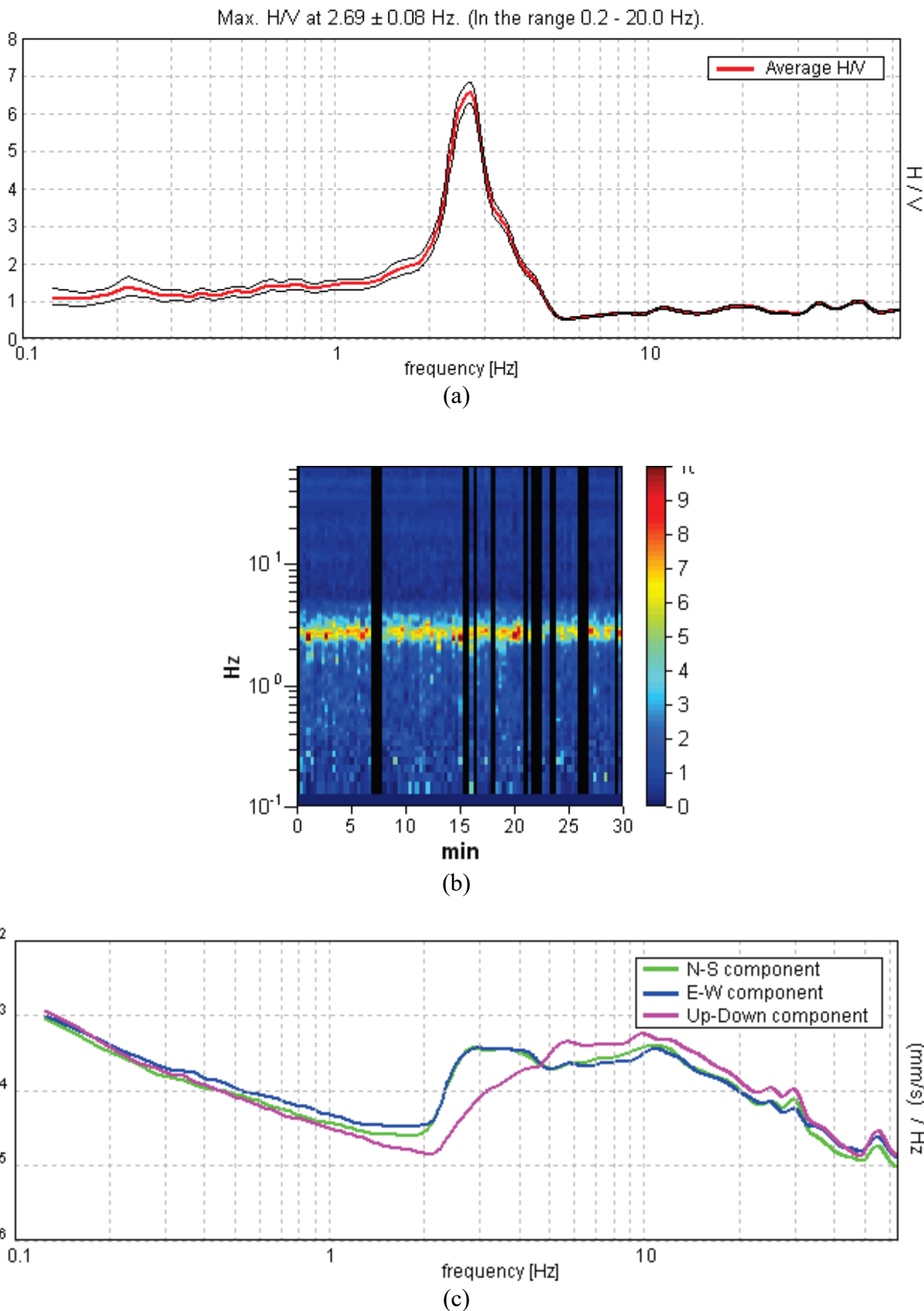


Fig. B-06 Tromino results at Masson landslide site MT06. (a) HVSR; (b) Spectral windows; (c) Horizontal and vertical average spectra for all windows used.

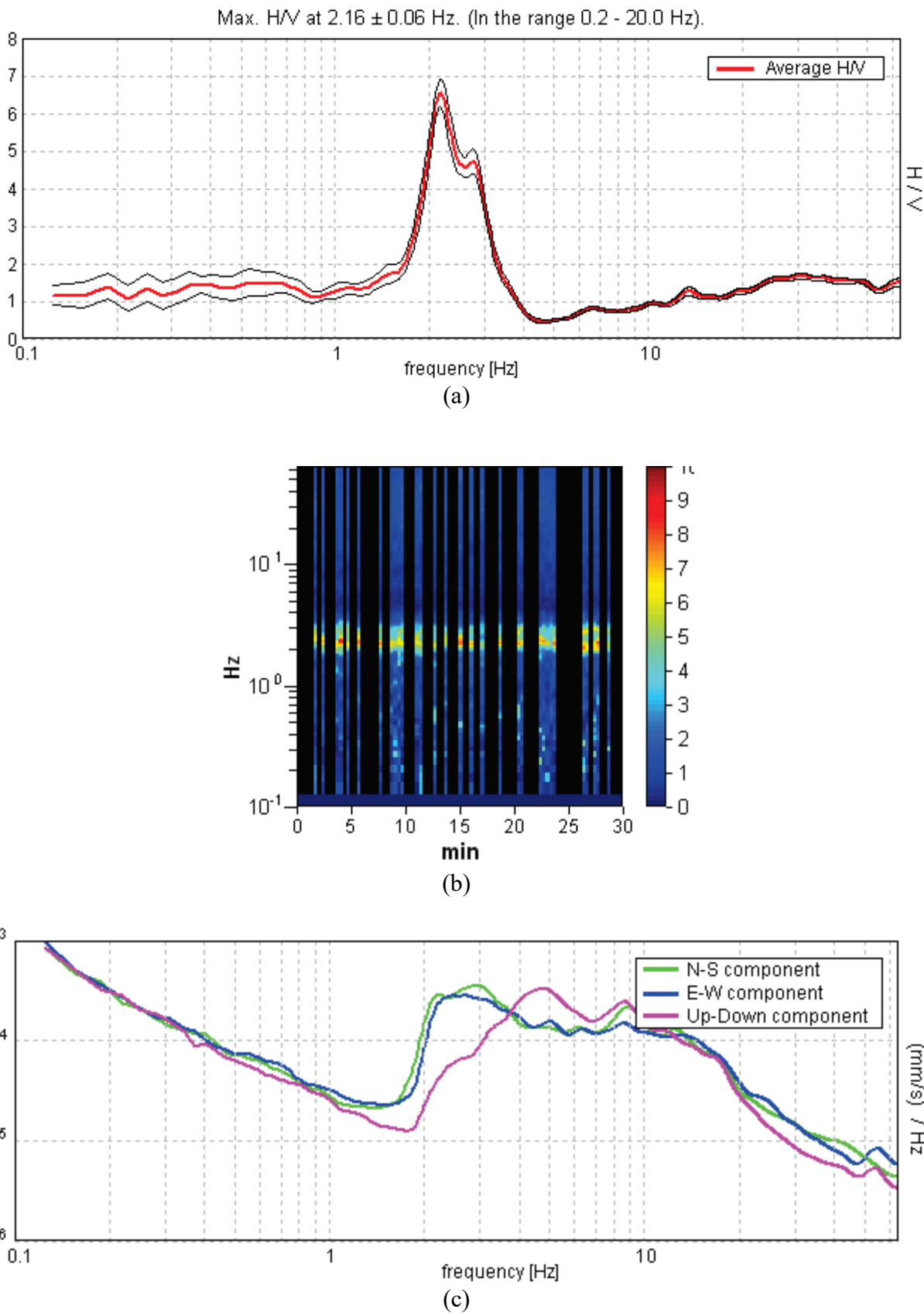


Fig. B-07 Tromino results at Masson landslide site MT07. (a) HVSR; (b) Spectral windows; (c) Horizontal and vertical average spectra for all windows used.

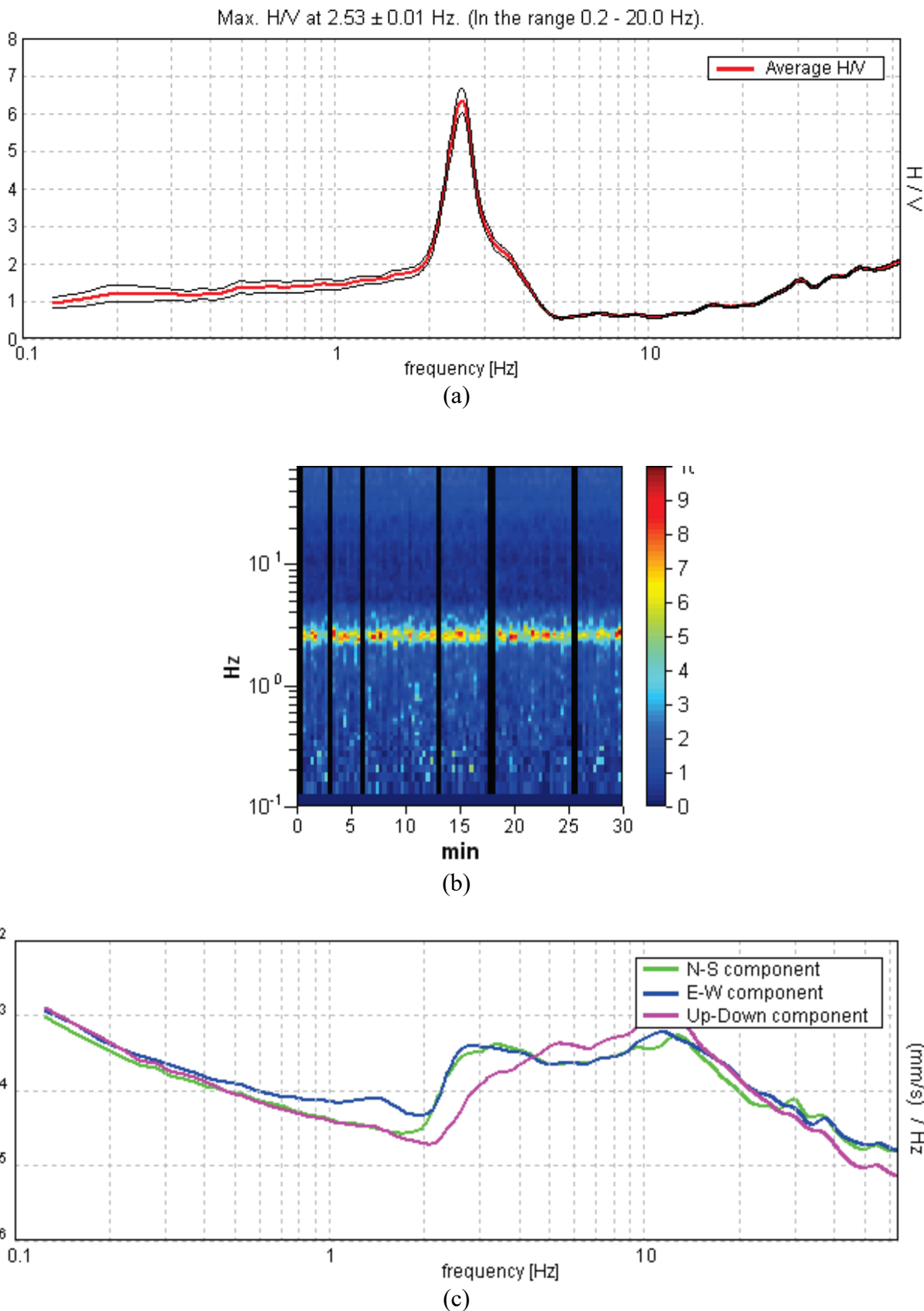


Fig. B-08 Tromino results at Masson landslide site MT08. (a) HVSR; (b) Spectral windows; (c) Horizontal and vertical average spectra for all windows used.

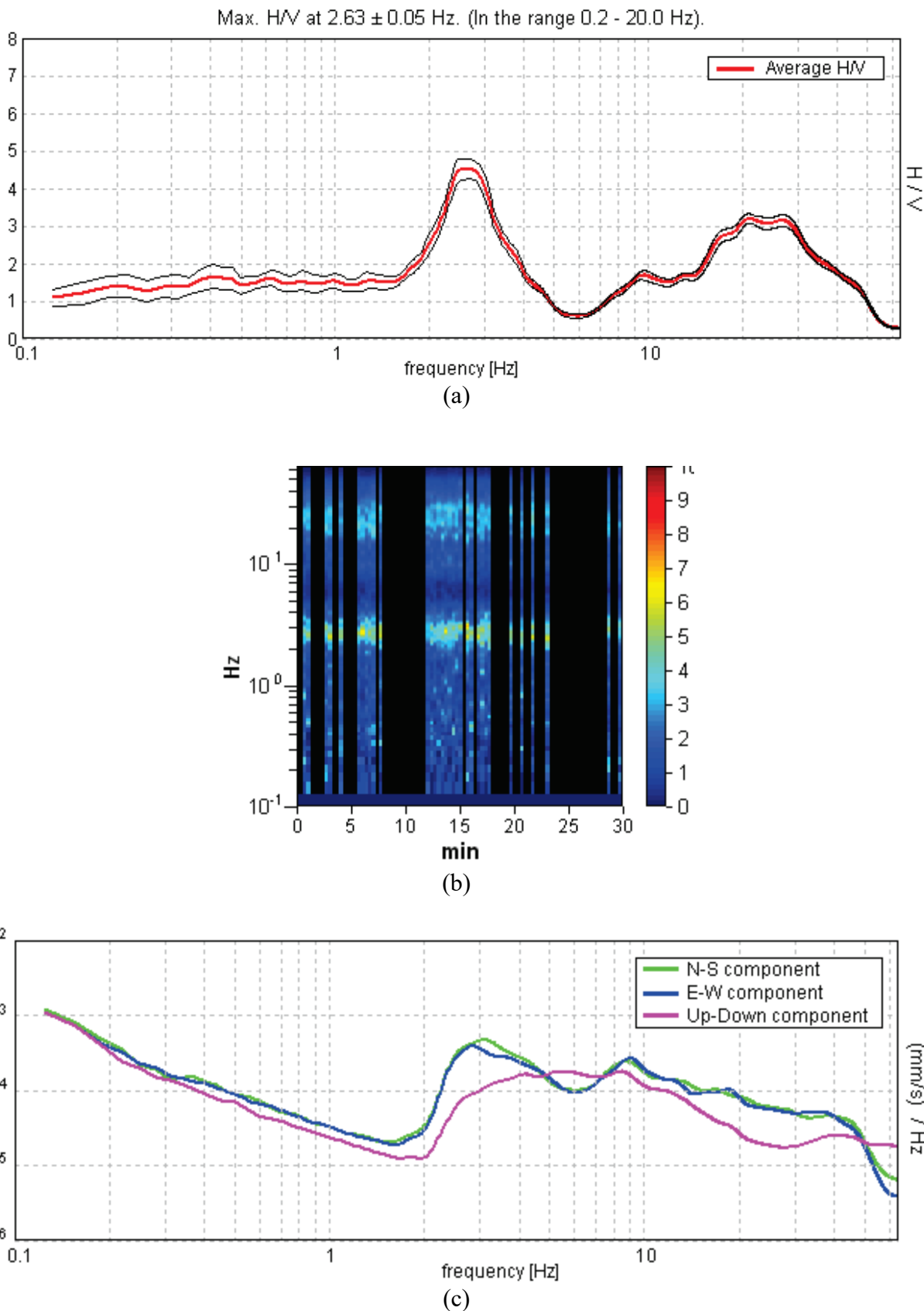


Fig. B-09 Tromino results at Masson landslide site MT09. (a) HVSR; (b) Spectral windows; (c) Horizontal and vertical average spectra for all windows used.

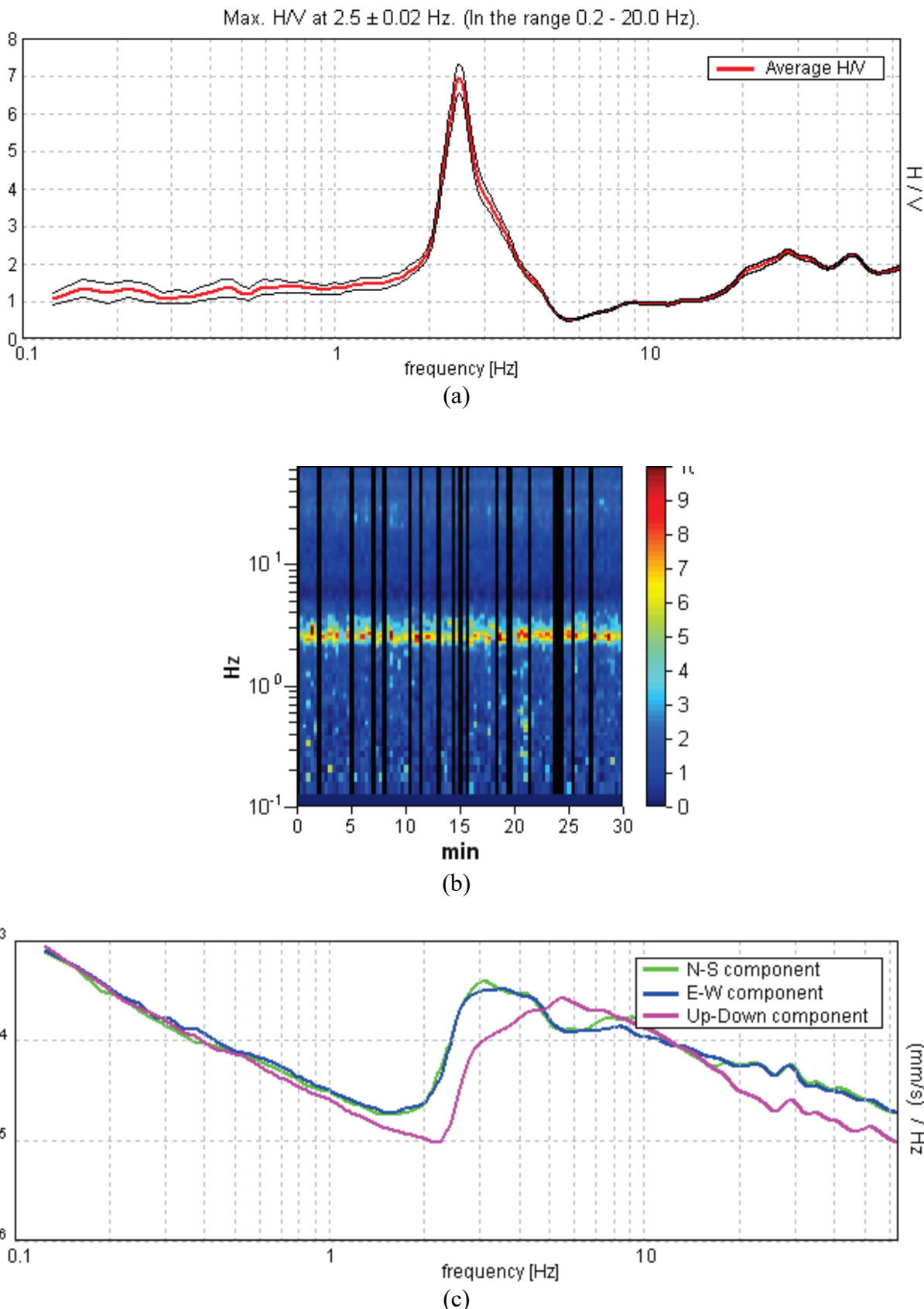


Fig. B-10 Tromino results at Masson landslide site MT10. (a) HVSR; (b) Spectral windows; (c) Horizontal and vertical average spectra for all windows used.

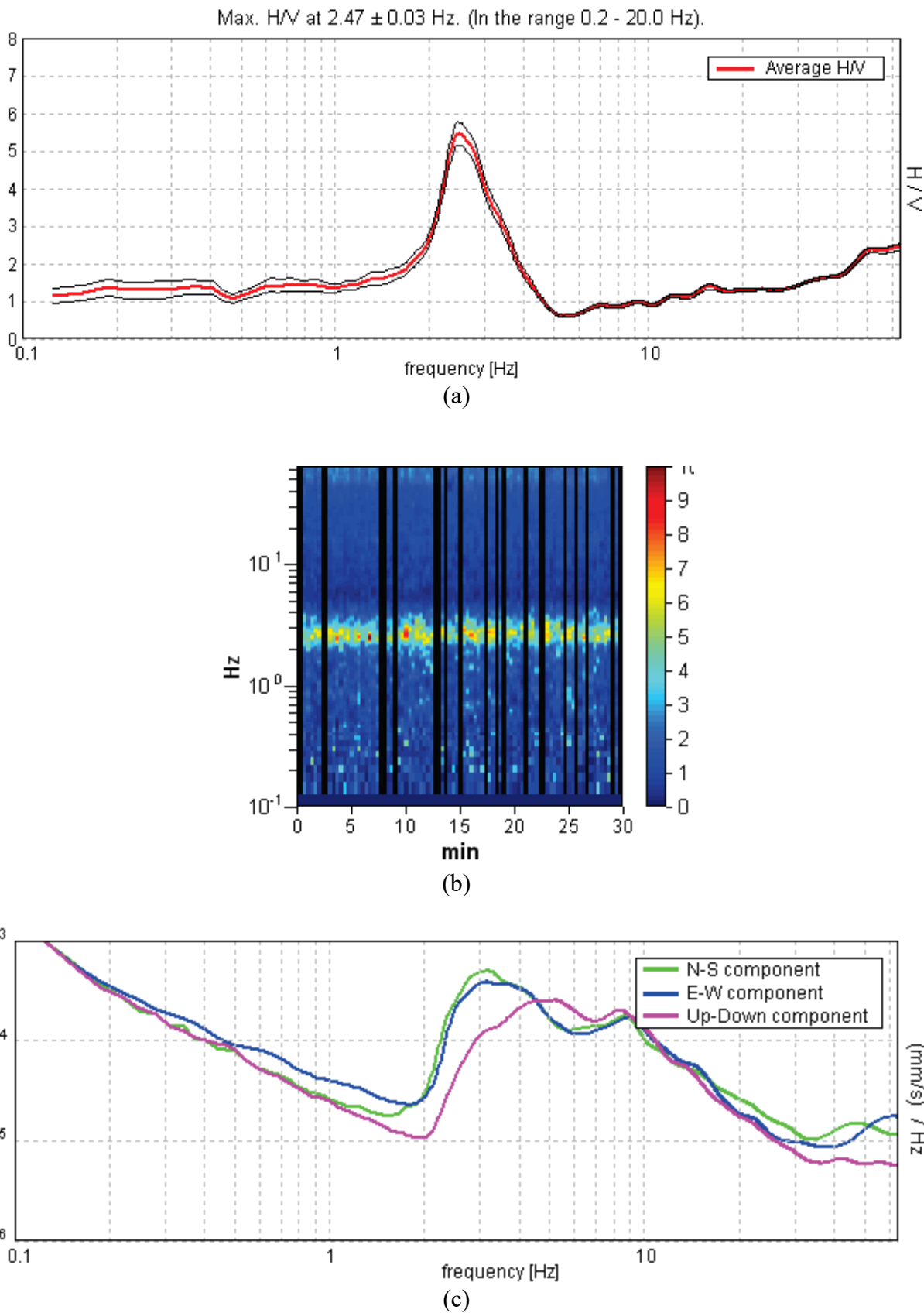


Fig. B-11 Tromino results at Masson landslide site MT11. (a) HVSR; (b) Spectral windows; (c) Horizontal and vertical average spectra for all windows used.

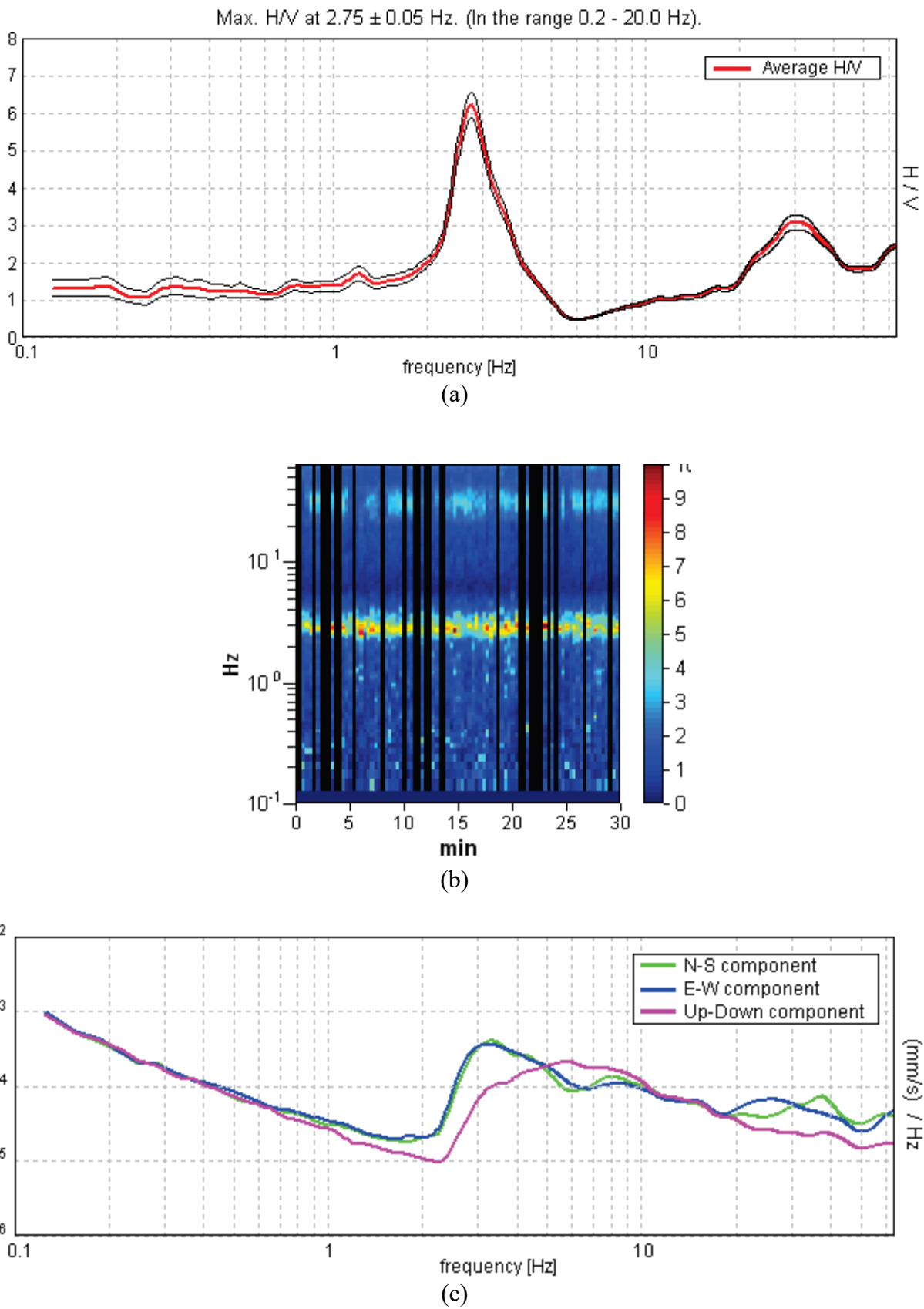


Fig. B-12 Tromino results at Masson landslide site MT12. (a) HVSR; (b) Spectral windows; (c) Horizontal and vertical average spectra for all windows used.

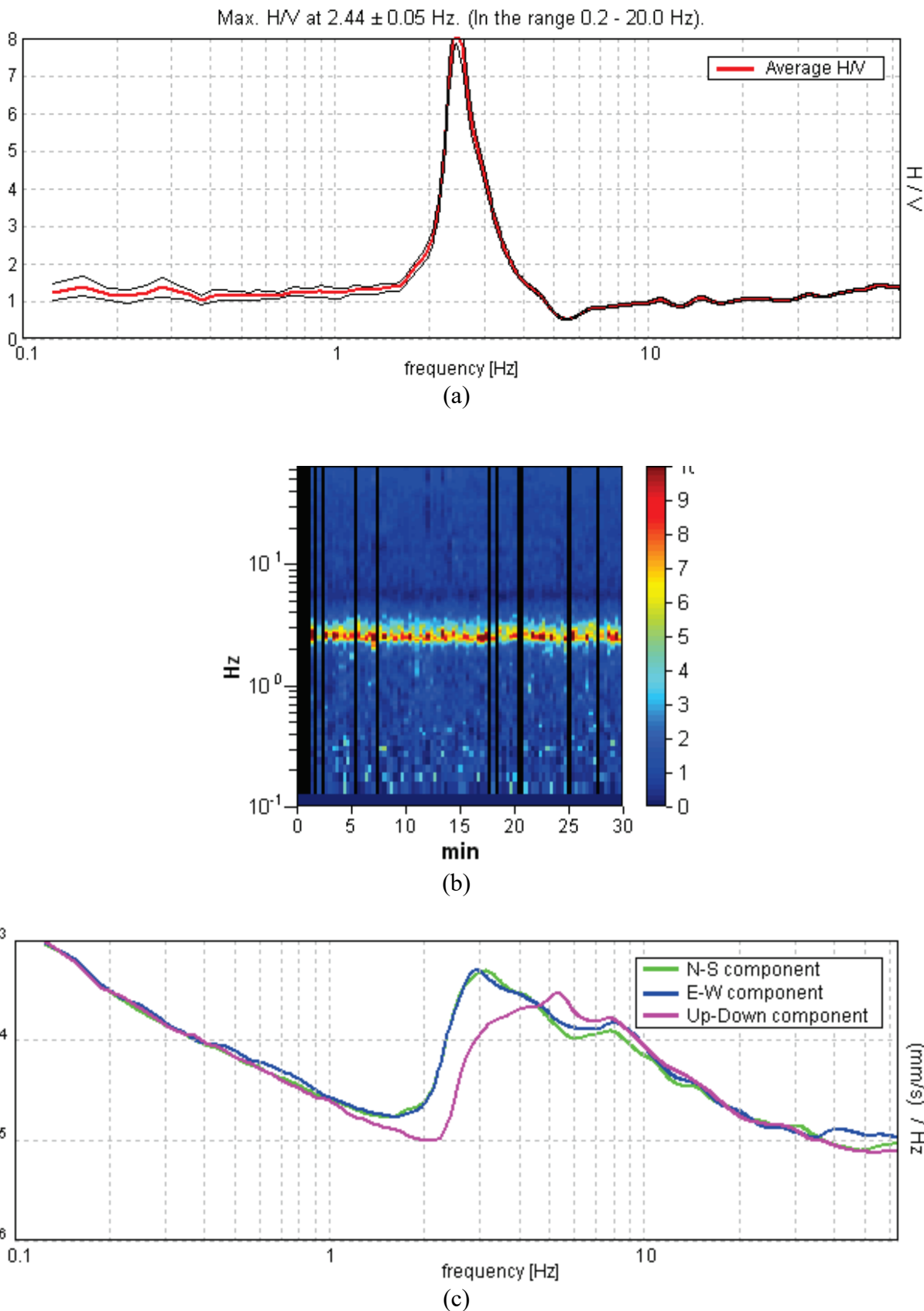


Fig. B-13 Tromino results at Masson landslide site MT13. (a) HVSR; (b) Spectral windows; (c) Horizontal and vertical average spectra for all windows used.

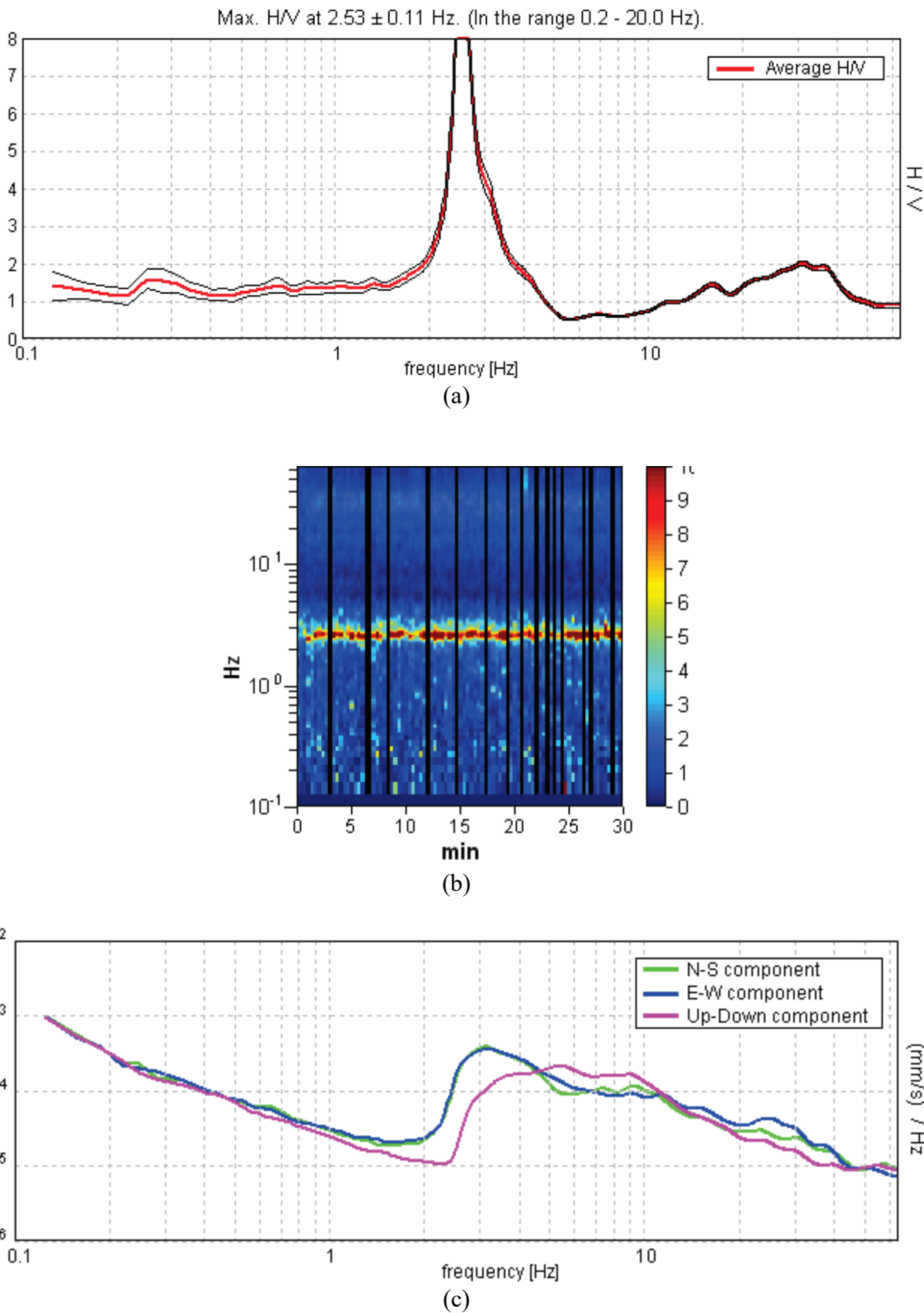


Fig. B-14 Tromino results at Masson landslide site MT14. (a) HVSR; (b) Spectral windows; (c) Horizontal and vertical average spectra for all windows used.

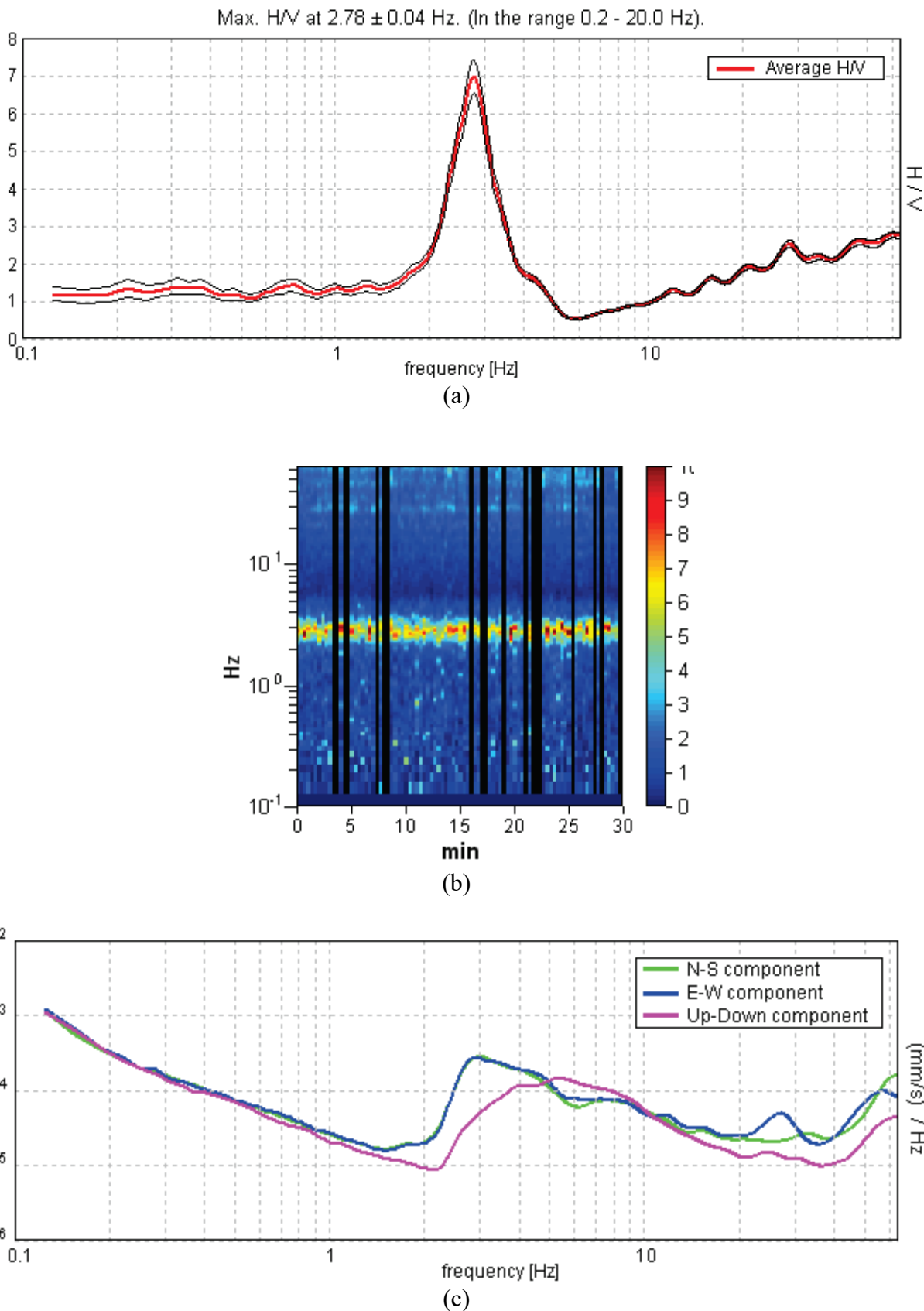


Fig. B-15 Tromino results at Masson landslide site MT15. (a) HVSR; (b) Spectral windows; (c) Horizontal and vertical average spectra for all windows used.

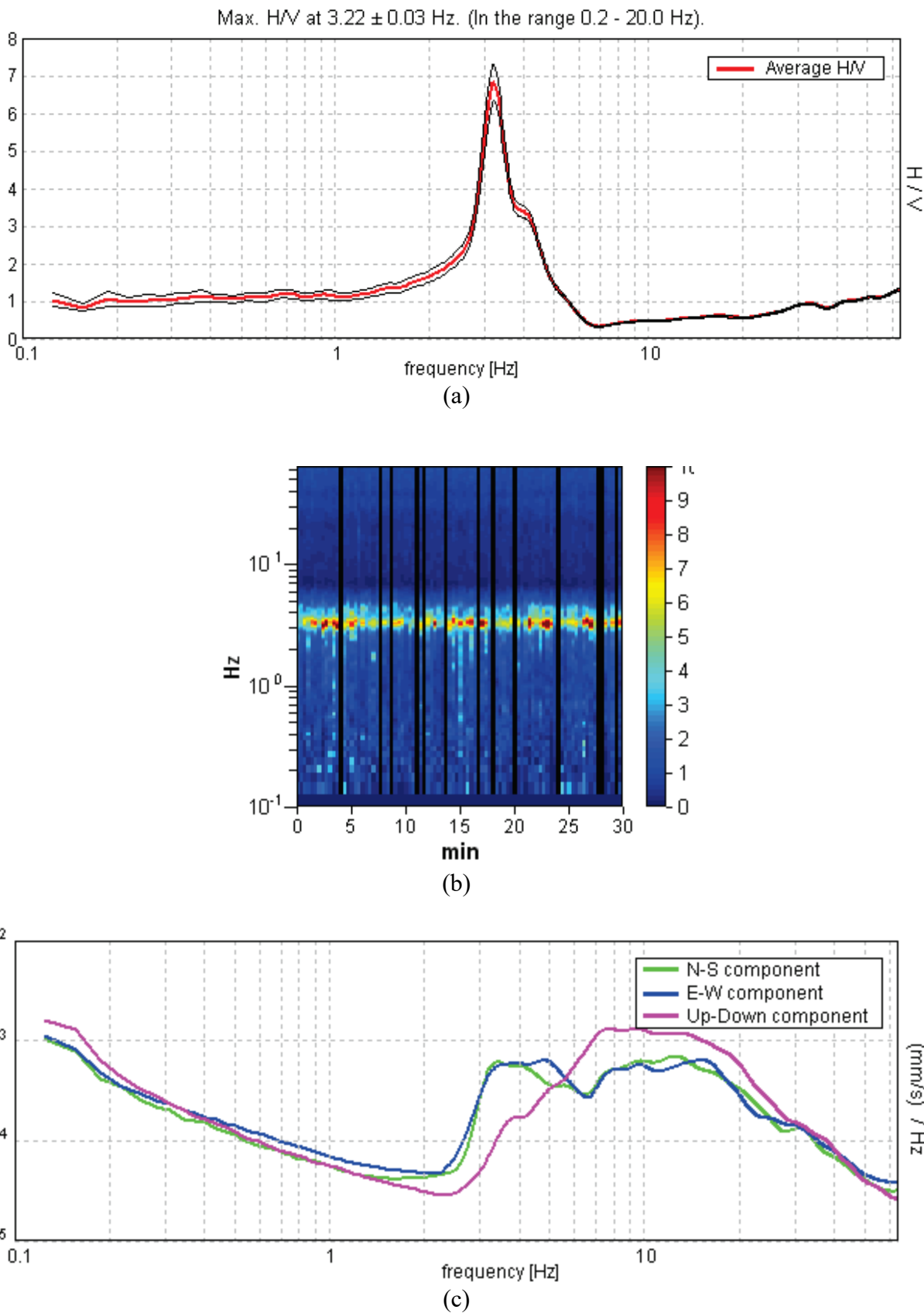


Fig. B-16 Tromino results at Masson landslide site MT16. (a) HVSR; (b) Spectral windows; (c) Horizontal and vertical average spectra for all windows used.

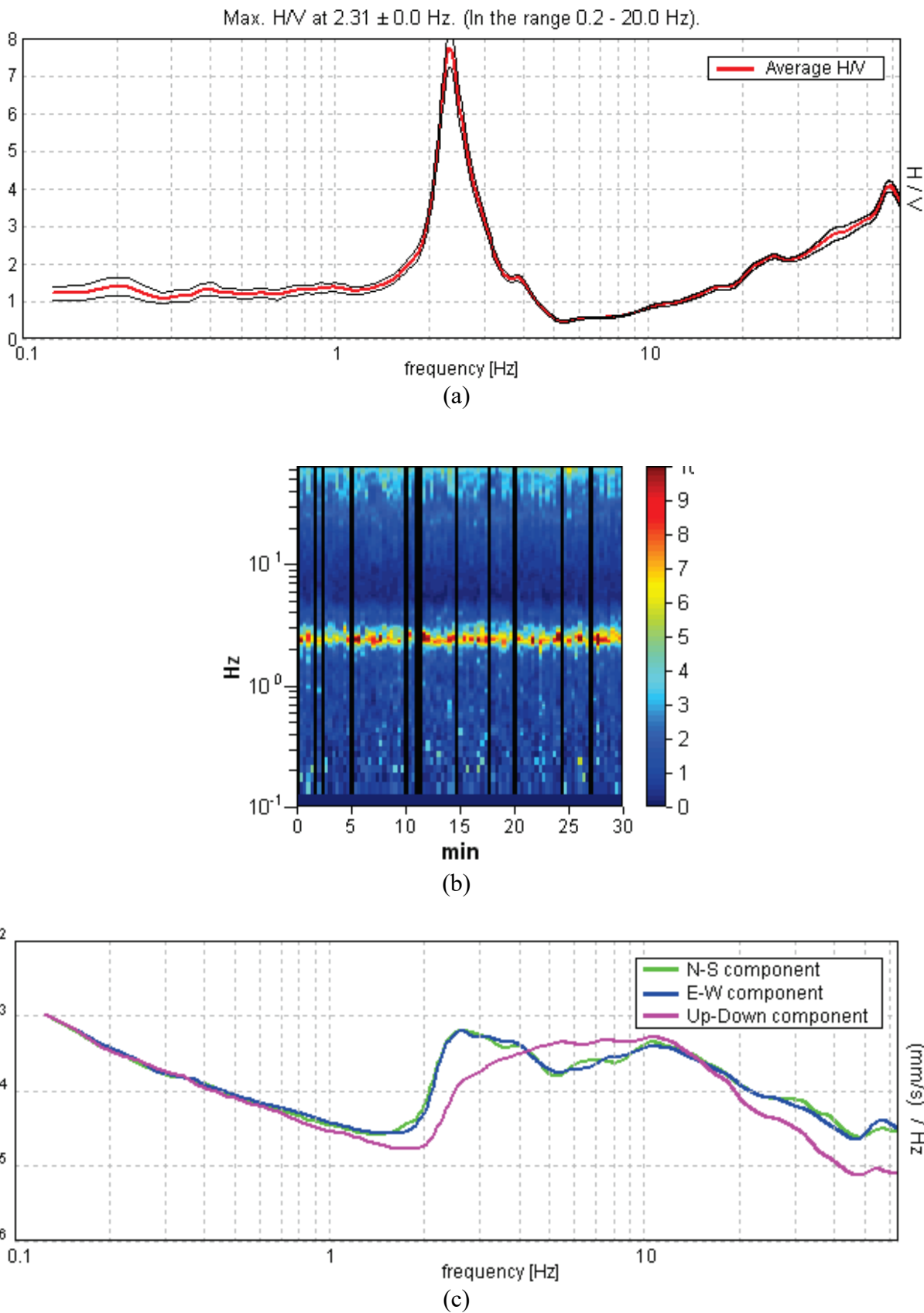


Fig. B-17 Tromino results at Masson landslide site MT17. (a) HVSR; (b) Spectral windows; (c) Horizontal and vertical average spectra for all windows used.

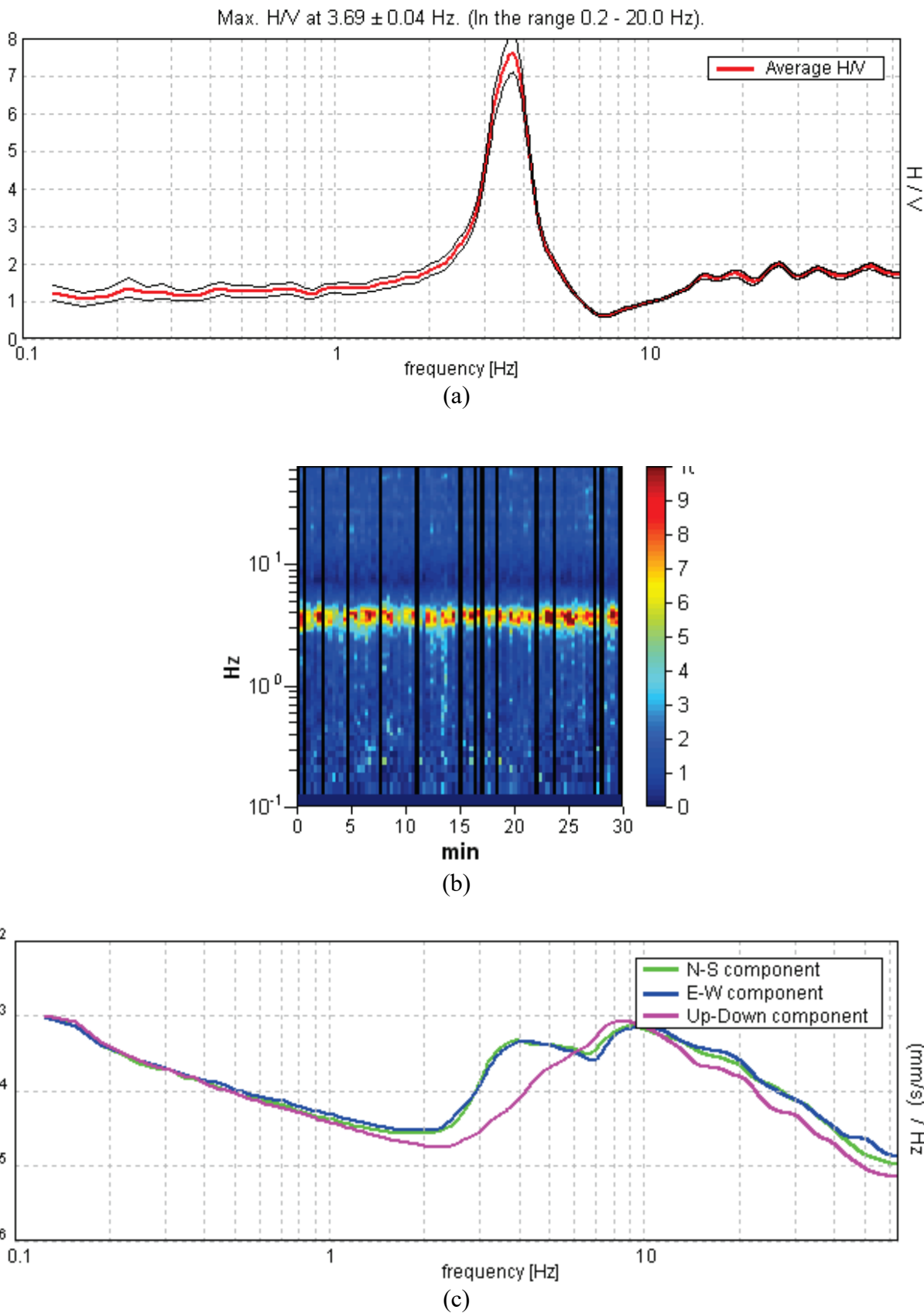


Fig. B-18 Tromino results at Masson landslide site MT18. (a) HVSR; (b) Spectral windows; (c) Horizontal and vertical average spectra for all windows used.

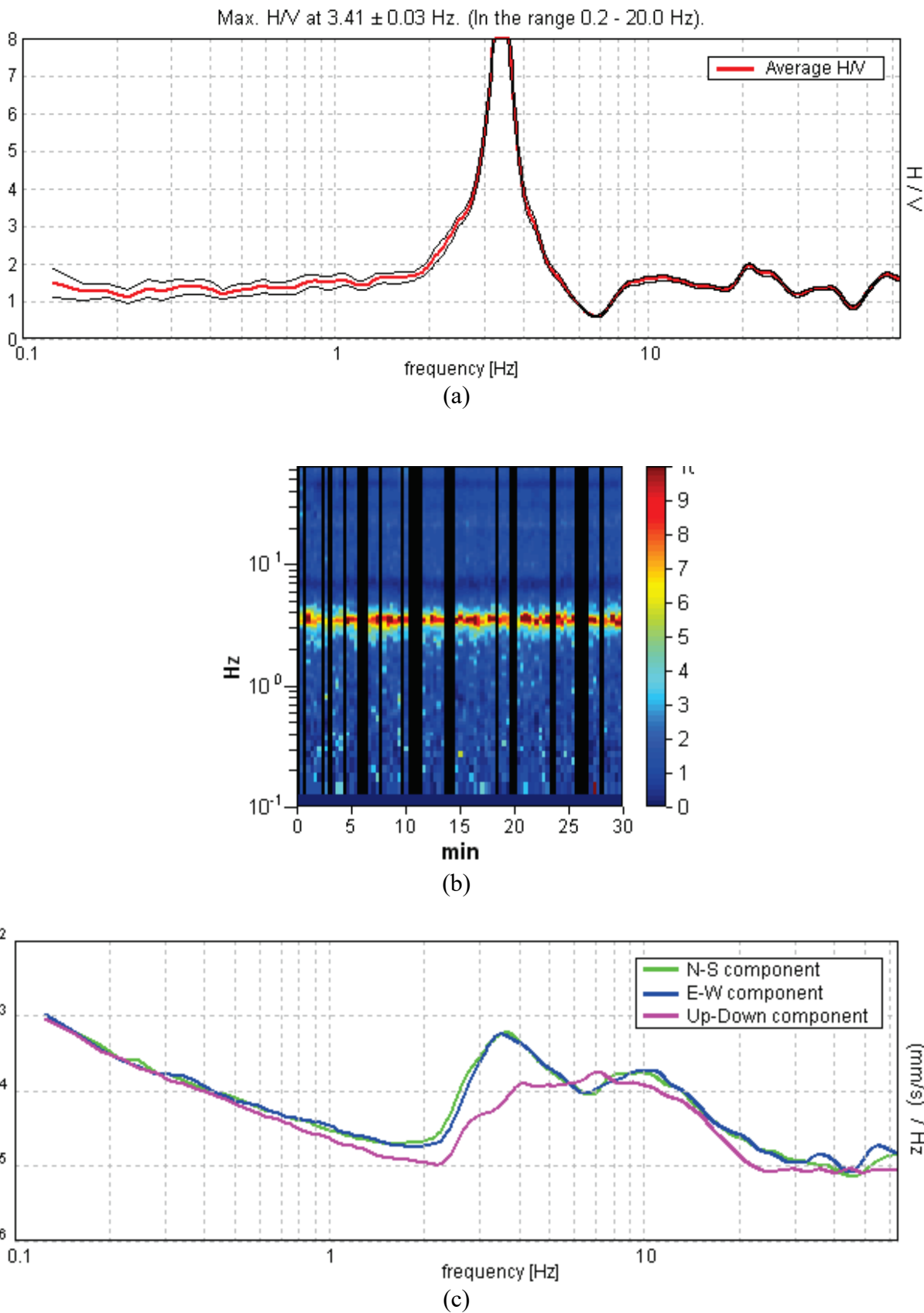


Fig. B-19 Tromino results at Masson landslide site MT19. (a) HVSR; (b) Spectral windows; (c) Horizontal and vertical average spectra for all windows used.

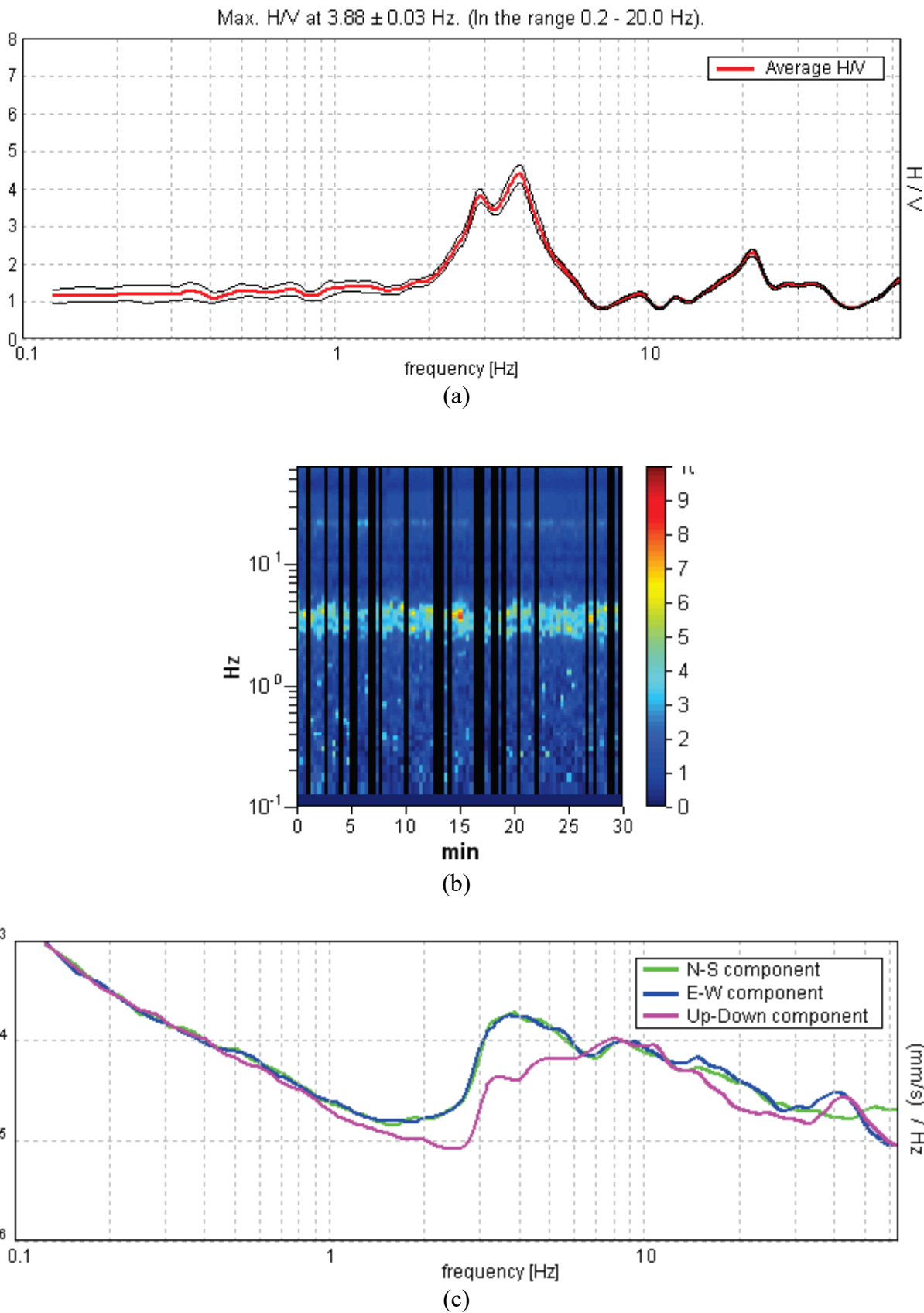


Fig. B-20 Tromino results at Masson landslide site MT20. (a) HVSR; (b) Spectral windows; (c) Horizontal and vertical average spectra for all windows used.

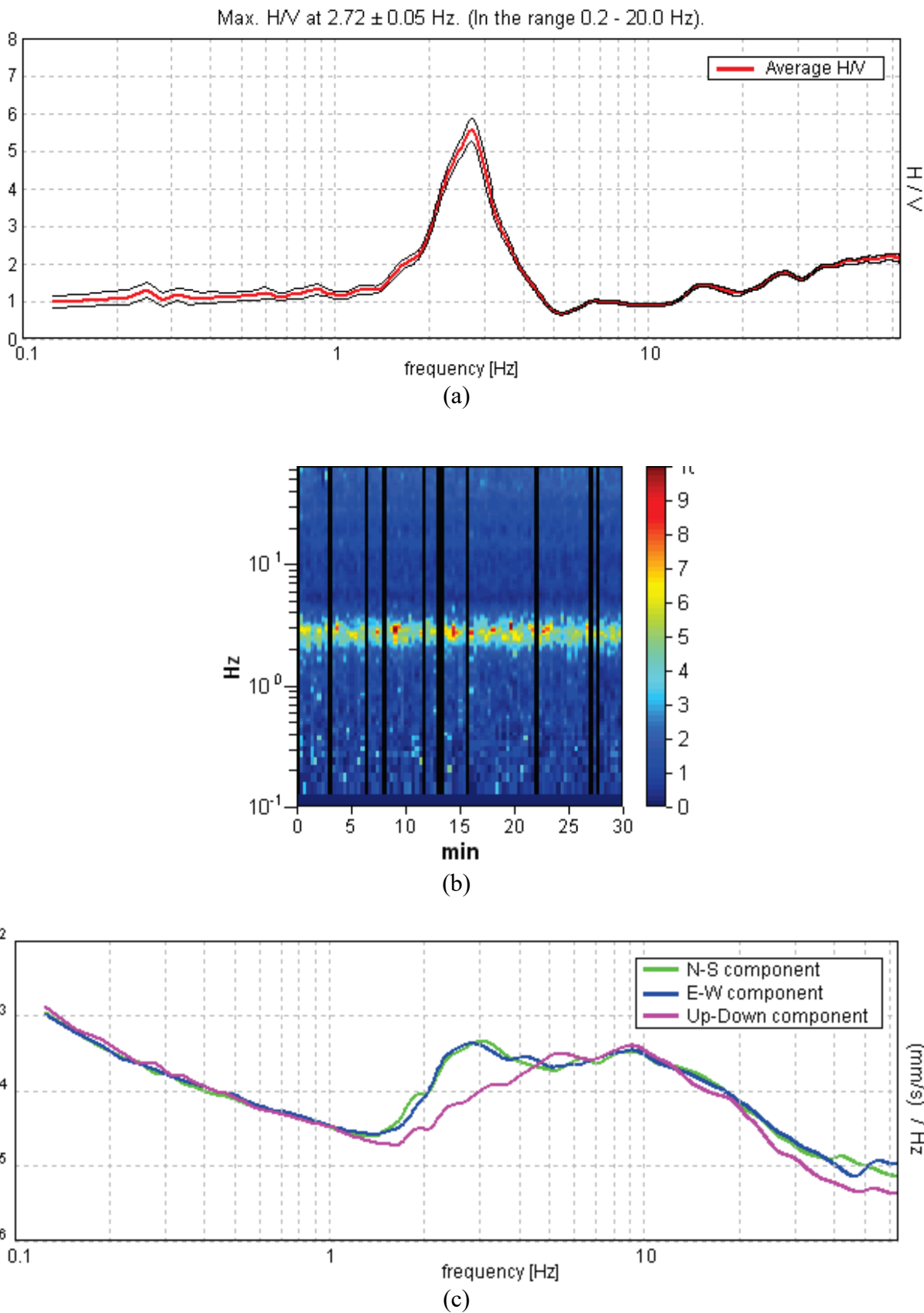


Fig. B-21 Tromino results at Masson landslide site MT21. (a) HVSR; (b) Spectral windows; (c) Horizontal and vertical average spectra for all windows used.

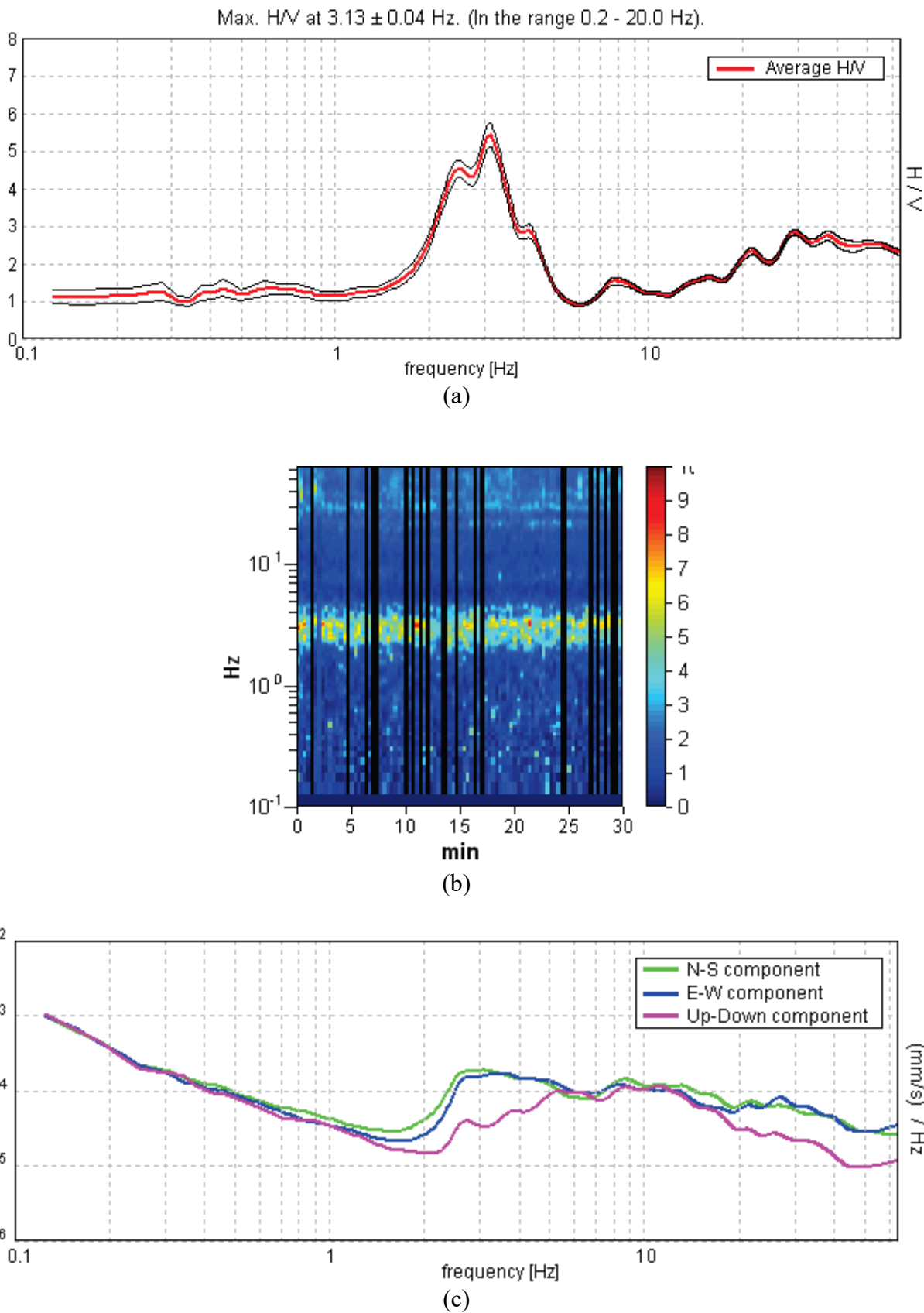


Fig. B-22 Tromino results at Masson landslide site MT22. (a) HVSR; (b) Spectral windows; (c) Horizontal and vertical average spectra for all windows used.

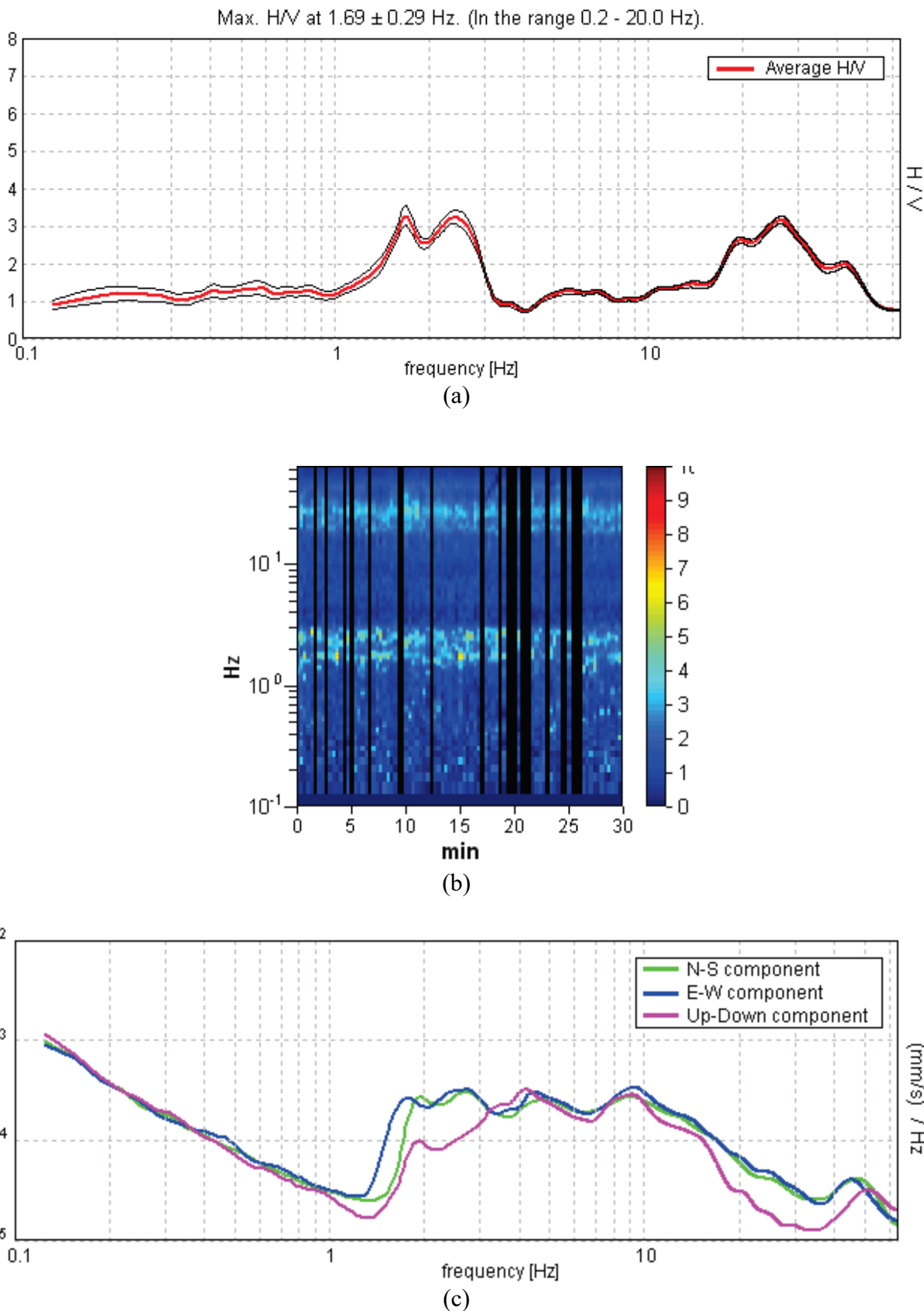


Fig. B-23 Tromino results at Masson landslide site MT23. (a) HVSR; (b) Spectral windows; (c) Horizontal and vertical average spectra for all windows used.

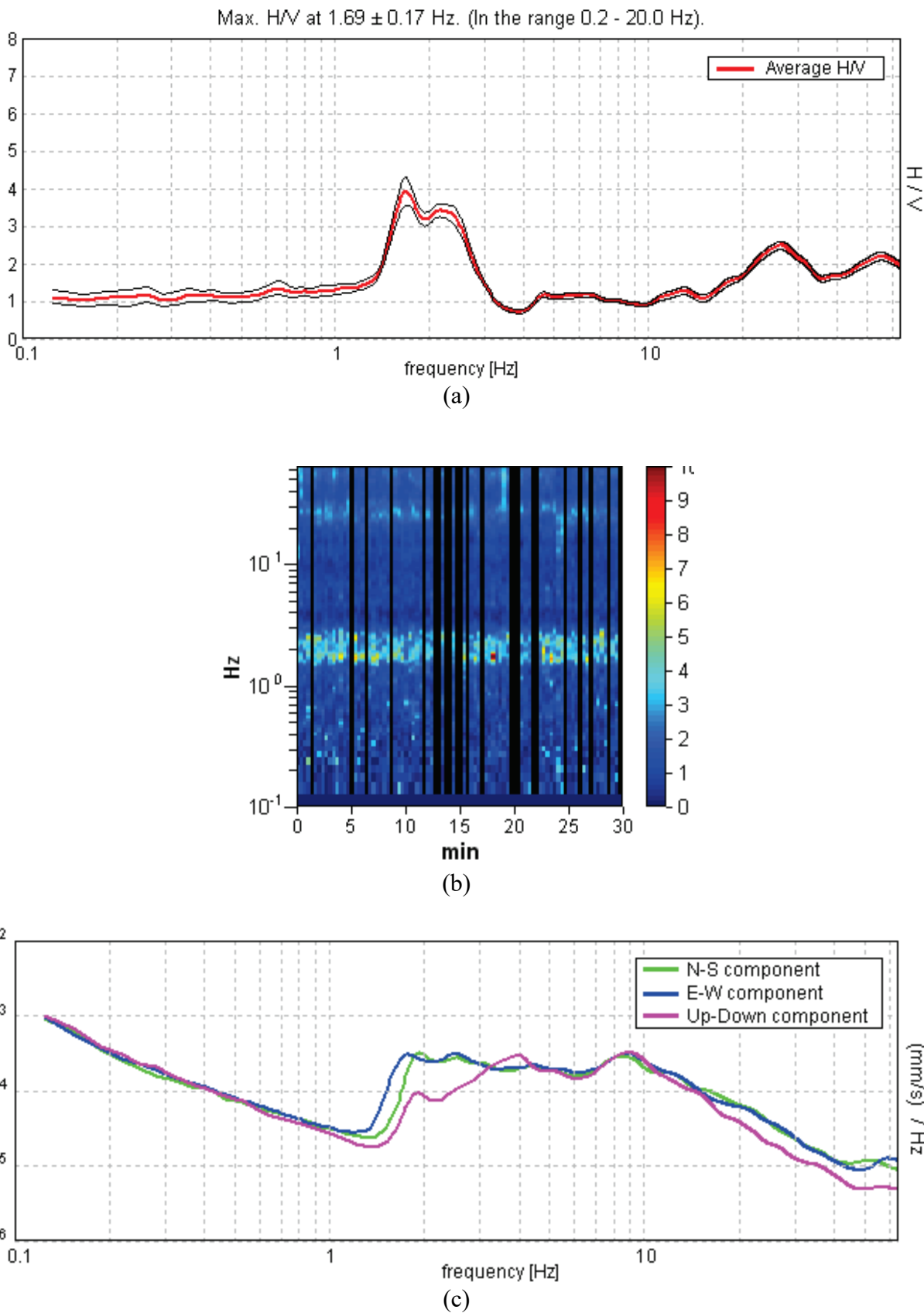


Fig. B-24 Tromino results at Masson landslide site MT24. (a) HVSR; (b) Spectral windows; (c) Horizontal and vertical average spectra for all windows used.

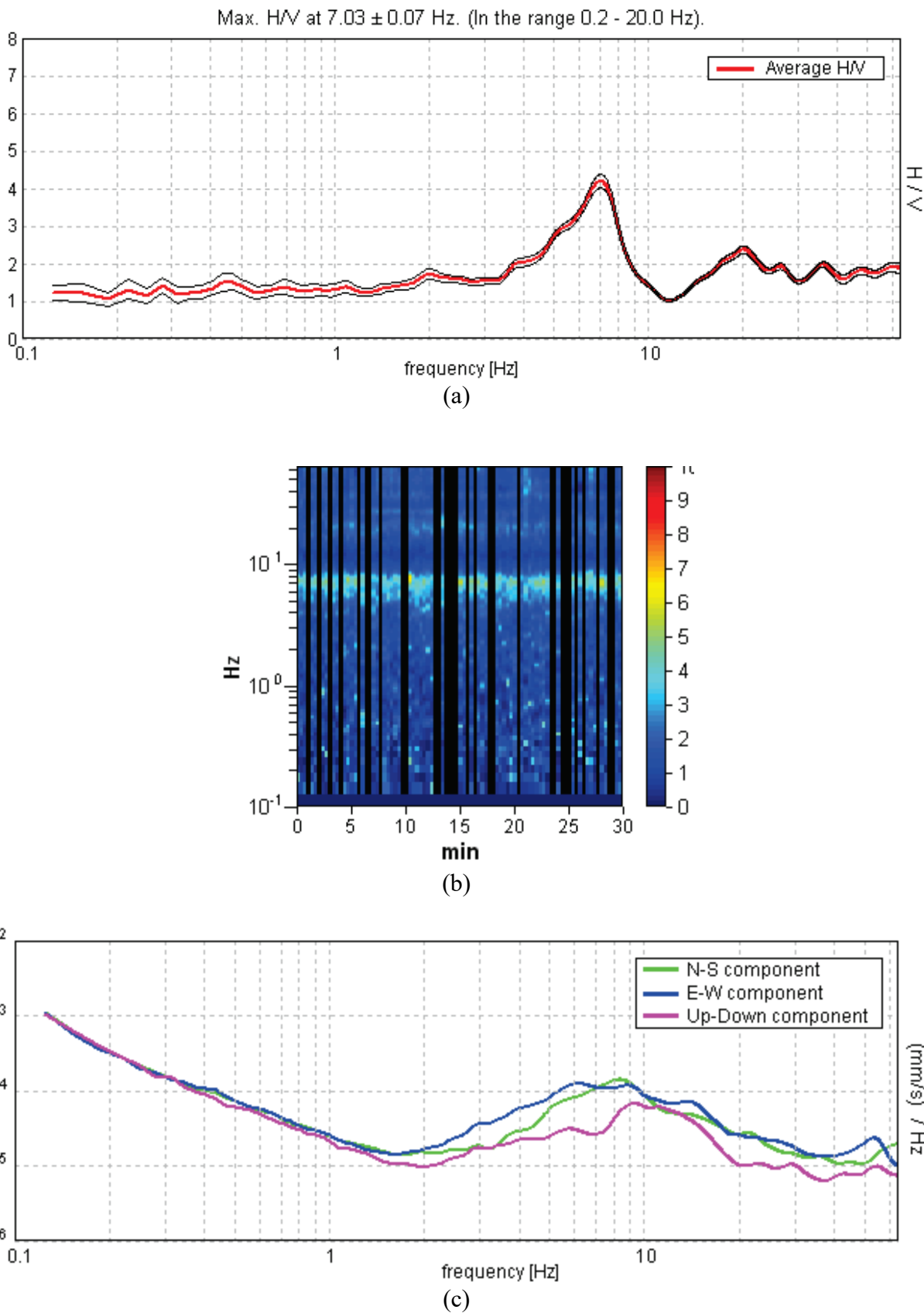


Fig. B-25 Tromino results at Masson landslide site MT25. (a) HVSR; (b) Spectral windows; (c) Horizontal and vertical average spectra for all windows used.

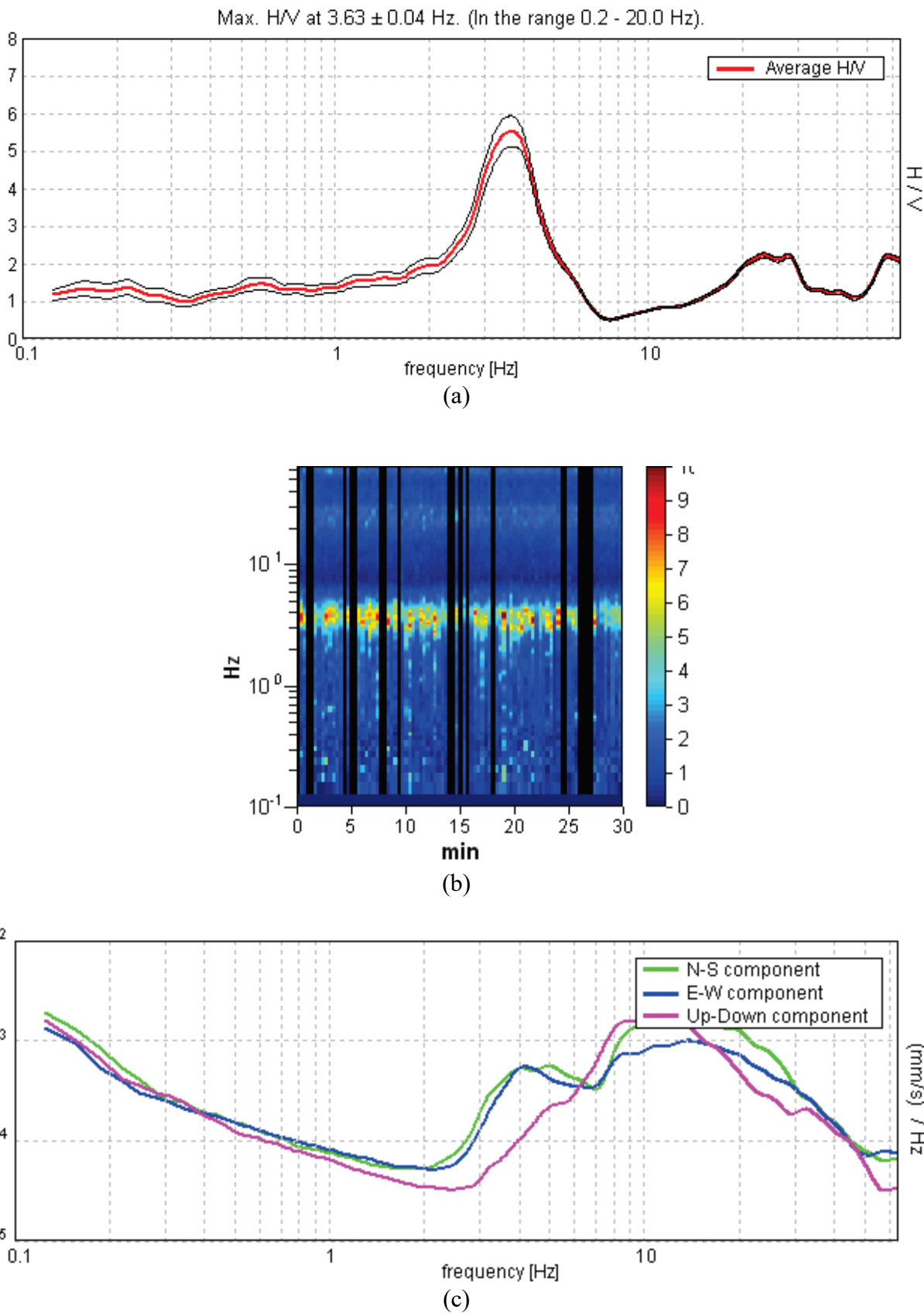


Fig. B-26 Tromino results at Masson landslide site MT26. (a) HVSR; (b) Spectral windows; (c) Horizontal and vertical average spectra for all windows used.

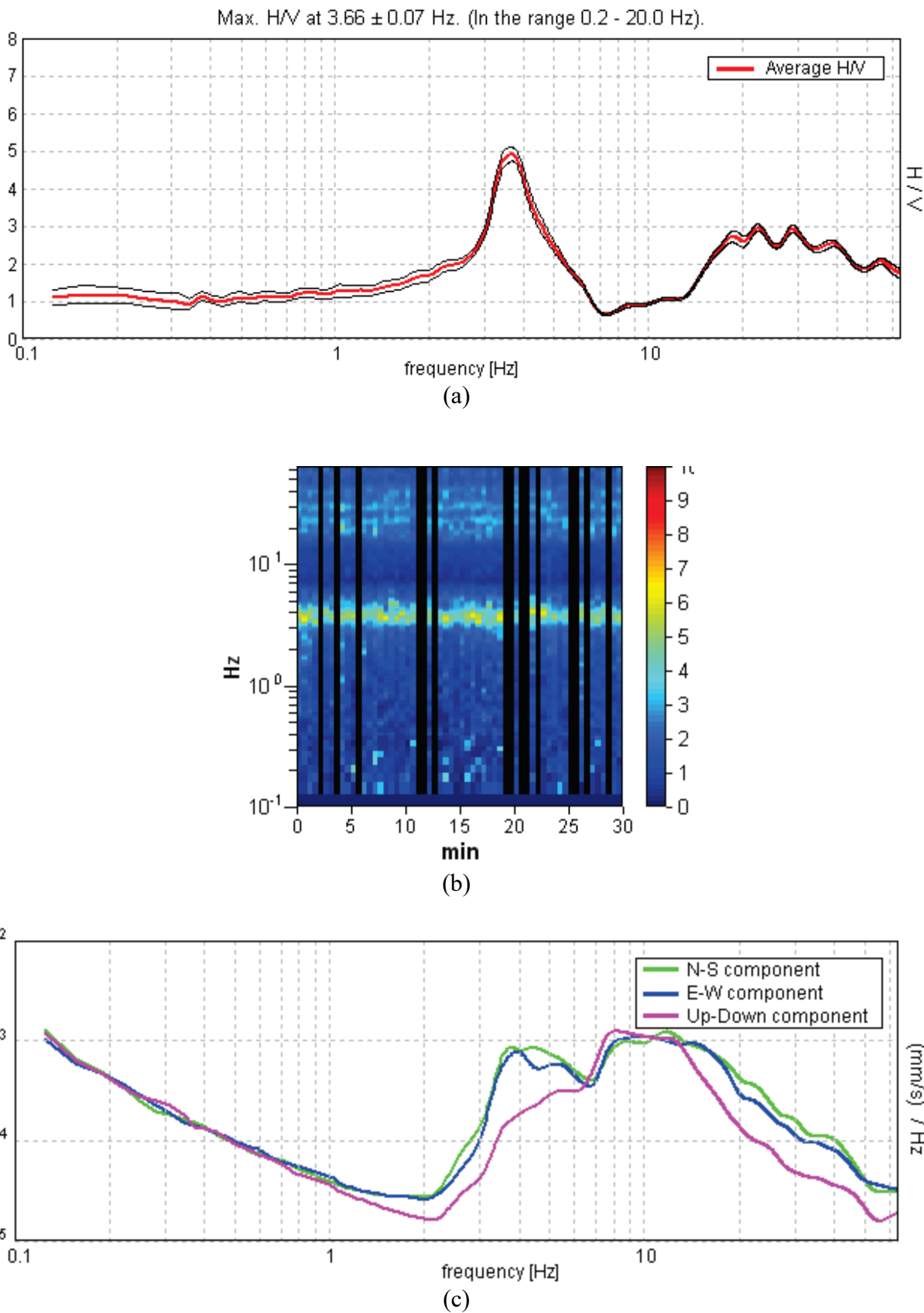


Fig. B-27 Tromino results at Masson landslide site MT27. (a) HVSR; (b) Spectral windows; (c) Horizontal and vertical average spectra for all windows used.

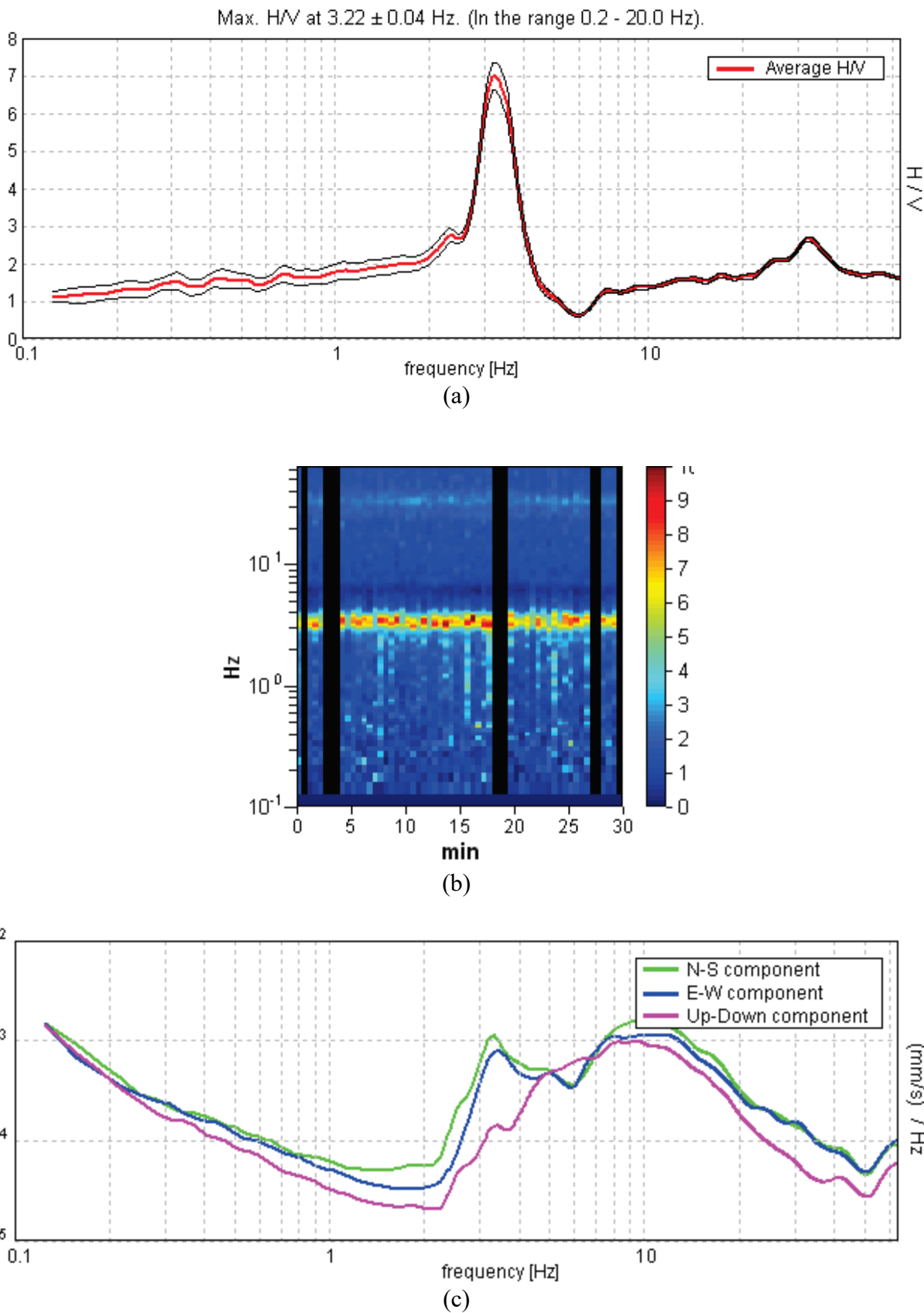


Fig. B-28 Tromino results at Masson landslide site MT28. (a) HVSR; (b) Spectral windows; (c) Horizontal and vertical average spectra for all windows used.

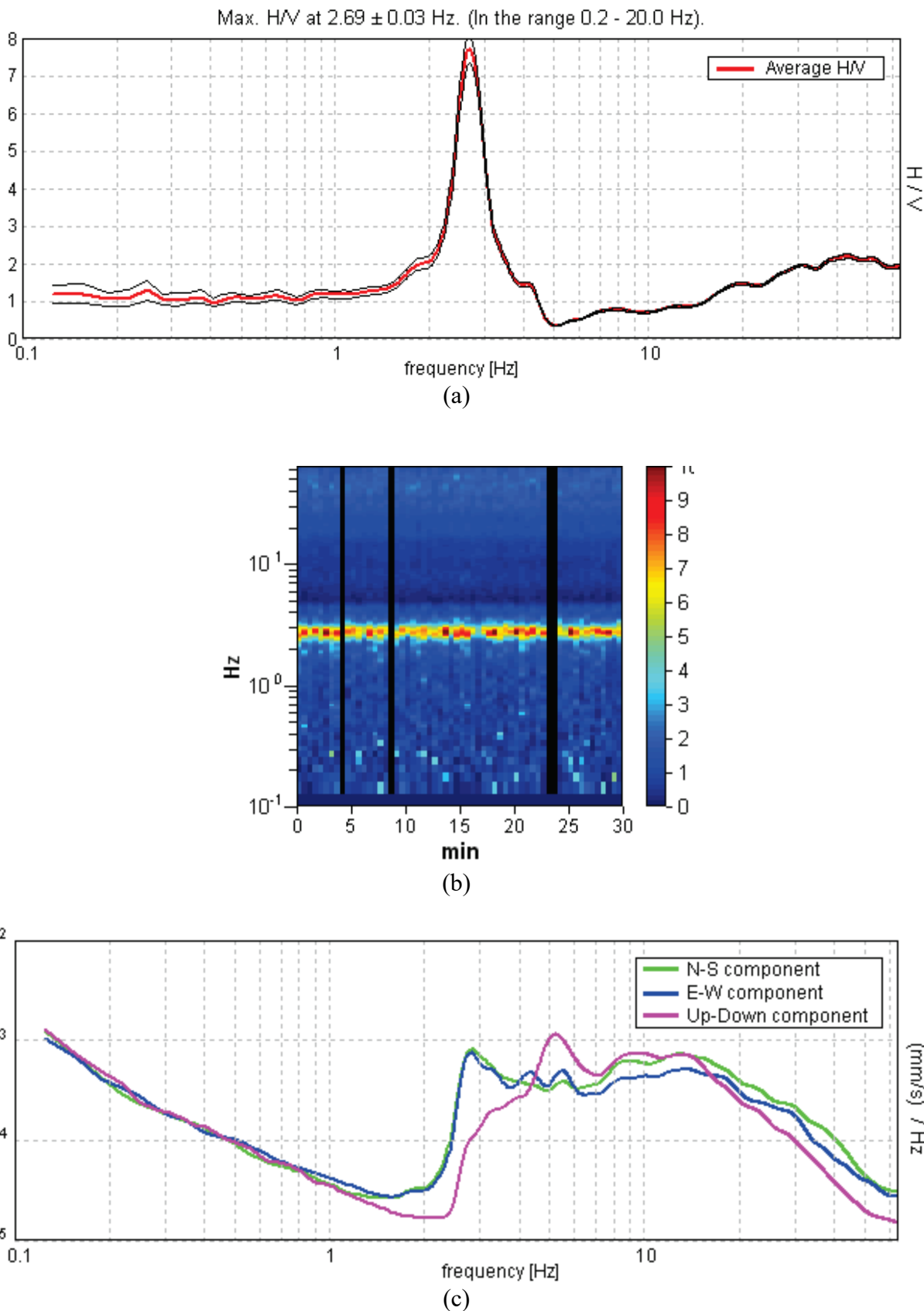


Fig. B-29 Tromino results at Masson landslide site MT29. (a) HVSR; (b) Spectral windows; (c) Horizontal and vertical average spectra for all windows used.

Appendix C

Charts of Tromino Measurements from Wendover Landslide Site

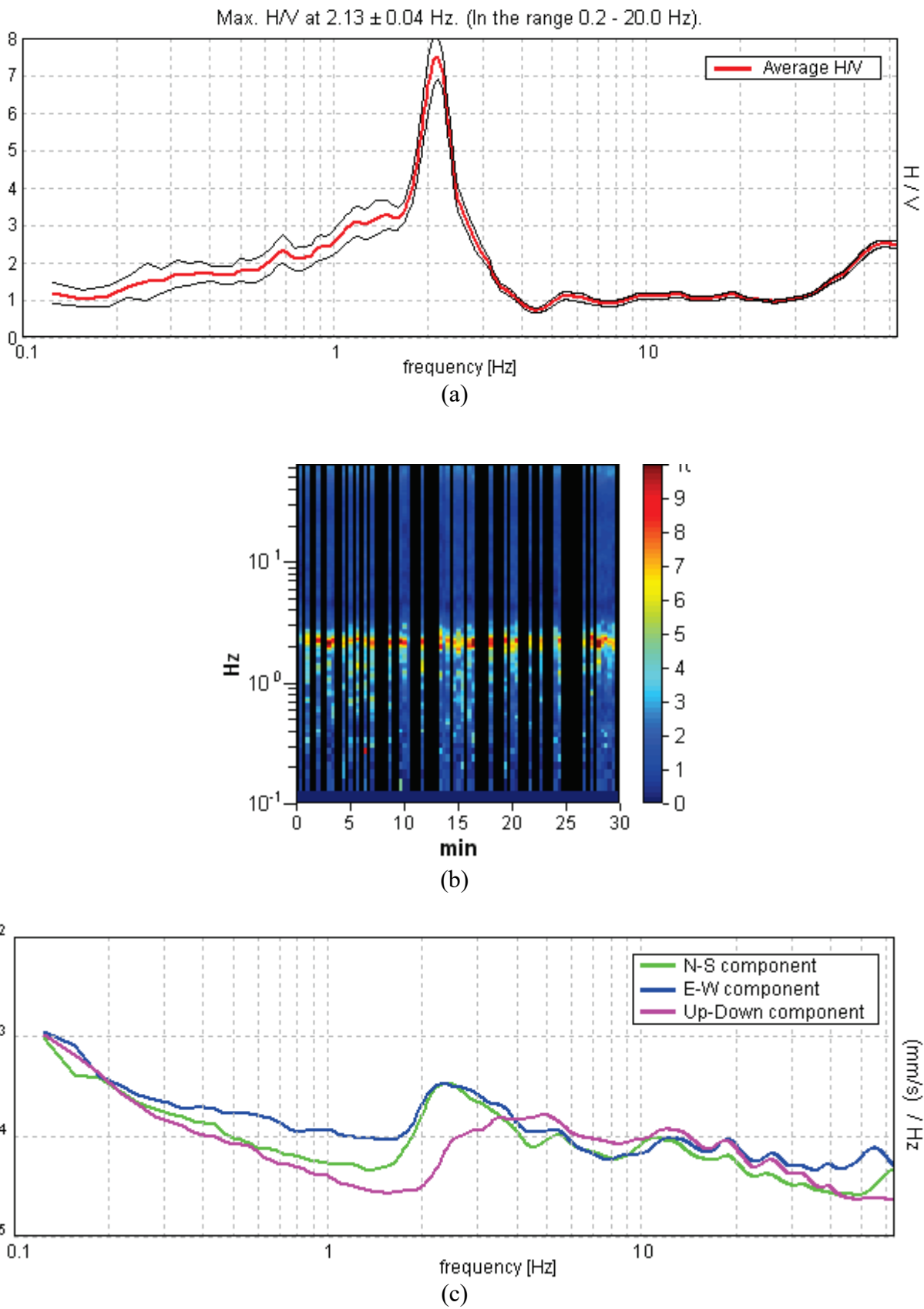


Fig. C-01 Tromino results at Masson landslide site WT01. (a) HVSR; (b) Spectral windows; (c) Horizontal and vertical average spectra for all windows used.

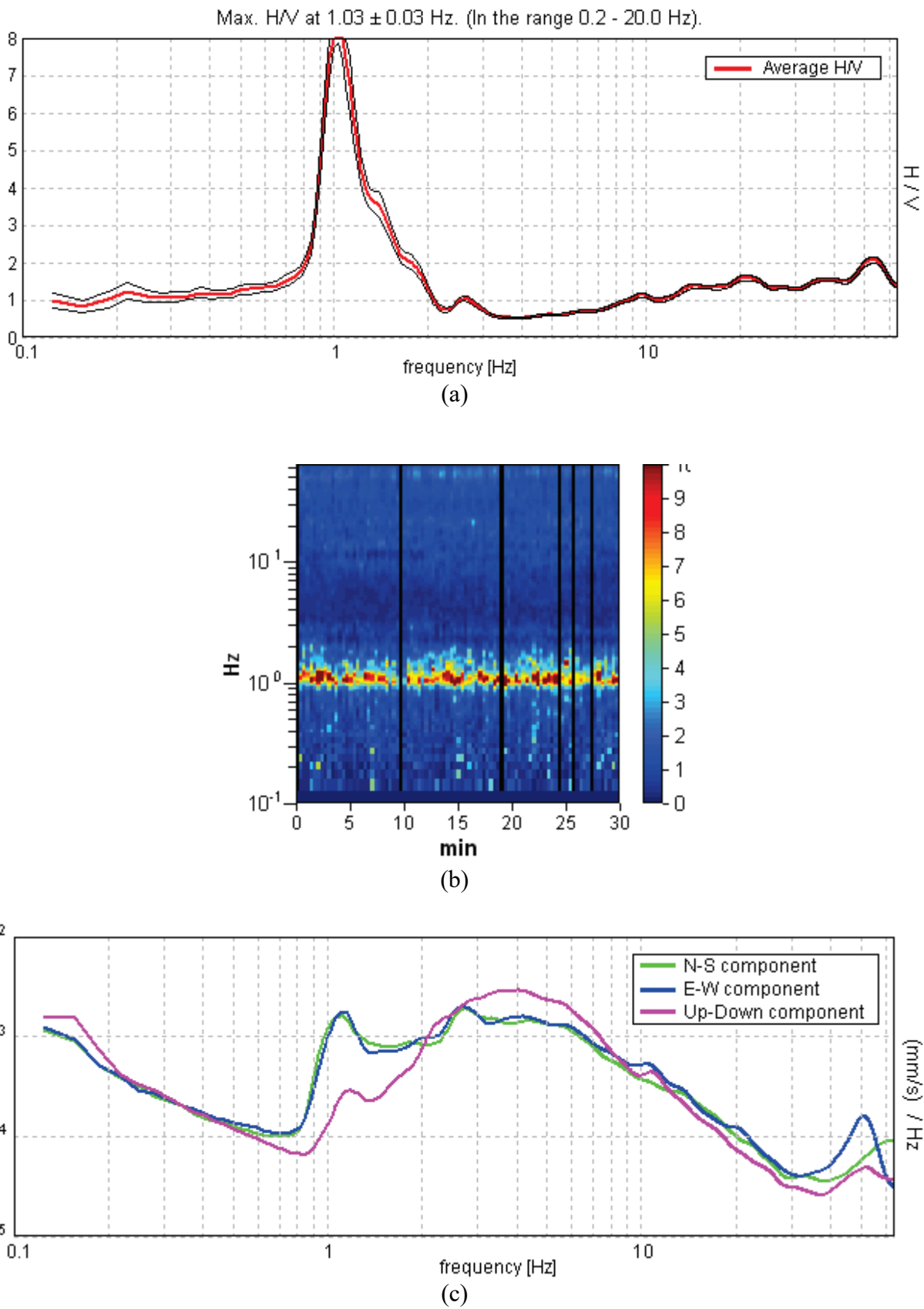


Fig. C-02 Tromino results at Masson landslide site WT02. (a) HVSR; (b) Spectral windows; (c) Horizontal and vertical average spectra for all windows used.

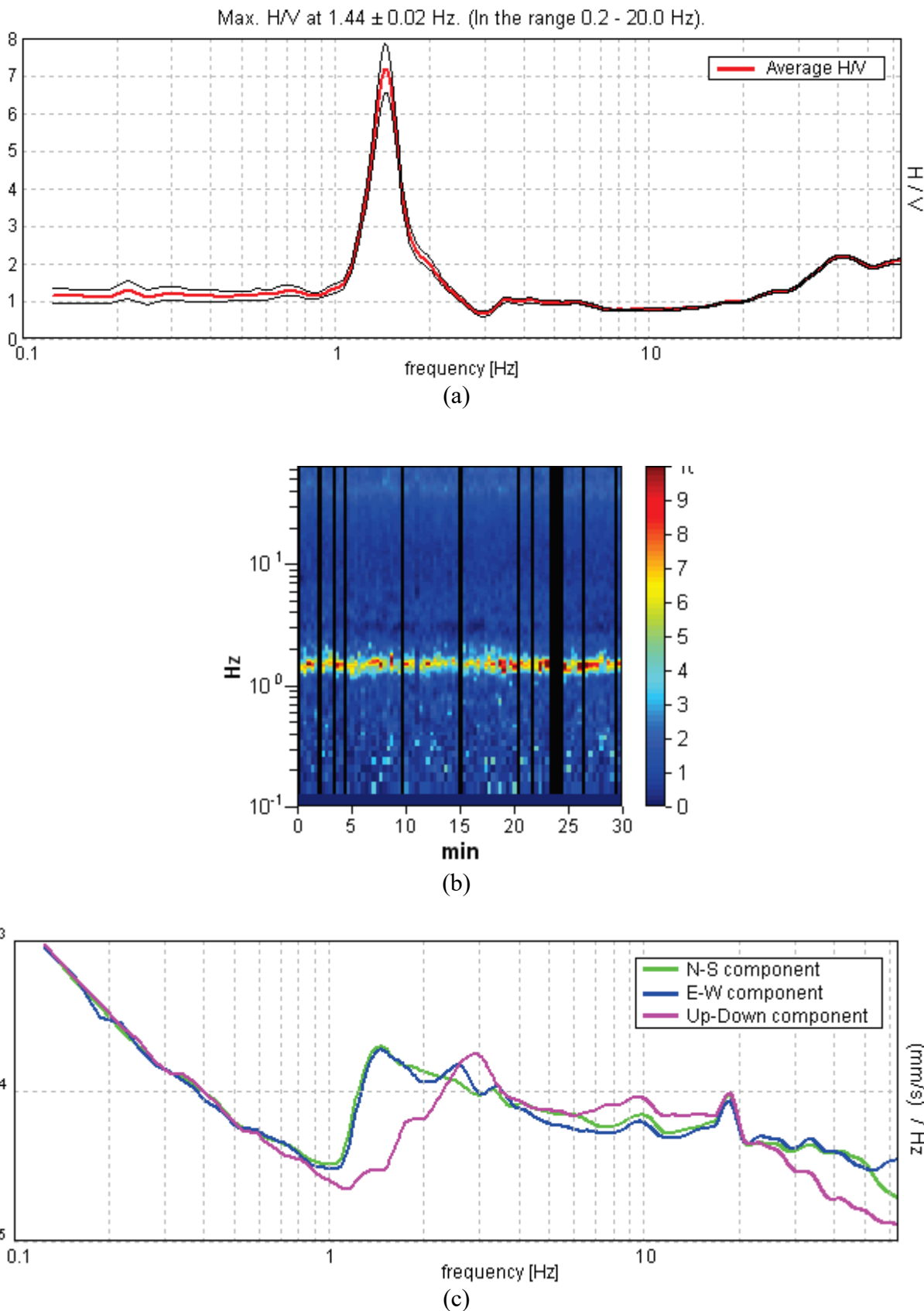


Fig. C-03 Tromino results at Masson landslide site WT03. (a) HVSR; (b) Spectral windows; (c) Horizontal and vertical average spectra for all windows used.

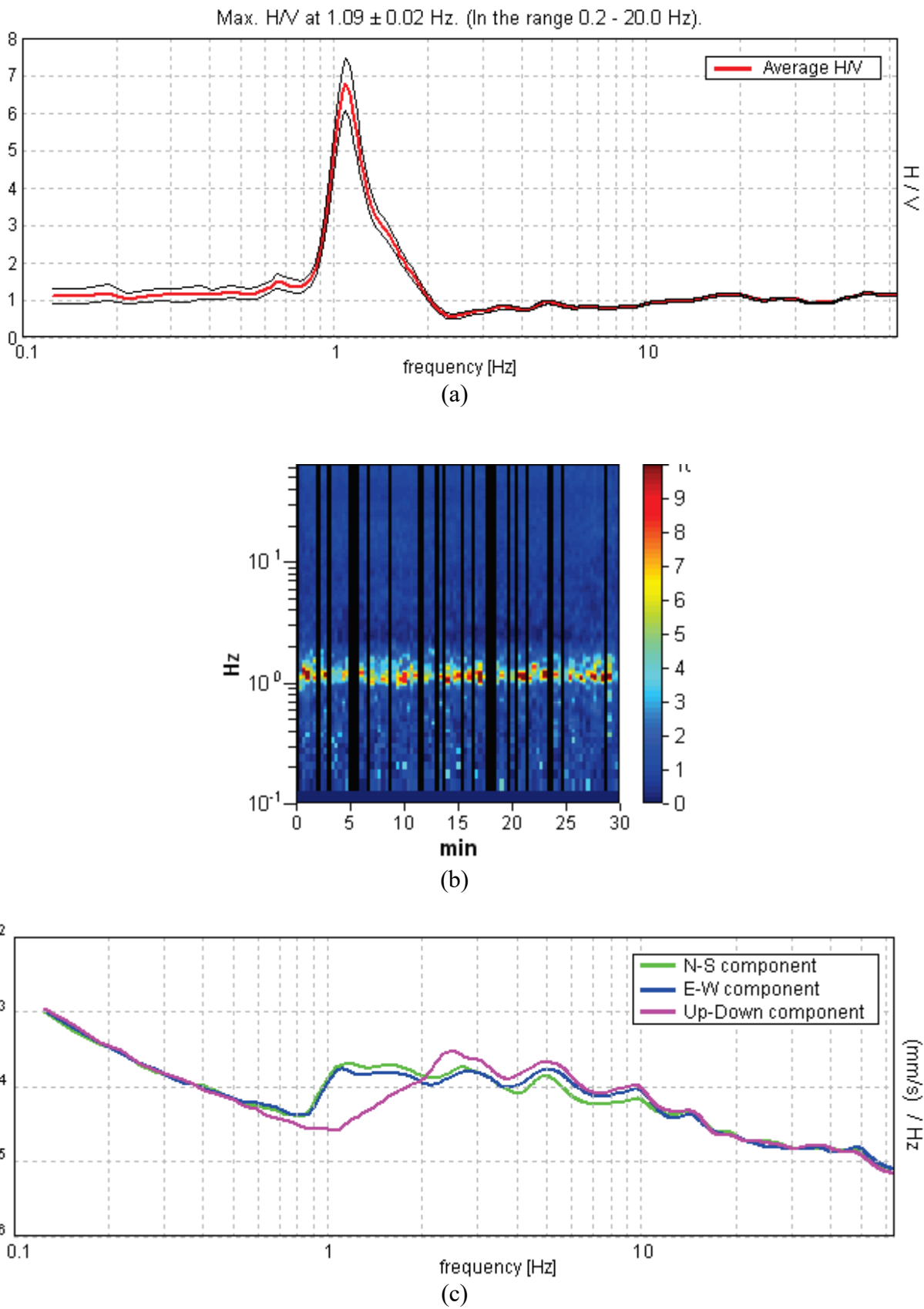


Fig. C-04 Tromino results at Masson landslide site WT04. (a) HVSR; (b) Spectral windows; (c) Horizontal and vertical average spectra for all windows used.

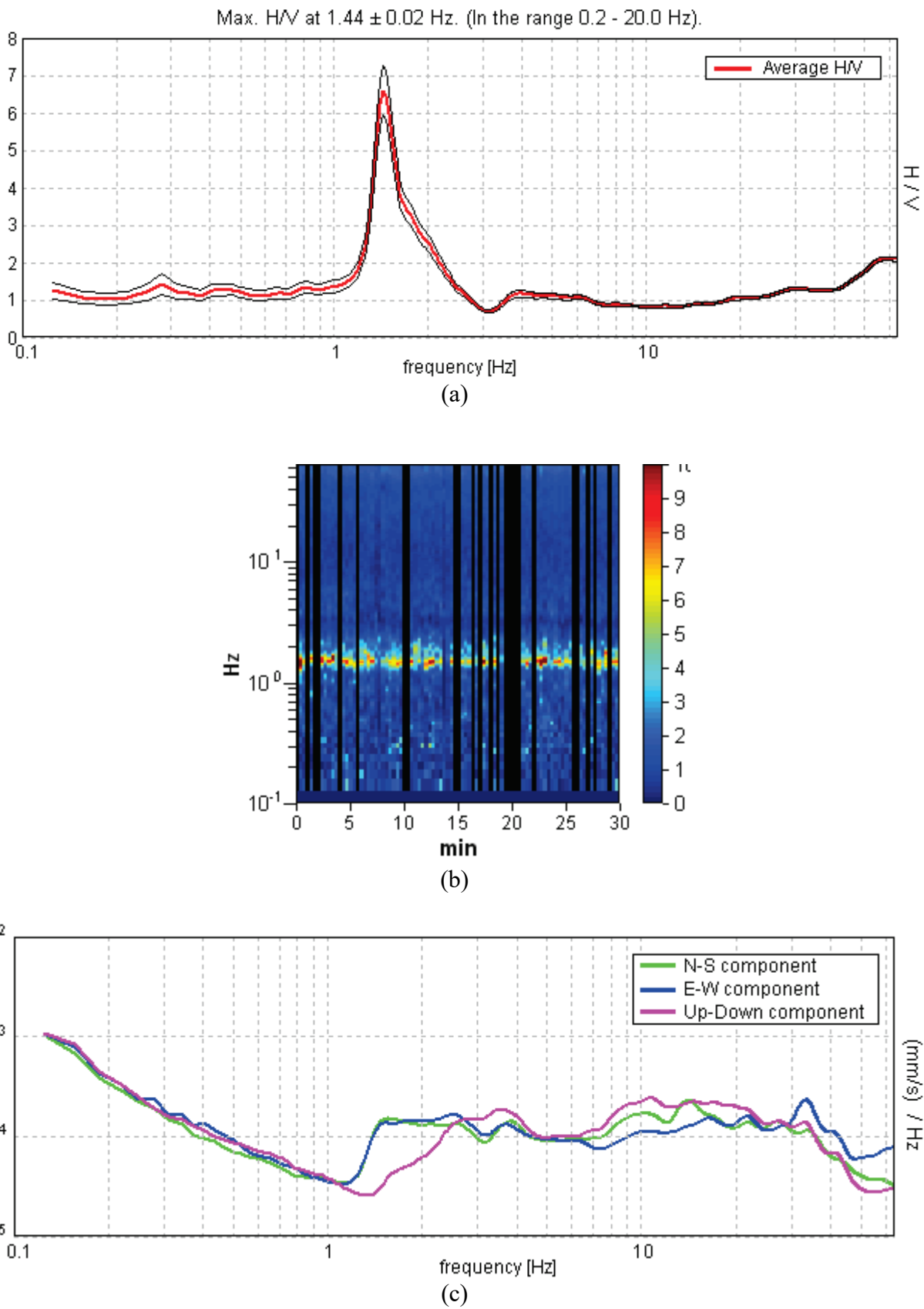


Fig. C-05 Tromino results at Masson landslide site WT05. (a) HVSR; (b) Spectral windows; (c) Horizontal and vertical average spectra for all windows used.

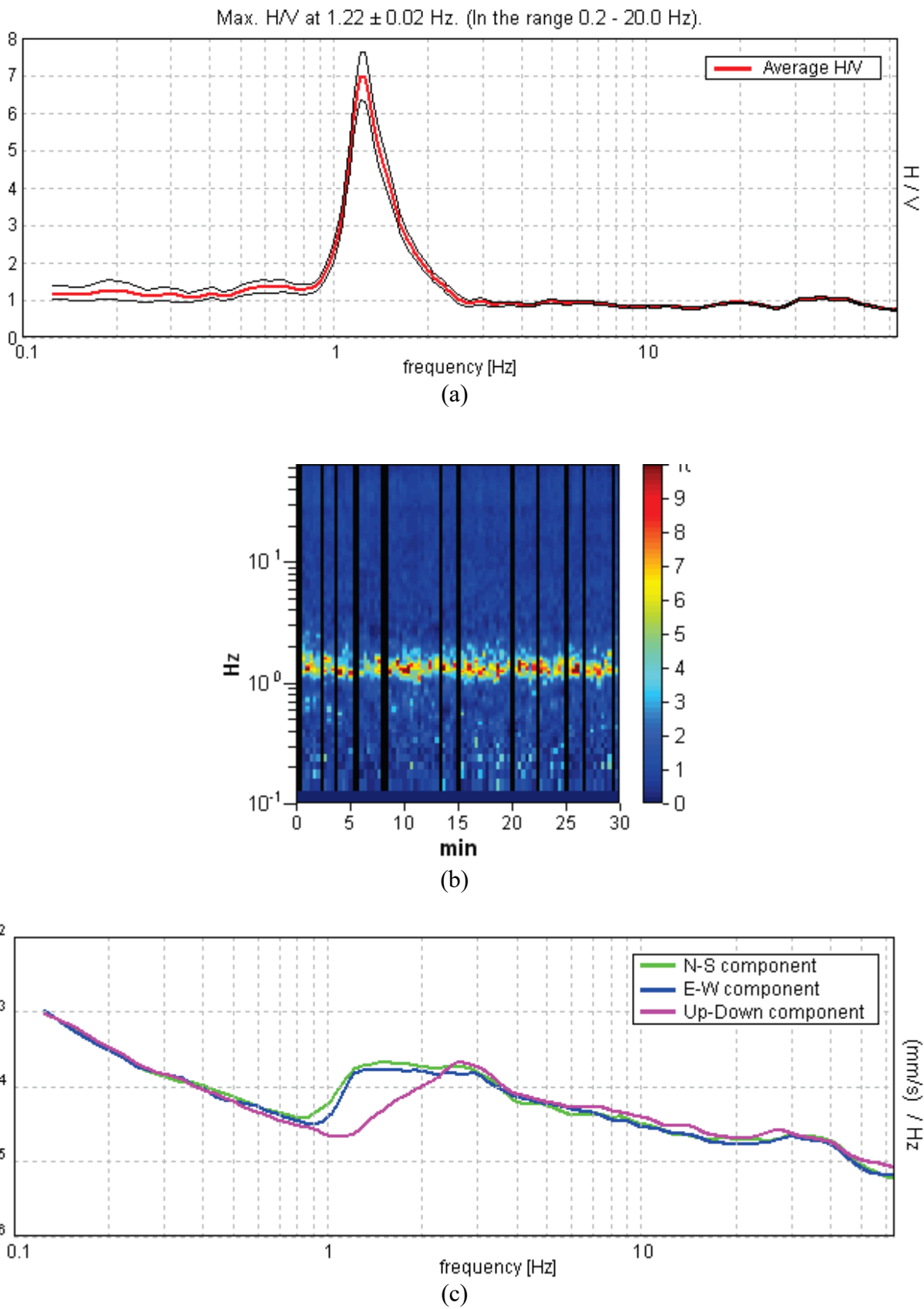


Fig. C-06 Tromino results at Masson landslide site WT06. (a) HVSR; (b) Spectral windows; (c) Horizontal and vertical average spectra for all windows used.

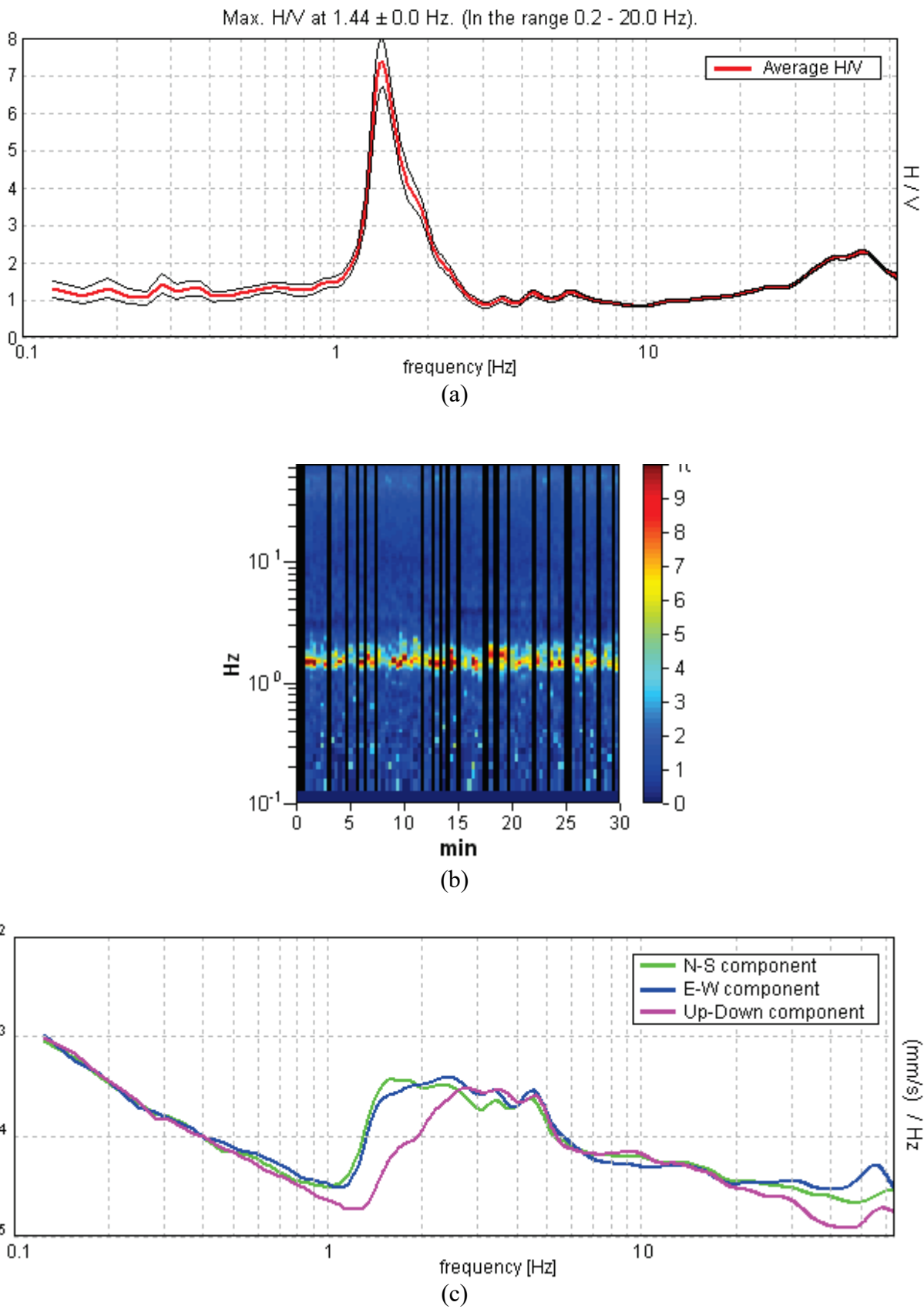


Fig. C-07 Tromino results at Masson landslide site WT07. (a) HVSR; (b) Spectral windows; (c) Horizontal and vertical average spectra for all windows used.

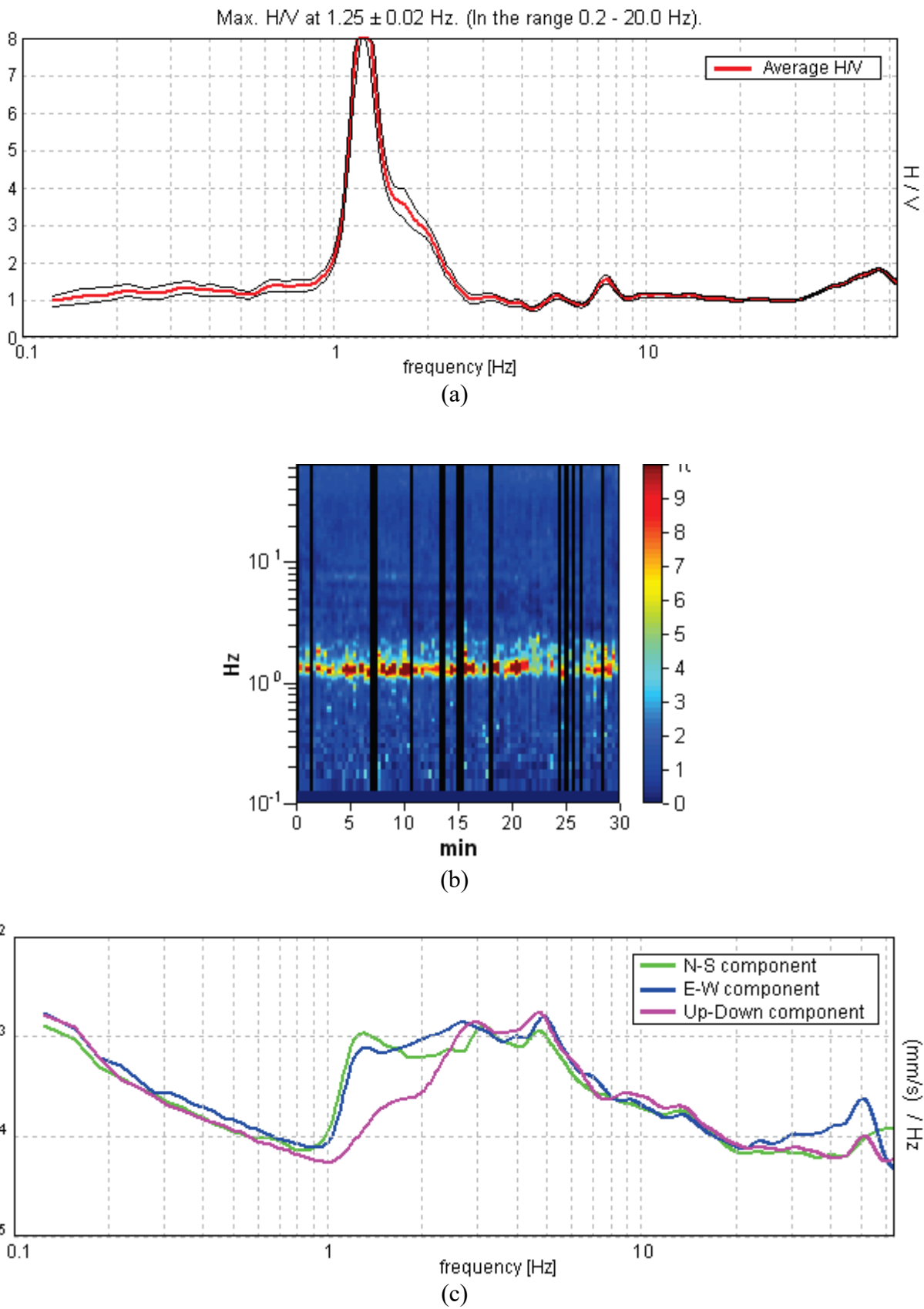


Fig. C-08 Tromino results at Masson landslide site WT08. (a) HVSR; (b) Spectral windows; (c) Horizontal and vertical average spectra for all windows used.

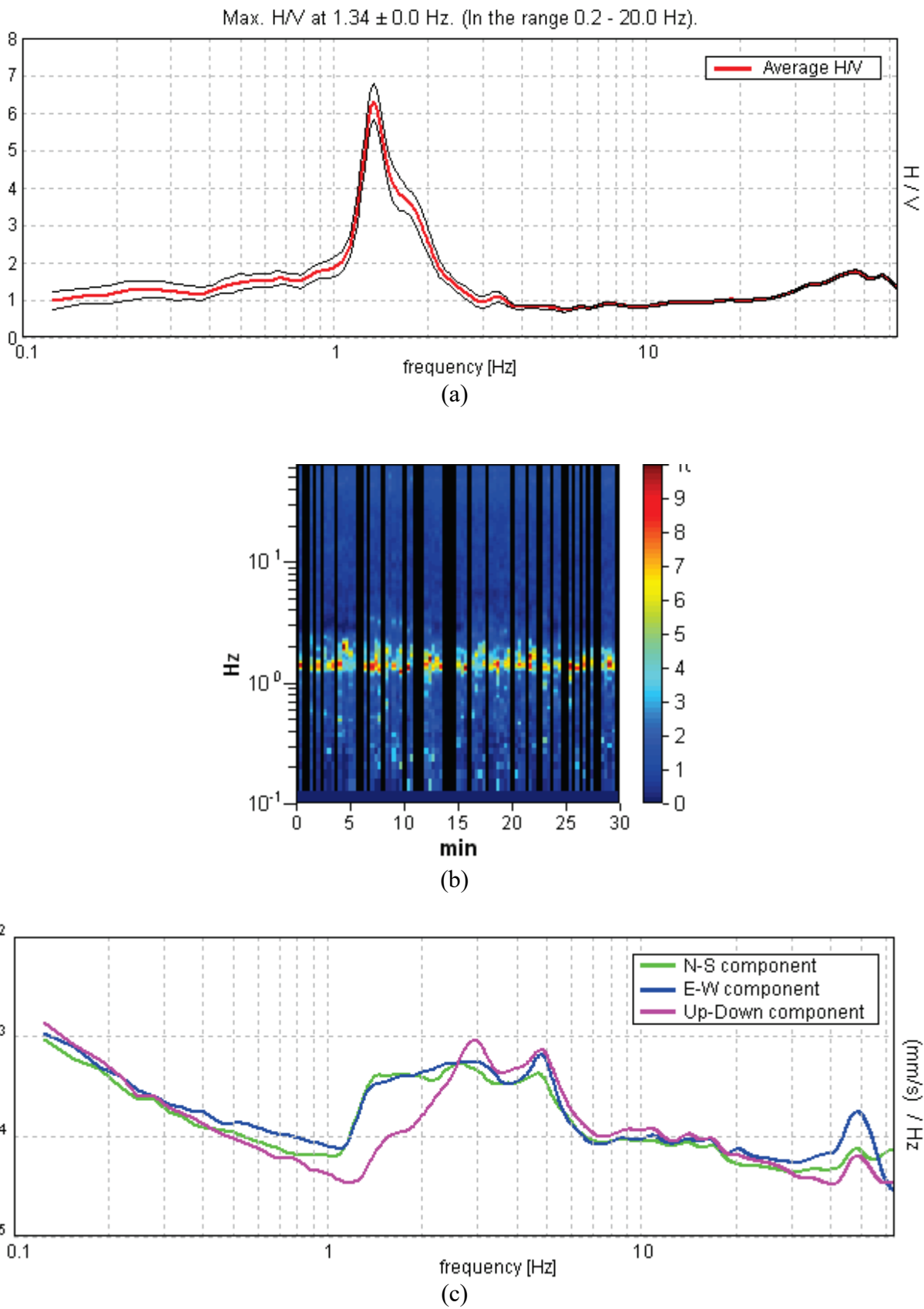


Fig. C-09 Tromino results at Masson landslide site WT09. (a) HVSR; (b) Spectral windows; (c) Horizontal and vertical average spectra for all windows used.

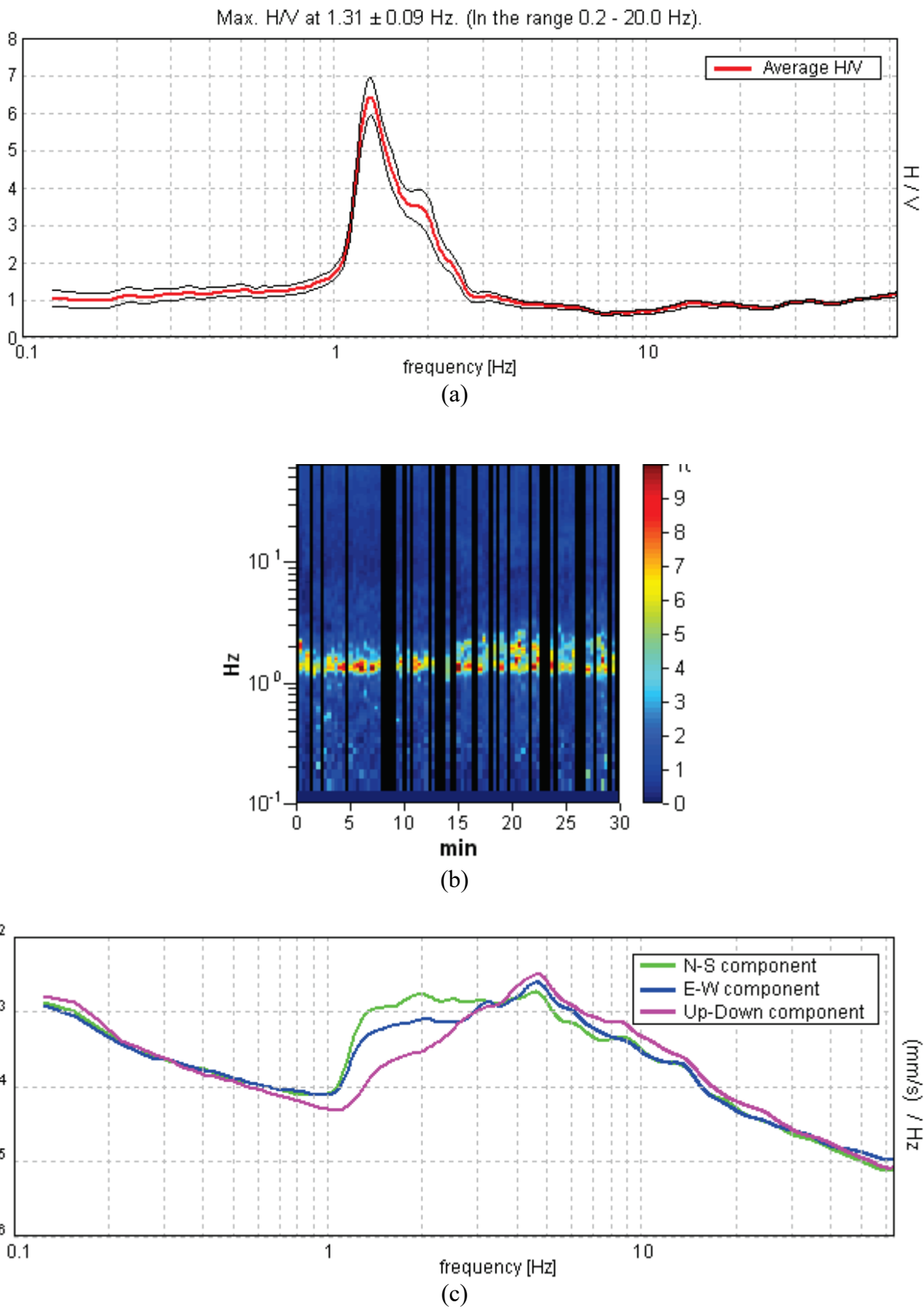


Fig. C-10 Tromino results at Masson landslide site WT10. (a) HVSR; (b) Spectral windows; (c) Horizontal and vertical average spectra for all windows used.

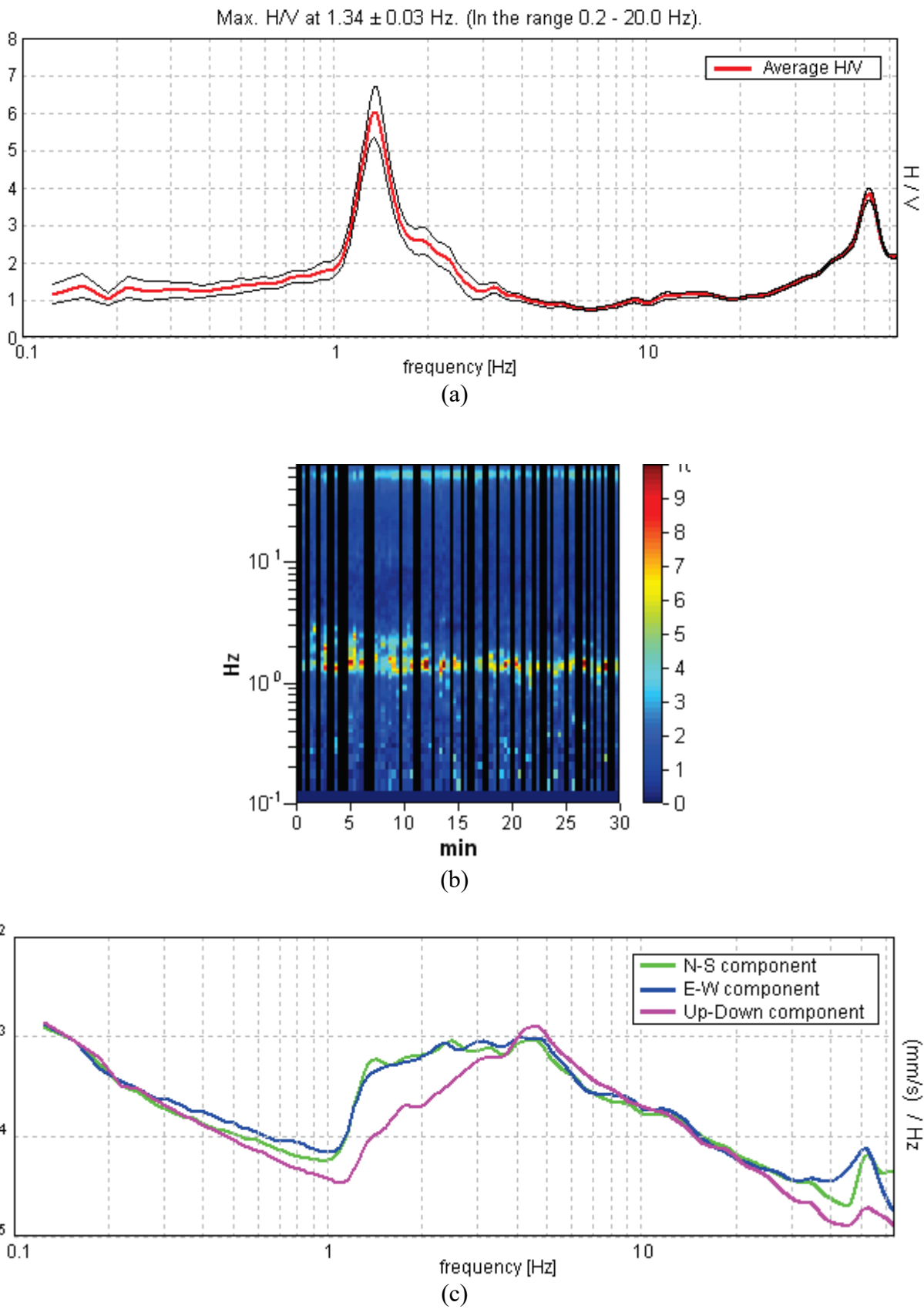


Fig. C-11 Tromino results at Masson landslide site WT11. (a) HVSR; (b) Spectral windows; (c) Horizontal and vertical average spectra for all windows used.